

72-3447

WALKER, Keith Gerald, 1941-
SIMULTANEOUS IONIZATION AND EXCITATION OF
NEON BY ELECTRON COLLISION.

The University of Oklahoma, Ph.D., 1971
Physics, atomic

University Microfilms, A XEROX Company, Ann Arbor, Michigan

THE UNIVERSITY OF OKLAHOMA

GRADUATE COLLEGE

SIMULTANEOUS IONIZATION AND EXCITATION OF NEON BY ELECTRON COLLISION

A DISSERTATION

SUBMITTED TO THE GRADUATE FACULTY

in partial fulfillment of the requirements for the

degree of

DOCTOR OF PHILOSOPHY

BY

KEITH GERALD WALKER

Norman, Oklahoma

1971

SIMULTANEOUS IONIZATION AND EXCITATION OF NEON BY ELECTRON COLLISION

APPROVED BY

Robert M. St. John

Subpanel Processes
Director

Keith D. Caswell

David C. Kay

DISSERTATION COMMITTEE

PLEASE NOTE:

**Some Pages have indistinct
print. Filmed as received.**

UNIVERSITY MICROFILMS

ACKNOWLEDGEMENT

From this research, a great amount of respect and appreciation has been generated for Dr. Robert M. St. John, and it is to him I give special thanks in the obtainment of this paper.

Much gratitude is due Dr. Ian Latimer for his helpful guidance in the initial stages of this research.

Sincere appreciation is expressed to Dr. C. C. Lin for his excellent lectures in atomic physics and helpful discussions in the research problem.

Many thanks to my colleagues Dr. James Walker, Jr., David Wilson, Max Lake and Roger Mickish for their assistance.

Gratitude to Mrs. Mary Lou Stokes, who has to be one of the best secretaries around, is certainly due for her many helps.

To Ron Stermer for his excellent glass work and the machine shop, a sincere thanks. Also, gratitude is expressed to the late Mr. James Hood for the monochromator slits and their superior quality.

Gratitude is expressed to the Air Force Office of Scientific Research for financial support of the work and to Dr. Ralph E. Kelley, scientific advisor of that agency, for his interest in and support of the work.

The role of my family, Rena, Barry and Trent, has been tremendous in this endeavor and their understanding and patience is deeply appreciated.

TABLE OF CONTENTS

	Page
ACKNOWLEDGEMENT	iii
LIST OF TABLES.	vi
LIST OF ILLUSTRATIONS	vii
ABSTRACT.	x
 Chapter	
I. INTRODUCTION.	1
II. SPECTRA AND TYPES OF COUPLING	3
III. EXPRESSION FOR THE CROSS SECTION.	9
IV. EXPERIMENT.	16
Apparatus	16
Standardization Procedures.	27
V. EXPERIMENTAL PARAMETERS	31
Electron Beam Current, I	31
Gas Pressure, p	31
Aperture Stops, D_C^2 and D_S^2	32
Electron Beam and Standard Lamp Intensity, I_C and I_S	32
Bandpass, $\Delta\lambda$	33
VI. APPARENT IONIZATION AND EXCITATION OF THE 3p LEVELS	36
Excitation Functions.	36
³ p Core	36
¹ d Core	45
¹ s Core	45
Apparent Cross Section.	45
³ p Core	45
¹ d Core	57
¹ s Core	57
Polarization.	58

TABLE OF CONTENTS (Cont'd.)

VII. CASCADE ANALYSIS.	67
³ P Core	67
¹ D Core	73
¹ S Core	82
Level Cross Section of the 3p, 3p' and 3'' Levels.	82
Comparison with Theoretical Cross Sections.	85
VIII. HIGH ENERGY CONSIDERATIONS.	89
³ P Core	89
¹ D Core	98
¹ S Core	104
IX. CASCADE INTO 3p ⁴ S _{3/2} AND RELATED TOPICS	107
X. RESONANT FEATURES IN ATOMIC NEON.	116
XI. SUMMARY	123
ADDENDUM.	125
REFERENCES.	126

LIST OF TABLES

TABLE	Page
I. Experimental Cross Sections for the (³ P)3p Configurations of NeII.	48
II. Comparison of Branching Ratios for 3p→3s Arrays	51
III. Branching Ratio Involving the 3p ⁴ S _{3/2} States.	53
IV. Experimental Cross Sections for the (¹ D)3p Levels	55
V. Comparison of Branching Ratios for 3p'→3s' Arrays.	56
VI. Experimental Cross Sections for the (¹ S)3p'' Levels	57
VII. Cross Sections for the Doublet 3d and 4s Levels	74
VIII. Cross Sections for the Quartet 3d and 4s Levels.	75
IX. Branching Ratios for the Cascade Levels.	76
X. Cross Sections of the 3d' and 4s' Levels	84
XI. Level Cross Sections of the 3p, 3p' and 3'' Levels	86
XII. Comparison of Sudden Perturbation Calculated Cross Sections and Experimental Level Cross Sections	87

LIST OF ILLUSTRATIONS

Figure	Page
1. Energy levels of 3P core of NeII	4
2. Energy levels of 1D core of NeII	5
3. Energy levels of 1S core of NeII	6
4. Interaction region between electrons and atoms	11
5. Electron gun	17
6. Impurity spectrum.	19
7. Vacuum system.	21
8. Optical arrangement for calibration.	26
9. Relative transmission of monochromator vs wavelength . .	27
10. Excitation functions of the $3p$ doublet levels.	37
11. Excitation functions of the $3p^4S$ and $3p^4P$ levels	38
12. Excitation functions of the $3p^4D$ levels.	39
13. Comparison of the excitation functions between NeII and ArII	42
14. Excitation functions of the $(^1D)3p'$ levels	46
15. Excitation functions of the $(^1S)3p''$ levels	47
16a. Rectangular reference frame for orientation of detector relative to electron beam.	59
16b. Dipole radiation for x, y and z dipoles.	59
17. Instrumental polarization for Jarrell-Ash $\frac{1}{2}$ -meter mono- chromator with 1180 grooves/mm grating	63
18. Polarization of the helium 4^1D level	65
19. Polarization of the NeII transitions	66

LIST OF ILLUSTRATIONS (Cont'd.)

20.	Excitation functions of the $4s^2P$ and $3d^2P$ levels	69
21.	Excitation functions of the $3d^2D$ and $3d^2F$ levels	70
22.	Excitation functions of the $4s^4P$ and $3d^4P$ levels	71
23.	Excitation functions of the $3d^4D$ and $3d^4F$ levels	72
24.	Excitation functions of the $4s'$ and $3d'$ levels	83
25.	High energy portion of the $3p$ doublet excitation functions.	90
26.	High energy portion of the $3p$ quartet excitation functions.	91
27.	$\ln Q'$ vs $\ln E$ for the $3p$ doublet levels.	92
28.	$\ln Q'$ vs $\ln E$ for the $3p$ quartet levels.	93
29.	High energy portion of excitation functions for the doublet cascade states of 3P core.	95
30.	High energy portion of excitation functions for the quartet cascade states of 3P core.	96
31.	$\ln Q$ vs $\ln E$ for those $3p$ levels where subtraction of cascade has changed their slope.	97
32.	$\ln Q$ vs $\ln E$ for the total ionization of NeI by electron impact	99
33.	High energy portion of the $3p'$ states' excitation functions.	100
34.	High energy portion of excitation functions for the cas- cade states of 1D core	101
35.	$\ln E$ vs $Q'E$ for the $3p'^2P$ levels.	102

LIST OF ILLUSTRATIONS (Cont'd.)

36.	$\ln Q'$ vs $\ln E$ for the $3p'^2D$ and 2F levels.	103
37.	High energy portion of the $3p''$ excitation functions. . .	105
38.	$\ln E$ vs $Q'E$ for the $3p''^2P$ levels.	106
39.	Levels involved in the calculation of the apparent and level cross section of $3p^4S_{3/2}$	108
40a.	Excitation function of the 2866\AA line from 0 to 500 eV .	110
40b.	Onset of the 2866\AA line.	110
41.	Excitation function of the 3329\AA line.	113
42.	Excitation function of the 3626\AA line.	113
43.	Optical excitation functions of the thresholds of the $2P$ levels in NeI	118
44.	Energy level diagram of the $2P$ levels of atomic neon and the associated negative ion states	119

ABSTRACT

The cross sections for simultaneous ionization and excitation of neon by electron impact to the 3p states of NeII have been measured at 150 eV by the optical method. Cascade into the 3p levels from the 4s and 3d levels was considered to obtain the level cross section of the 3p states. Comparison was made between these experimental values and those obtained by the sudden perturbation approximation.

The excitation functions were examined from onset to 1000 eV and compared to ArII and the ionization excitation function. The NeII excitation functions were much broader than expected. In general, the doublet curves were broader than the quartet levels for the 3P core configuration. The levels associated with the 1D and 1S core configurations have exceptionally broad excitation functions.

Polarization effects were examined and found to be very small, less than 5 per cent in most cases.

The spectrum of NeII is quite complex and has several errors in line assignments. Recent work has corrected some of these errors but the results of this research have suggested more work is needed in this area.

CHAPTER I

INTRODUCTION

Cross sections for the simultaneous ionization and excitation by electron impact of neon have been measured and are examined in this work. Neon is used frequently in high temperature gaseous devices and astrophysical observations, and of late, ion lasers; collision information has been needed, but not been readily available.

Recent experimental work on NeII includes experiments on line strengths^(1,2) and lifetimes^(2,3). Hertz⁽⁴⁾ has obtained some of the optical excitation functions for simultaneous ionization and excitation of the 3s states of NeII which lie in the vacuum ultraviolet. Theoretical work consists of lifetime calculations⁽⁵⁾ of the $2p^43p$ states of NeII, Hartree-Fock results for some of the excited states⁽⁶⁾ and excitation cross sections for the upper laser states of the $2p^43p$ configuration utilizing the method of sudden approximation.^(7,8)

This paper contains the absolute cross sections for simultaneous ionization and excitation by electron collision to the 3p states of NeII with cascade contributions from the 3d and 4s states. Several of these 3p states have been found as laser states⁽⁹⁾ and are of particular interest. The optical excitation functions have been obtained from threshold to 1000 electron volts (eV). Polarization effects were examined as well.

One of the difficulties encountered in this research was the obtainment of an accurate table concerning the classification of spectral transitions for the single ionized states of neon. Until 1967 there had been no classification of lines other than those originating from the 3s, 3p, 3d, 4s and 4f levels. Some of the 3d and many of the 4f levels were of doubtful assignment. Persson and Minnhagen^(10,11) have been analyzing the spectrum of NeII and have published some of their results. The complete analysis of NeII by them is as of this writing yet to be published⁽¹²⁾. We have used the published results of Persson to classify our transitions. This work still questions some of the assignments and we have illustrated how the optical excitation function can be used as a tool for identifying spectra.

Also presented in this paper is a discussion on some resonance peaks which have been discovered in the optical excitation functions of the 3p levels of NeI. These have been attributed to cascade from the negative ion states of neon.

CHAPTER II

SPECTRA AND TYPES OF COUPLING

Figures 1, 2 and 3 are the energy level diagrams of NeII. The energy scale is referred to the ground state of the ion. The ground state of the ion is a $2s^22p^5$ configuration which gives rise to a 2P term. The excited NeII configuration can be expressed as $2s^22p^4n\ell$ where $2s^22p^4$ represents the core and $n\ell$ the configuration of the running, or excited, electron. The $2s^22p^4$ core configuration, based on the LS coupling scheme, will contain three different terms: 3P , 1D and 1S . Associated with the 3P core is a doublet and quartet system. A doublet system only is generated by the 1D and 1S core.

In the $J_c\ell$ scheme, where J_c is the total angular momentum quantum number for the core and ℓ is the orbital angular momentum of the running electron, there would be associated with the 3P core three systems designated as 3P_2 , 3P_1 and 3P_0 . For the 1D and 1S core, we would have 1D_2 and 1S_0 .

Garstang⁽¹³⁾ calculated the relative line strengths for lines of the $3s-3p$ and $3p-3d$ arrays under the assumption of intermediate coupling. In 1964, Koopman's⁽¹⁾ relative line strengths obtained from intensity measurement on the $3s-3p$ transitions with an electrically driven shock tube correlated better with the LS coupling scheme values than with the intermediate coupling values. Koopman's results on the $3p-3d$ transitions were limited but tended to agree with the

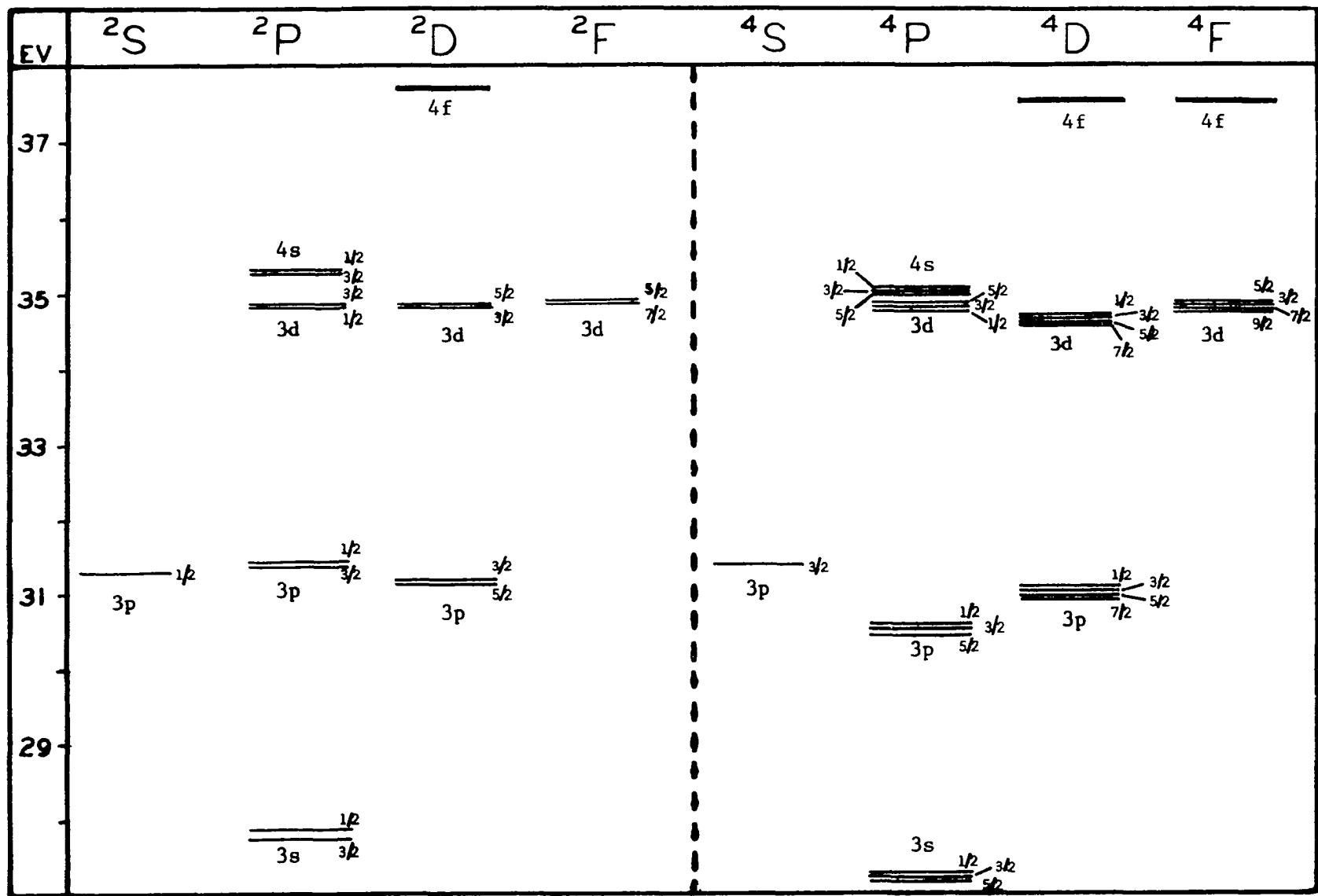


FIGURE 1. Energy levels of $3P$ core of $NeII$

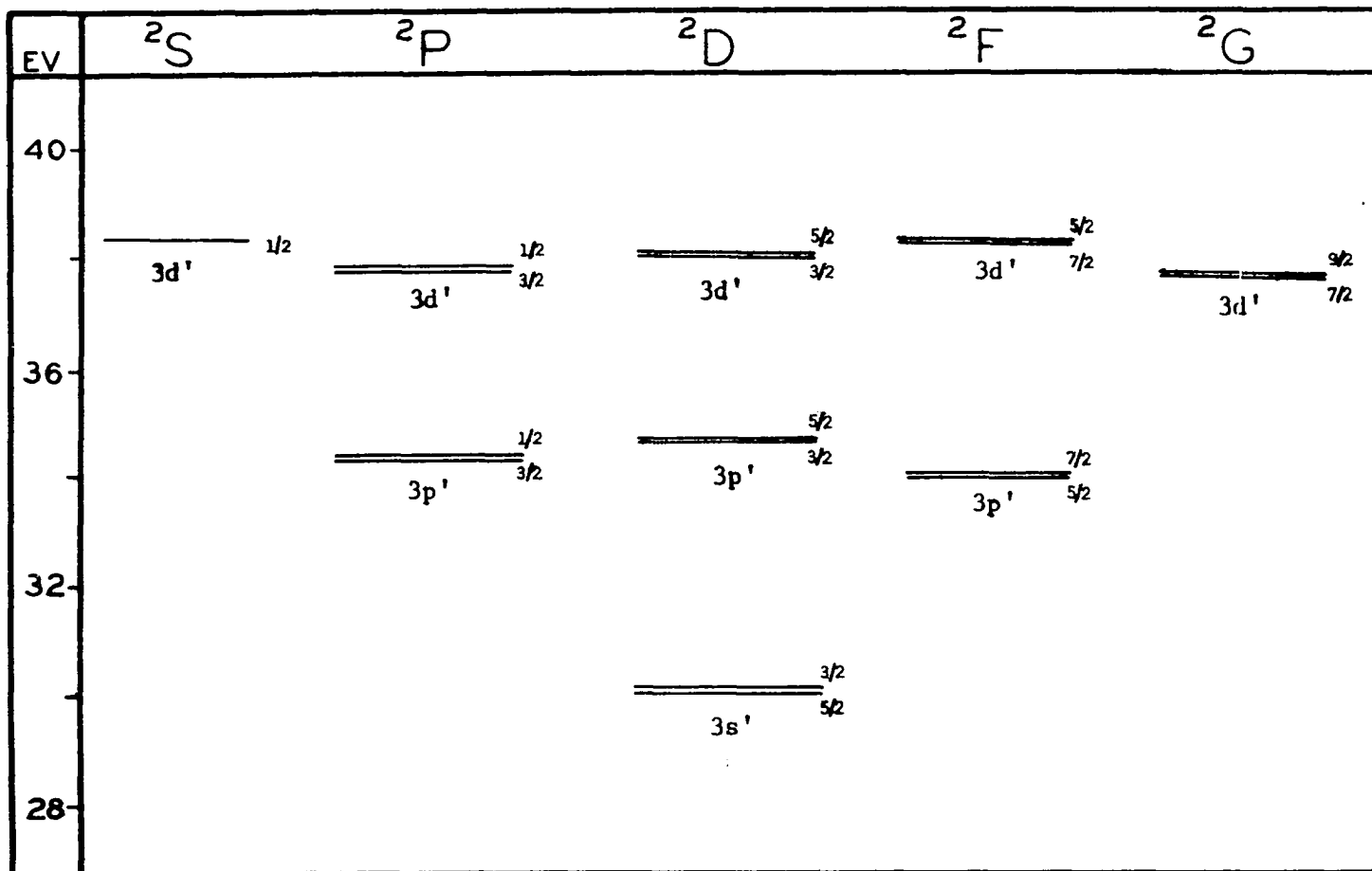


FIGURE 2. Energy levels of 1D core of NeII

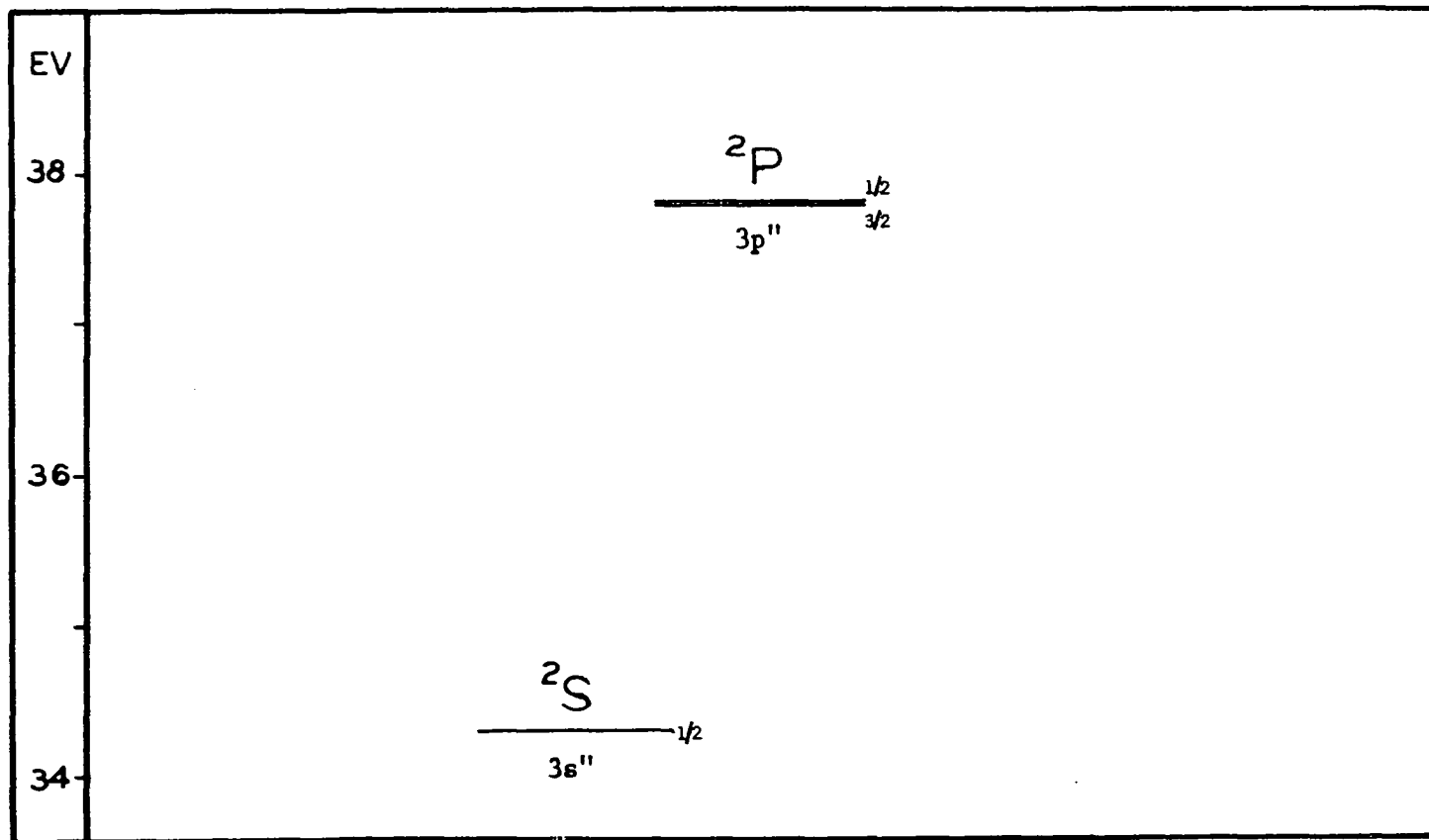


FIGURE 3. Energy levels of $1S$ core of $NeII$

intermediate coupling. The experiment of Hodges *et al.*,⁽²⁾ using a cw neon laser discharge as a spectroscopic source, determined the line strengths of the 3s-3p, 3p-3d and 3p-4s arrays. Their results indicated that many of Koopman's values were in error and that Garstang's intermediate coupling calculations for the 3s-3p transitions are better than previously thought.

Persson⁽¹⁴⁾ has found in his work that the 3p levels are fairly good in LS coupling with the $3p^4S_{3/2}$ and $3p^4D_{7/2}$ very pure in LS coupling (99-100% pure). He also has found that the 3d configurations are intermediate between LS and $J_C\ell$ coupling.

In $J_C\ell$ coupling the electrostatic interaction between the outer electron and the p^4 core is strong compared to the spin-orbit interaction of the external electron but still weak relative to spin-orbit interaction of the core. The orbital angular momentum $\vec{\ell}$ of the running electron is coupled to the total angular momentum of the core \vec{J}_C . This vector coupling forms the quantized result $\vec{J}_C + \vec{\ell} = \vec{K}$. The total angular momentum \vec{J} of the atom is then found by the coupling of \vec{K} with the spin \vec{s} of the running electron, $\vec{J} = \vec{K} + \vec{s}$. In this type of coupling relative strong transitions would be allowed between quartet and doublet states in Fig. 1. Such transitions have been observed in the 3p-3d array in this research; particularly from the $3d^2F$ and $3d^4F$ states. Persson has found that $3d^4F_{7/2}$ and $3d^2F_{7/2}$ levels are mixed about half and half. This means that the LS designations are insignificant for some levels as far as the nature of the quantum states is concerned. Persson's study of those transitions from the $2p^4nf$ levels have revealed almost pure $J_C\ell$ coupling.

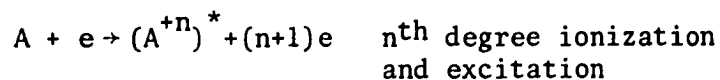
Throughout this paper the LS designations for the states will be used even though for some states, as the ${}^2F_{7/2}$ and ${}^4F_{7/2}$ mentioned above, it has no relationship whatsoever to the nature of the quantum state involved.

Minnhagen's^(15,16) work on ArII, which has the same $p^4\ell$ configuration as NeII, showed the same type of coupling, i.e., good LS coupling for the deep lying 4p states and greater tendency to $J_c\ell$ coupling the higher the levels. Therefore, it will be of interest to compare this present work with the earlier work on ArII by Latimer and St. John⁽¹⁷⁾.

CHAPTER III

EXPRESSION FOR THE CROSS SECTION

The experiment consists simply of subjecting a gas of known density to an electron beam which is well defined, both geometrically and energetically. The impact of the electrons upon the gas atoms create various effects. These can be classified into three types of collisions: elastic, superelastic and inelastic. The elastic collision between electron and atom involves no exchange of energy whereby the atom is left in some excited state. The superelastic collision is associated with the phenomena where an electron receives energy from an excited atom upon collision. The inelastic collision brings about such conditions as the excitation, ionization or simultaneous ionization and excitation of the atom. The various inelastic processes can be expressed as follows:



One of the main purposes of this paper is to determine a quantitative result (commonly called a cross section) relating to the probability of singly ionizing and exciting the neon atom to the 3p levels of NeII by a single electron impact.

To extract such a quantity we begin with an equation expressing the rate by which atoms are excited to the i^{th} state. If $N(i)$ is the number of atoms in the i^{th} state which exist in the collision region, then

$$\frac{dN(i)}{dt} = \begin{array}{l} \text{Rate of population} \\ \text{(of state } i \text{ by di-} \\ \text{rect electron impact} \end{array} - \begin{array}{l} \text{Rate of depopulation} \\ \text{(of state } i \text{ by spon-} \\ \text{taneous emission.} \end{array} \\ + \begin{array}{l} \text{Rate of population of} \\ \text{(state } i \text{ by cascade)} \\ \text{from higher levels.} \end{array} \pm \begin{array}{l} \text{Rate of excitation} \\ \text{(or deexcitation)} \\ \text{by atom-atom col-} \\ \text{lision.} \end{array}$$

The last term can be made negligible by using sufficiently low pressures.

At equilibrium, $\frac{dN(i)}{dt} = 0$ and

$$\begin{array}{l} \text{Rate of Populating} \\ \text{(of state } i \text{ by di-} \\ \text{rect electron impact} \end{array} = \begin{array}{l} \text{Rate of depopulation} \\ \text{(of state } i \text{ by spon-} \\ \text{taneous emission} \end{array} - \begin{array}{l} \text{Rate of population} \\ \text{(of state } i \text{ by } \\ \text{cascade from higher} \\ \text{levels.} \end{array}$$

The rate of depopulation by spontaneous emission will betray itself by the emission of radiation from the level i to all allowed lower levels. If the total photon flux from the interaction region between the electrons and atoms due to transitions from the state i is measured, then we possess a quantity which expresses the number of atoms which must be entering state i each second.

Likewise, the cascade contributions can be found by measuring the total flux of the lines terminating on level i and it will yield that number of atoms in state i due to cascade.

The difference in these photon counts would yield that number of atoms which are excited each second to state i by a direct electron

impact in the interaction region.

Consider Fig. 4,

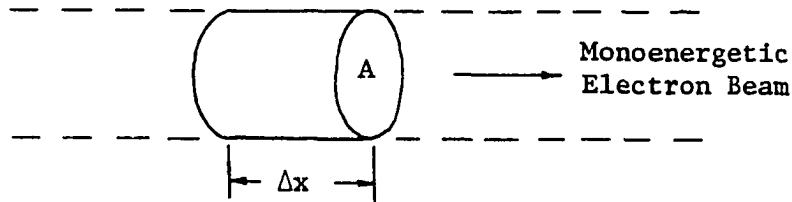


Figure 4. Interaction region between electrons and atoms.

where Δx is the length of the electron beam from which radiation is gathered by the detecting system and defines the interaction region, hereafter designated as the collision chamber. Also,

A = cross sectional area of electron beam

N = number of gas atoms per unit volume

N_e = number of electrons per unit volume

v = velocity of electrons.

Then $\int_A N_e v dA'$ is the number of electrons passing through A each second and $NA\Delta x$ is the number of atoms in the collision chamber. Hence, the fractional part of A which is opaque to electrons because of inelastic collision can be written as $NA\Delta x \frac{Q}{A}$ where Q is defined as the total inelastic cross section per atom (in units of area) and is made up of all the before mentioned types of inelastic collision processes. Therefore, $NA\Delta x \frac{Q(i)}{A}$ represents that fractional part of A which is opaque to electrons because of collisions which excite the atom to state i . $Q(i)$

is then defined as the level cross section of state i and is dependent on the energy of the impacting electron. The curve representing $Q(i)$ as a function of electron energy is called the excitation function of the i^{th} state.

Then the total number of electrons which will suffer a collision per second in the collision chamber with an atom in which that atom will end up in state i is $N\Delta x Q(i) \int_A N_e v dA'$. Substituting, we have $N\Delta x Q(i) \frac{I}{e}$ where I is the electron beam current and equals $e \int_A N_e v dA'$. Designating the photon flux from the interaction region due to a transition from state i to state j as $F(ij)$, Eq. (1) is obtained

$$N\Delta x Q(i) \frac{I}{e} = \sum_{i>j} F(ij) - \sum_{k>i} F(ki) \quad . \quad (1)$$

To obtain the level cross section $Q(i)$ optically, one must measure the total photon flux arising from all transitions into and out of state i . In general it is impossible to completely resolve all these lines and determine each ones cross section. In such instances, Eq. (1) can be simplified as follows.

$$F(ij) = A(ij) \int N(i) A' dx \quad (2)$$

where $A(ij)$ is the Einstein coefficient for spontaneous emission from state i to state j and $N(i)$ is the number of gas atoms per unit volume which are in the i^{th} state. The integration is over the observational length of the electron beam. The total photon flux out of state i is

$$\sum_{\ell} F(i\ell) = \sum_{\ell} A(i\ell) \int N(i) A' dx \quad . \quad (3)$$

Combining Eqs. (2) and (3) yields

$$\sum_{\ell} F(i\ell) = \frac{\sum A(i\ell)}{A(ij)} F(ij) \quad (4)$$

The quantity $\frac{A(ij)}{\sum_{\ell} A(i\ell)}$ is defined as the branching factor of the $i \rightarrow j$ transition and denoted by $B(ij)$. These branching factors are quite commonly obtained theoretically and sometimes are available experimentally. Hence, if only one transition is measured then by use of the appropriate branching factor the total flux can be obtained. Equation (1) can now be written as

$$N\Delta x Q(i) \frac{I}{e} = F(ij)/B(ij) - \sum_{k>i} F(ki) . \quad (5)$$

The cascade flux can also be made more complete by use of branching factors. The expression for the direct cross section is then

$$Q(i) = \frac{1}{B(ij)} \frac{F(ij)}{N\Delta x(I/e)} - \sum_{k>i} \frac{F(ki)}{N\Delta x(I/e)} . \quad (6)$$

Setting

$$Q(ij) = \frac{F(ij)}{N\Delta x(I/e)} , \quad (7)$$

we have what is defined as the optical cross section of the spectral line due to the $i \rightarrow j$ transition. Equation (6) can now be written

$$Q(i) = \frac{Q(ij)}{B(ij)} - \sum_{k>i} Q(ki) . \quad (8)$$

The quantity $Q(ij)/B(ij)$ is called the apparent cross section of the level i , $Q'(i)$. It is best if branching factors can be avoided in the

calculation and $Q'(i)$ be determined by the actual measured sum of the optical cross-sections. This is because branching factors are sometimes quite sensitive to the scheme in which they were generated.

The experimental data will then consist of as many optical cross sections as possible of those transitions originating from, and terminating on, level i . From Eq. (7), it is seen that the experimental parameter which will be the most difficult to measure is the total photon flux, $F(ij)$. The detecting system will gather radiation in a certain solid angle, Ω , from the observation region. Then

$$F(ij) = \frac{4\pi}{\Omega} F(ij, \Omega) \quad (9)$$

where $F(ij, \Omega)$ is that flux gathered in the solid angle Ω . Equation (9) is based upon the assumption that the emitted radiation is isotropic. Such a condition is not true in general and gives rise to polarization of the emitted radiation. This effect and its affect on $Q(i)$ will be discussed later.

The detector will then register a signal which is proportional to $F(ij, \Omega)$. The proportionally constant will consist of the spectral sensitivity, $S(\lambda)$, of the detecting device and the transmission factors, $\gamma(\lambda)$, of the various optical components. This can be expressed as

$$I_c = \gamma(\lambda)S(\lambda)F(ij, \Omega_c) \quad , \quad (10)$$

where I_c is the signal displayed by the detector.

Equation (7) can be rewritten as

$$Q(ij) = \frac{4\pi I_c}{\Omega N \Delta x (I/e) \gamma(\lambda) S(\lambda)} \quad . \quad (11)$$

$S(\lambda)$ is determined from a known flux source. In this work a tungsten ribbon lamp whose calibration is traceable to the National Bureau of Standards in Washington, D. C. was used.

CHAPTER IV

EXPERIMENT

Apparatus

As was mentioned in the previous chapter, an electron beam is necessary in which the energy and geometry are well defined. Figure 5 is a drawing of the electron gun used in this experiment. It was designed and constructed by Sharpton⁽¹⁸⁾. The cathode is 3mm in diameter and was indirectly heated; it is of the impregnated barium type. The cathode is at a negative potential which is the accelerating voltage. The first two grids control the current and focusing properties of the beam. The third grid is at cathode potential and essentially stops all electrons whose energy is less than the cathode potential. This helps the energy resolution of the beam which is estimated to be 0.4 to 0.5 eV from the examination of resonant features in excitation functions. The last two grids are at ground potential as is the Faraday cage which serves as the collision chamber. The beam upon emerging from the last grid is about 3mm in diameter. The currents used in this experiment were 500 microamperes although the gun is capable of currents around 1.0 milliampere. Secondary electrons which have been created by the primary electrons hitting the back side of the Faraday cup can distort the excitation curves since they are at much lower energy. To help negate this effect the end of the Faraday cup is constructed of

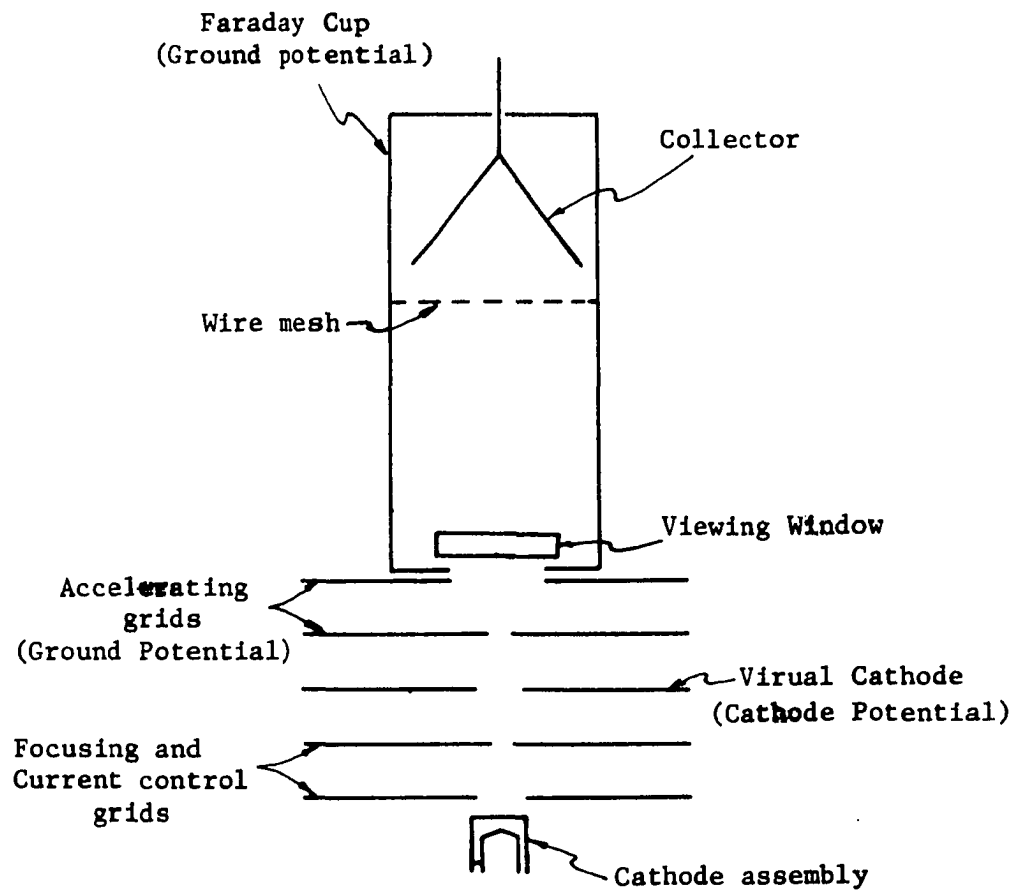


FIGURE 5. Electron Gun

a wire mesh which is transparent to the electrons but opaque to external fields. The cup-shape collector is operated at a positive voltage with respect to the cage and collects secondary electrons before they can enter the interaction region.

One aspect of the apparatus which required extensive modification was the vacuum system. Figure 6(a) is a recording of the impurity spectra of the collision chamber before modification. The gun was activated and the system was cut off from the vacuum pumps for over one hour. The spectrum of interest in this paper lies between 3000 Å and 4000 Å. The impurities consist of CO^+ and N_2^+ and various other molecules which are due to impurities in the system components and those contaminants vaporized from the hot cathode. Figure 6(b) is the same spectrum under the same conditions but after modifications. Only ultra-high vacuum components were used. They were made of glass and type 304 stainless steel. This eliminated much of the previous impurities but still those molecules and ions emitted from the cathode existed in the chamber. To rid the system of these gases a Norton Sorb-Ac non-evaporable getter pump was utilized. This operates by a new way of pumping the active gases, chemisorption and bulk diffusion into a zirconium-aluminum alloy getter. This getter alloy is coated by a special process onto a steel cartridge which is then pleated into a circular configuration to give a maximum surface area in a small volume. This getter was then mounted next to the collision chamber for maximum effect. Figure 6(c) is the same region of the spectrum under the identical conditions as in Figs. 6(a) and 6(b) but now with the getter pump. No impurities were detected.

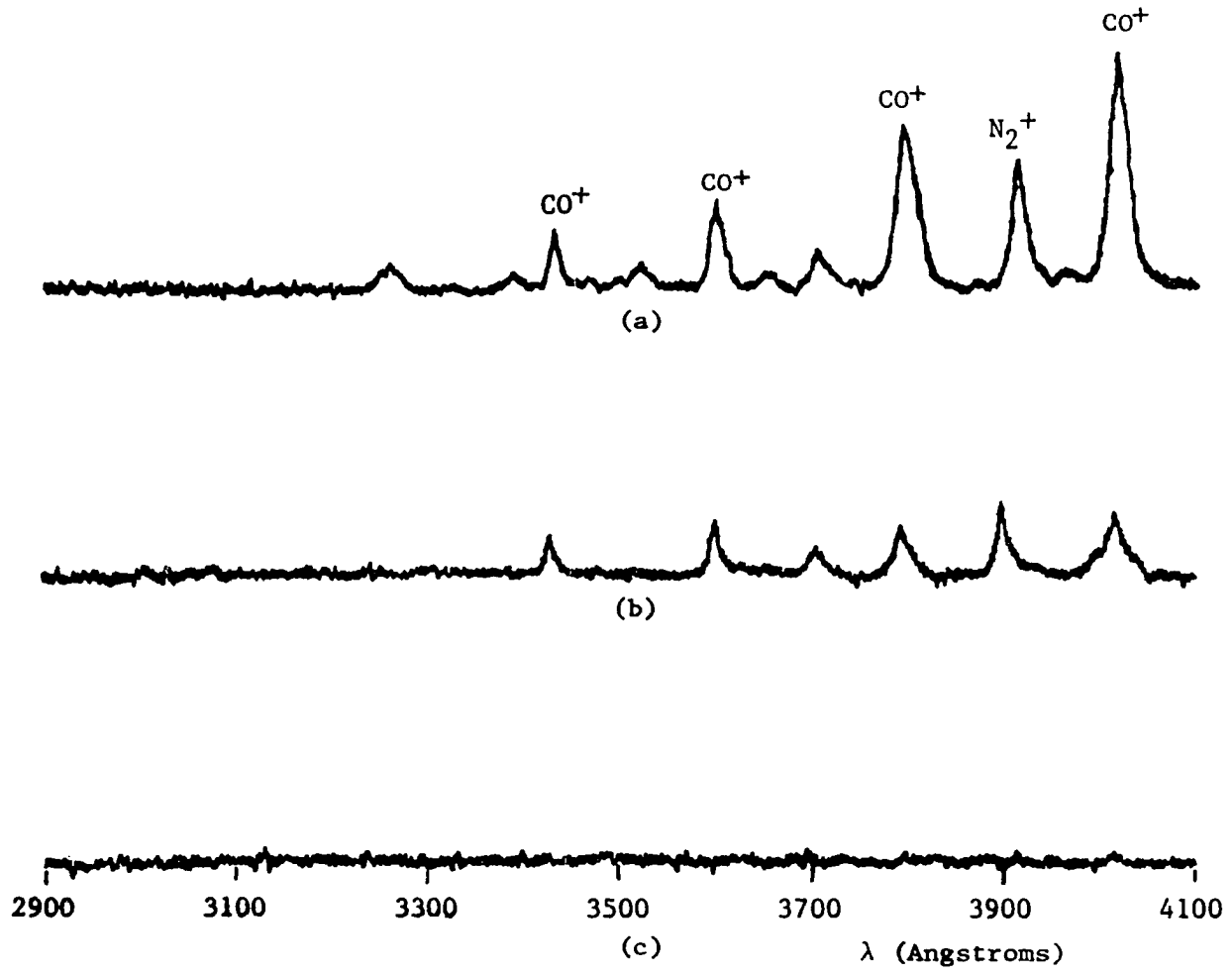


FIGURE 6. Impurity spectrum (a) before modification of system, (b) after modification and (c) with addition of getter pump.

Also, the slit width of the monochromator used in the above tests was twenty times larger than widths used in taking excitation data. The biggest advantage of this getter pump over other types of getters and absorption pumps as far as this experiment is concerned is that it will not pump the inert gases. This was verified with this particular pump for neon by monitoring the neon pressure in the chamber with respect to time.

Figure 7 is a drawing of the vacuum system. The area enclosed by the dotted line is bakeable at 450° C. The gas is inserted from flasks containing spectroscopically pure gas into a small evacuated region by the use of stopcocks. It is then fed into the ultra-high vacuum region by a bakeable, high vacuum valve. The gas travels over liquid nitrogen before entering the chamber. Any contamination suffered by the gas because of stopcocks or residual contaminants in the gas bottle which are not condensed out by the liquid nitrogen are pumped readily by the getter pump. In fact, the getter pump can be used commercially to separate out pure neon. Hence, a great degree of confidence is present in the purity of the sample and that all lines seen in the resulting spectrum have their origin in the neon atom. No distortions of the excitation functions because of unwanted contaminants should exist. One other improvement concerning the vacuum system was in the ability to keep the use of the oil diffusion pump to an extreme minimum. Its only purpose is to pump the sample out of the system at the end of the day so that a 15 liter/sec Varian Vac-Ion, model 911-5011, magnetic ion pump can take over. This is necessary since the ion pump will not pump inert gases and its minimum starting pressure is 10^{-4} torr. The reason for restricting the use of an oil diffusion pump is due to backstreaming

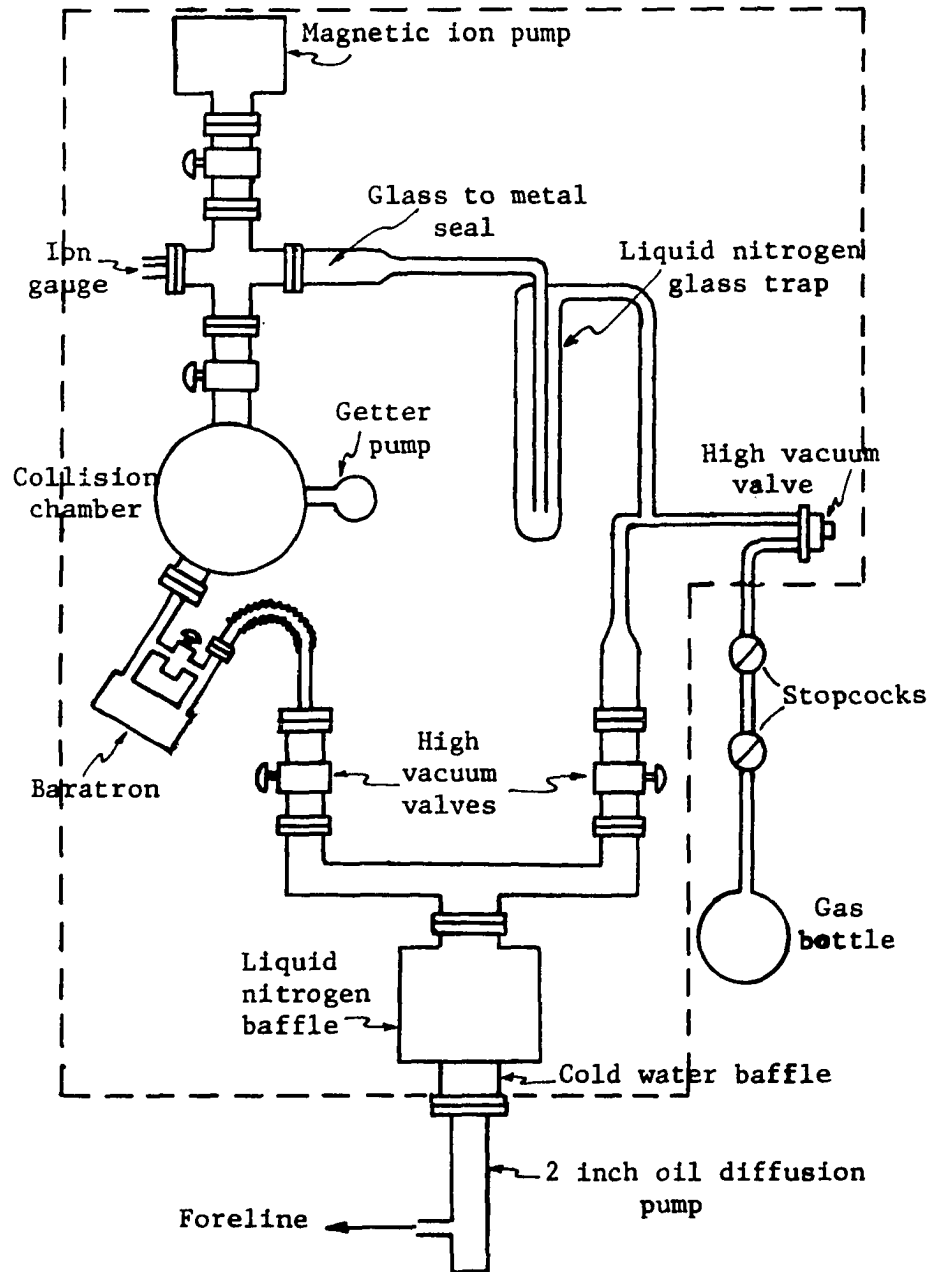


FIGURE 7. Vacuum system

and creeping of oil into the system. Even though these effects are very small they can cause highly detrimental results. Silicon oil DC704 is used as the diffusion pump oil in most pumps since it has high thermal stability, being able to withstand accidental exposure to air while at operating temperatures without decomposition. Octoil diffusion pump fluid is a better oil as far as ultimate pressure and backstreaming is concerned but care must be exercised in that it does not have high thermal stability. Santovac 5 diffusion pump oil is recommended for use in ultra high vacuum systems. Its extremely low backstreaming and creep properties coupled to an unusually high thermal stability made it the best choice for the present system. Christy⁽¹⁹⁾ has found that DC704, when bombarded by electrons, is transformed into a polymer with a high electrical resistivity (greater than 10^{14} ohm-cm). The mechanism of such a process is the free radical polymerization by the incident electrons of the oil molecule absorbed on the bombarded surface. Poole⁽²⁰⁾ has found this phenomena to hold for numerous organic compounds. The backstreaming oil eventually forms a thin film over the grids of the gun and the subsequent electron bombardment turns the grids into insulating sheets which can accumulate charge and create potential barriers to the beam. This phenomenon coupled with space charge effects results in the electrons entering the collision area of the Faraday cage with an energy less than that indicated by the voltage on the cathode. Such a difference in the effective accelerating voltage and cathode voltage is termed contact potential and must be measured by the appearance potential of the thresholds of known spectral lines. To further decrease this effect even for the small time in which the oil diffusion pump is used, a water baffle and liquid nitrogen chevron cold trap were set on top of the pump. According to manufacturers specifications,

this essentially eliminates all backstreaming. The effectiveness of the traps and the cleaner components illustrated itself in a reduction of the contact potential. Before the system was modified a contact potential between 2.0-3.5 eV was common. Presently, it is less than 1.0 eV for neon. Another more subtle feature of this film on the plates is that the insulating properties change with the energy of the impacting electrons. Poole found that at electron energies above 300 eV the film is broken down and is the source of some of the black deposit found on the grids. This would cause a change in the contact potential of the beam and produce distortions in the excitation function.

The pressure of the gas is monitored continuously by an MKS Baratron type 90 capacitance manometer. This has a range of 10^{-5} torr to 1.0 torr at $\frac{1}{2}\%$ accuracy. The sensor head contains an LC bridge network with two capacitors of the bridge formed by a thin diaphragm and a plate on either side. One cell is exposed to the unknown pressure and the other to a reference pressure. When a change in the pressure differential occurs each capacitor is changed and the bridge becomes unbalanced. The resulting voltage across the bridge is nulled by the control unit and the pressure is read on decade switches. The sensor head, type 90H-1, is bakeable to 450° C. Since the elasticity constants of the diaphragm are temperature dependent, it is best to keep the head at a constant temperature. This was done with the MKS type 1090-1 temperature control unit. The temperature can be adjusted from 25° C to 150° C and held within 0.1C°. Very little zero drift was noticed on the Baratron when such temperature precautions were taken. The reference side of the sensor was put directly above the oil diffusion pump with a liquid nitrogen chevron baffle between them. This put the reference

side in the 10^{-8} torr range. Since all the cross sectional data was measured from 10-20 millitorr, the decade readings were essentially absolute. The pressure side of the sensor was connected directly to the chamber.

The advantages of the capacitance manometer over a McLeod gauge are:

- i. The McLeod gauge gives the gaede effect which can amount to 5-10% error depending upon the gas. The capacitance manometer reading is independent of the gas.
- ii. There is no mercury contamination or corrosion of the system with the capacitance manometer as there is with the McLeod.
- iii. A higher degree of accuracy and precision in reading is obtainable. The capacitance manometer is calibrated with deadweights to better than $\frac{1}{2}\%$.
- iv. The Baratron can be placed next to the region in question while the McLeod is usually farther away because of its awkwardness and the necessity of a liquid nitrogen trap.
- v. Continuous monitoring of the pressure is possible with the capacitance manometer plus a much greater ease in taking a measurement.

Utterback and Griffith⁽²¹⁾ have compared extensively the McLeod and the capacitance manometer and found the latter to perform better even in the submillitorr range.

The radiation was viewed at right angles to the electron beam. The detecting portion of the apparatus is a half-meter Jarrell-Ash monochromator coupled to a 6256B EMI photomultiplier tube. This is an

S-13 type tube with a spectral response from 1900 Å to 6600 Å. The grating is 1180 grooves/mm and blazed at 5000 Å. The minimum resolution is 0.32 Å and in many instances in the course of this work such resolution was required. In general, the slits were set for 1.0 Å resolution in order to resolve the sought for lines. The radiation was chopped mechanically before entering the monochromator. This was accomplished by a bladed synchronous motor which was driven by the reference output signal of a Princeton Applied Research, model 122, lock-in-amplifier. The chopped frequency used in this work was 85 Hz. The photomultiplier tube signal was then amplified by the same lock-in-amplifier. This method of driving the chopping mechanism with the same amplifier which is used to detect the signal eliminates any difficulties encountered with phasing of the reference and measured signal.

The D.C. output of the lock-in-amplifier was then fed to the vertical deflecting plates of a Tektronic type 561A oscilloscope. The horizontal sweep was driven by the accelerating voltage of the electron beam whose current was kept constant. The resulting curve is termed an optical excitation function and displayed on an oscillogram.

The optical cross sections were measured at a predetermined fixed energy. The intensity of the line was recorded on a model V.O.M. 7, Bausch and Lomb time base chart recorder. By comparing this intensity with the intensity measured from a tungsten filament lamp whose photon flux for various filament temperatures has been standardized, the optical cross section can be obtained at that particular electron energy. These data in conjunction with the optical excitation function will give the absolute optical cross section at any energy covered by the excitation function.

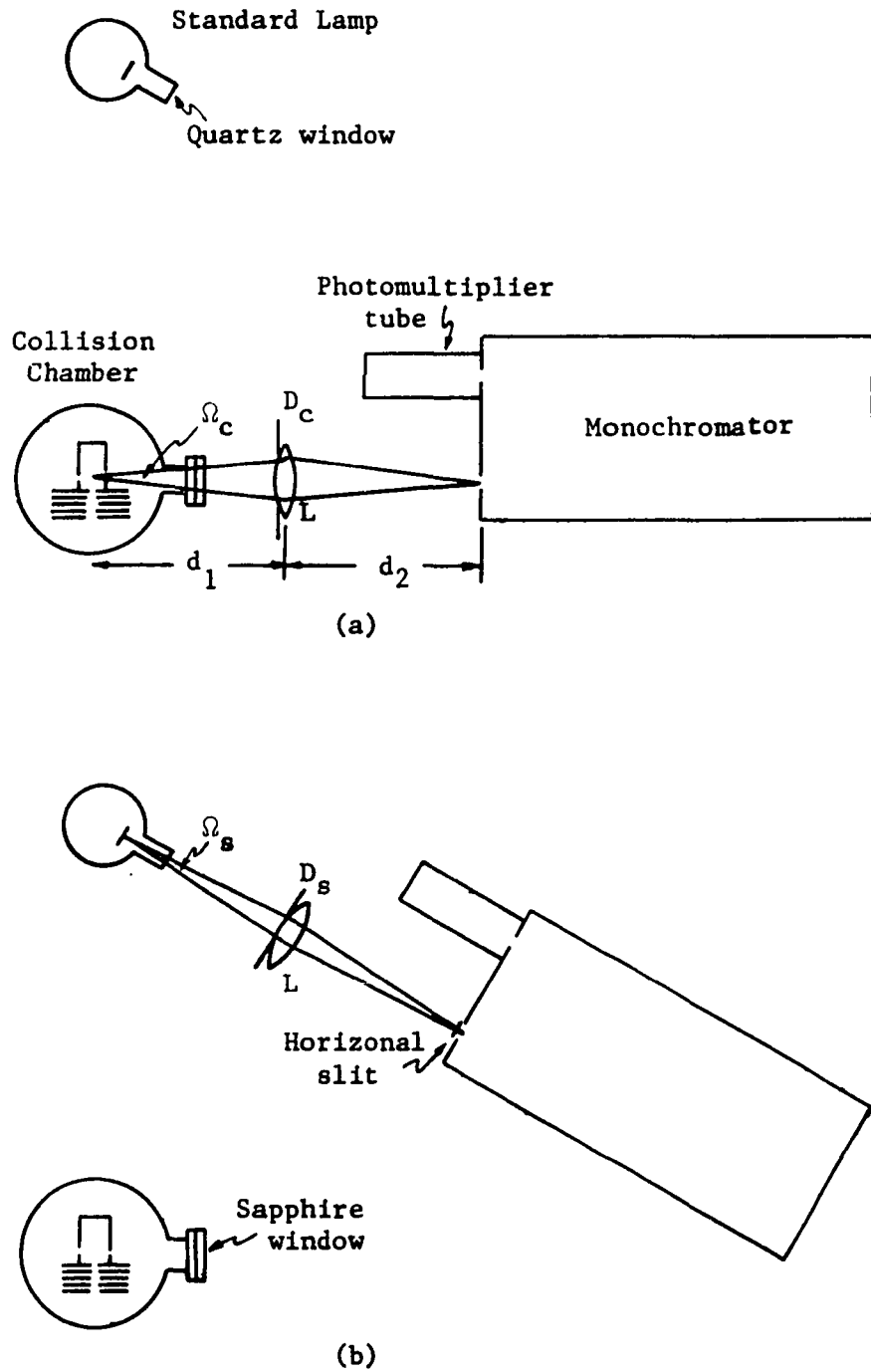


FIGURE 8. Optical arrangement for calibration

Standardization Procedures

The standardization of the detection system involves the determination of the spectral sensitivity, $S(\lambda)$, of the photomultiplier tube. Figure 8(a) is a drawing of the optics when the spectrum line is being monitored. In Fig. 8(a), D_c is the diameter of the aperture stop when the beam is observed and the solid angle Ω from which radiation is gathered is given by $\pi D_c^2/d_1^2$. L is the lens whose focal length permits d_1 to be equal to d_2 and unit magnification at the image position, i.e., at the entrance slit. Hence the slit width w will be the length of the observation region, Δx . The various optical elements which radiation must pass through are the chamber window and the focusing lens with transmission factors γ_w and γ_L respectively. The relative transmission function of the monochromator is given as

$$\gamma_R = \begin{cases} 1 + \frac{\lambda - \lambda_0}{\Delta\lambda} & \text{for } \lambda_0 - \Delta\lambda \leq \lambda \leq \lambda_0 \\ 1 - \frac{\lambda - \lambda_0}{\Delta\lambda} & \text{for } \lambda_0 < \lambda < \lambda_0 + \Delta\lambda \end{cases} \quad (12)$$

where $\Delta\lambda$ is the bandpass of the monochromator and λ_0 is the peak of the transmission function. Figure 9 is a plot of γ_R versus λ . It should

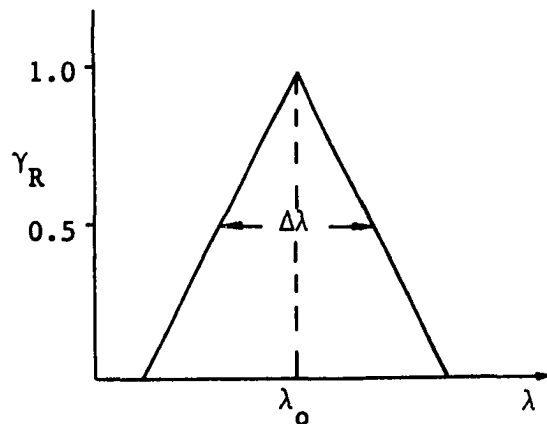


Figure 9. Relative transmission of monochromator vs wavelength

be mentioned that Eq. (12) is valid only if the entrance and exit slit widths are equal. St. John⁽²²⁾ has analyzed this situation as well as the case where the slits are not equal. Identical slit widths were used throughout this experiment.

If the lines in question are observed at the wavelength for maximum intensity, then γ_R is unity and Eq. (11) can be written

$$Q(ij) = \frac{4d_1^2 I_c}{D_c^2 w N(I/e) \gamma_w \gamma_L S(\lambda)} \quad (13)$$

Now $S(\lambda)$ must be determined by a known flux source. A General Electric tungsten ribbon lamp type 30AT24/13, serial number 431-P-724, was used.

In order to eliminate many sources of error in the standardization process, the monochromator and associated lens are mounted on a movable table. The table is then rotated and the optical distances remain the same for both the electron beam and standard lamp measurements as shown in Fig. 8(b).

If I_S is the output of the photomultiplier tube when in the standardization configuration then

$$I_S = S(\lambda) F_S \quad (14)$$

where F_S is the photon flux hitting the detector. F_S can be expressed as

$$F_S = A_S \Omega_S \gamma_w \gamma_L \int_{\lambda_0 - \Delta\lambda}^{\lambda_0 + \Delta\lambda} R_N(\lambda, T) \gamma_R d\lambda \quad (15)$$

where

A_S = the area of tungsten ribbon from which photons are emitted and which enter the monochromator.

Ω_s = the solid angle which light is gathered when in the standard lamp arrangement.

γ_w = the transmission of the standard lamp window.

$R_N(\lambda, T)$ = the photon radiancy and gives the rate of emission of photons per area per unit wavelength interval into a unit solid angle normal to the surface whose temperature is T.

$R_N(\lambda, T)$ can be obtained from blackbody considerations since

$$R_N(\lambda, T) = e(\lambda, T) R_N^B(\lambda, T) \quad (16)$$

where $e(\lambda, T)$ is the emissivity of tungsten and $R_N^B(\lambda, T)$ is the photon radiancy of a black body. St. John⁽²²⁾ has shown from Planck's black-body theory that

$$R_N^B(\lambda, T) = \left(\frac{c_1}{hc\lambda^4} \right) \frac{1}{\exp(c_2/\lambda T) - 1} \quad (17)$$

where $c_1 = 3.7405 \times 10^{-16}$ W-m² and $c_2 = 1.43879 \times 10^{-2}$ m-°K.

For wavelengths below the peak of the black body density curve, Wien's law can be used and Eq. (17) becomes

$$R_N^B(\lambda, T) = \frac{c_1}{hc\lambda^4} \exp\left(-\frac{c_2}{\lambda T}\right) \quad (18)$$

Jobe⁽²³⁾ has calculated the integral

$$R_{16}(\lambda_o, T) = \int_{\lambda_o - 16\text{\AA}}^{\lambda_o + 16\text{\AA}} R_N(\lambda, T) \gamma_R d\lambda \quad (19)$$

for temperatures ranging from 1400° K to 3000° K and for λ_o between 2200 Å and 30,000 Å. In doing so, the emissivity values of de Vos⁽²⁴⁾ were used and, since $e(\lambda, T)$ is a slowly varying function of wavelength it

was assumed constant at $e(\lambda_0, T)$ over the integration interval. Also, only the linear terms in the Taylor expansion of $R_N^B(\lambda, T)$ about λ_0 were integrated over. This introduces negligible error as long as $\Delta\lambda < 200\text{\AA}$. Hence,

$$R_{\Delta\lambda}(\lambda_0, T) = \frac{\Delta\lambda}{16} R_{16}(\lambda_0, T) \quad . \quad (20)$$

Utilizing Eqs. (14) and (15) and Eq. (20) yields

$$S(\lambda) = \frac{16 I_s}{A_s \Omega_s \gamma_w \gamma_L \Delta\lambda R_{16}(\lambda, T)} \quad . \quad (21)$$

If a horizontal slit of width H is placed over the entrance slit of the monochromator, then Hw will equal A_s since L gives unit magnification. If D_s represents the diameter of the aperture stop for standardization, then $\pi D_s^2/d_f^2$ will yield Ω_s .

Equation (13) becomes with the aid of Eq. (21)

$$Q(ij) = \frac{4\pi e H \Delta\lambda R_{16}(\lambda, T) I_c D_s^2 \gamma_w'}{N I 16 I_s D_c^2 \gamma_w} \quad . \quad (22)$$

Under the assumption that the temperature of the gas is 300° K and using the ideal gas law,

$$N = 3.22 \times 10^{13} p \quad (23)$$

where p is measured in mTorr. The chamber window was made of sapphire and the standard lamp window was made of quartz. The transmission of these windows is constant over the wavelength region examined and

$$\frac{\gamma_w'}{\gamma_w} = 1.05 \quad . \quad (24)$$

CHAPTER V

EXPERIMENTAL PARAMETERS

From Eq. (22) we see the various parameters which must be measured.

Electron Beam Current, I

A Keithley, model 160, digital multimeter was used to monitor the beam current with an accuracy of 0.2%. To insure that no appreciable multiple excitations occur in the observation region, the intensity of the lines was checked as a function of I. Linearity was observed in the range of currents at which this work was done. The beam's resolution was checked by use of the resonant feature on 3^3D line in helium⁽²³⁾ and on the resonant features in neon discussed in Chapter IX of this paper. These experiments indicated an energy resolution of at least 0.5 eV at 500 μ A. Another Keithley, model 160, digital multimeter monitored the electron energy.

Gas Pressure, p

This was measured by the previously discussed MKS Baratron to 0.5%. To insure that the gas density does not become so great that a single electron will make multiple collisions in the observation region and that significant atom-atom collisions will not occur with subsequent energy exchange, the intensity was plotted versus the pressure; the experiments were subsequently performed in the linear region. It was found

that NeII signal was linear for pressures up to at least 100 mTorr. This work was done in the 10-20 mTorr range.

Aperature Stops, D_c^2 and D_s^2

Aluminum disks were machined and the aperature openings were measured on a traveling microscope which could be read to 0.5 microns. One must be certain that the aperature which is used is not so large that the radiation overfills the grating of the monochromator. Certainly if this happens, not all the radiation which is collected in Ω is gathered on the cathode of the photomultiplier tube. To make sure the above does not happen a plot is made of the intensity versus D^2 . As long as all the energy is collected by the grating and cathode this plot will be linear. When the curve begins to depart from this linear relationship, the grating is being overfilled. This departure from linearity will occur at different D^2 for different wavelengths. This is due to the fact that the angle which the grating makes with the first mirror in the monochromator will determine the exposed area of the grating in which radiation will fall. In essence, the f-value of the instrument is wavelength dependent. In this experiment, an aperature diameter was used which fell in the middle of the linear portion and thereby insuring that all energy was collected.

Electron Beam and Standard Lamp Intensity, I_c and I_s

As mentioned previously, these intensities are monitored on a time base chart recorder. In determining I_s , the current through the standard lamp must be known and held constant. Its temperature was maintained at 2000° K with a current of 23.90 amperes. Also connected with

these intensity measurements are the various gain values associated with the amplifiers. This is especially important since generally a different gain setting is used for I_C than the larger I_S . Therefore, careful measurement of the gain vs dial settings was a prerequisite to all work. In order to evaluate the accuracy of these values, the cross section of a line was determined using various gain factors to insure identical results. Where possible, the gain factor for I_C and I_S was made the same and compared to those results when they are different. One final note concerning I_S . Since the lines of NeII fall mainly between 3000 Å and 4000 Å and the flux from the standard lamp is quite low in this region, a slight amount of light of other wavelengths scattered in the monochromator will completely overwhelm the desired flux. Hence a band pass filter was required which cut out the more intense wavelengths above 4000 Å from the standard lamp. When the filter was not used it was found that 90 per cent of I_S was made up of scattered radiation. With the filter, the scattered light made an unmeasurable effect on I_S . The filter was left in for both I_C and I_S measurements so that γ_f will cancel out in Eq. (22).

Bandpass, $\Delta\lambda$

This is determined by scanning the spectral line in question and measuring its width at half-height. In this experiment, very small bandpasses were necessary in order to resolve the lines. Hence, great care was necessary to insure the linearity of the monochromator and chart recorder drive. A slight error in the bandpass would correspond to a large per cent error due to the smallness of $\Delta\lambda$ and $\Delta\lambda$ becomes a sensitive parameter in the measurement of this paper's cross sections. The slits

used in this experiment were of excellent quality and gave triangular bandpasses down to minimum separation of the slits.

Ideally, one would like to take every line and follow the above procedures. But practically, and particularly in this experiment, this is not possible and still be able to obtain good precision. Only on the strong lines will you still retain a nice degree of intensity when the stop with diameter D_c is inserted. Also, since most of the lines were done with the slits practically closed (0.32 \AA to 1.00 \AA for $\Delta\lambda$), the intensity suffered even more. In this experiment, the cascade levels were particularly weak and upon closing the slits and stopping down the aperture, the feasibility of a good measurement was poor. Weak lines also make it difficult to obtain an accurate value for $\Delta\lambda$ which we have previously mentioned to be an important parameter in the calculation of $Q(ij)$.

To overcome these difficulties, let us once again consider Eq. (22),

$$Q(ij) = \frac{4\pi e \Delta\lambda I_c (1.05)}{N I_{16} D_c^2} H \left[\frac{R_{16}(\lambda_0, T) D_s^2}{I_s} \right] .$$

The term in brackets contains those quantities associated with the standardization procedure. It is independent of any beam characteristics. If a plot of $[R_{16}(\lambda, T) D_s^2 / I_s]$ versus λ is made, a curve is obtained which is a composite of the filter, standard lamp and photomultiplier tube spectral characteristics. Now I_s will change in value from day to day because of differing thermal conditions but the shape of the curve $[R_{16}(\lambda, T) D_s^2 / I_s]$ will not change and the ratio of any two points on the curve will remain invariant.

Filmed as received

without page(s) 35.

UNIVERSITY MICROFILMS.

CHAPTER VI

APPARENT IONIZATION AND EXCITATION OF THE 3p LEVELS

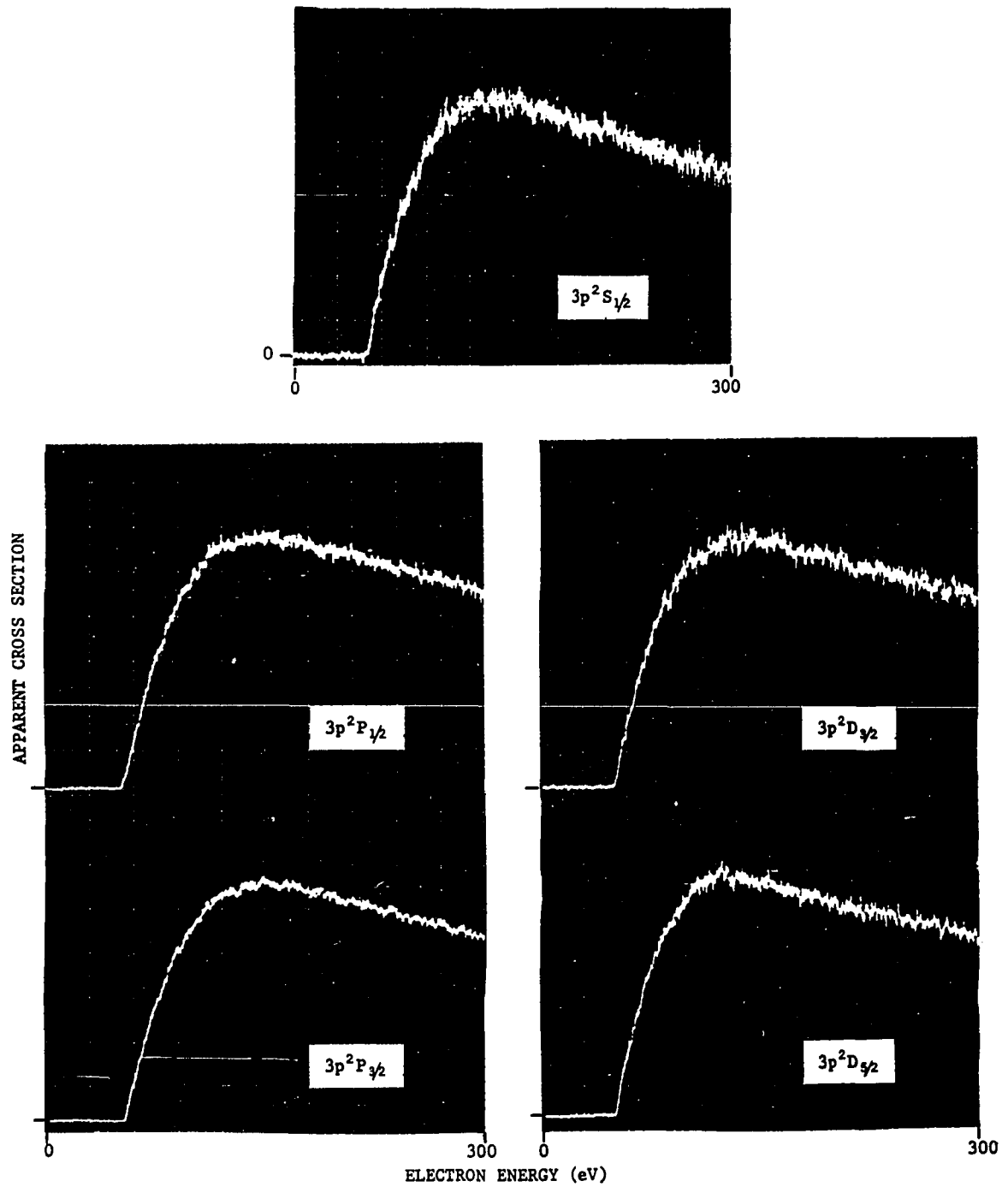
Transitions from the 3p levels of the 3P , 1D and 1S core configurations are the strongest of the entire NeII spectrum. The experimental results are segregated in this paper according to the core configuration. To designate which core is being referred to, the following notation is adopted. The unprimed l values for the running electron are those associated with the 3P core. Those levels coupled to the 1D core are designated with primes. Finally, the levels in conjunction with the 1S core have double primes. Comparison of Figs. 1, 2 and 3 reveals that the 3P core levels are the most plentiful and the 1S core the most anemic.

Excitation Functions

3P Core

Figure 10 gives the excitation functions of the 3P doublet levels from 0-300 eV. The energy scale has been adjusted to compensate for contact potential. Figures 11 and 12 are the excitation functions of the 3P quartet levels for the same energy range.

These excitation functions are very broad. The quartet functions are in general more narrow than the doublets. This is not surprising since in generating a quartet state a spin "flip" is necessary. This comes from the fact the neon ions' ground state is a 2P configuration.

FIGURE 10. Excitation functions of the (3P)3p doublet levels

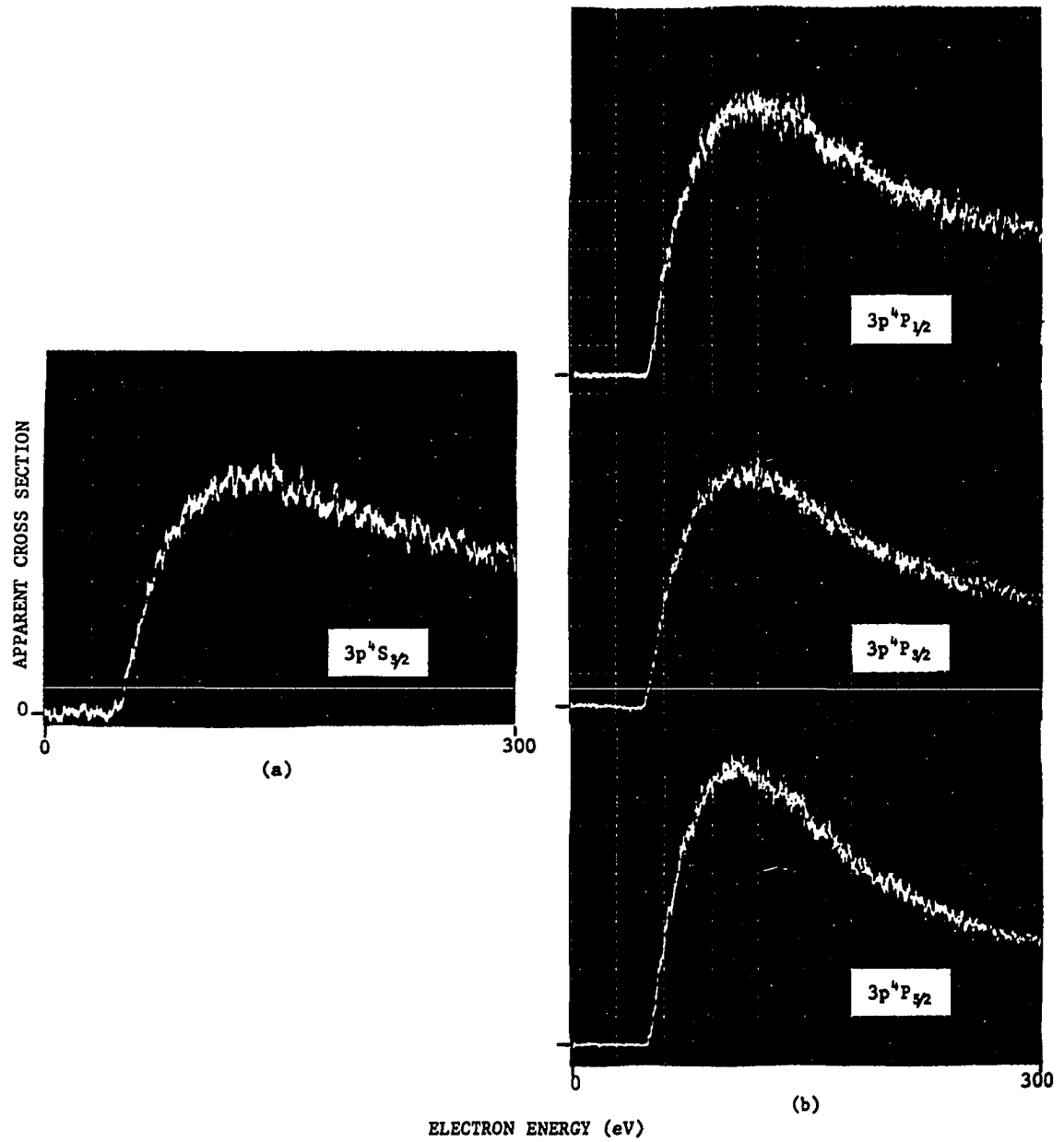
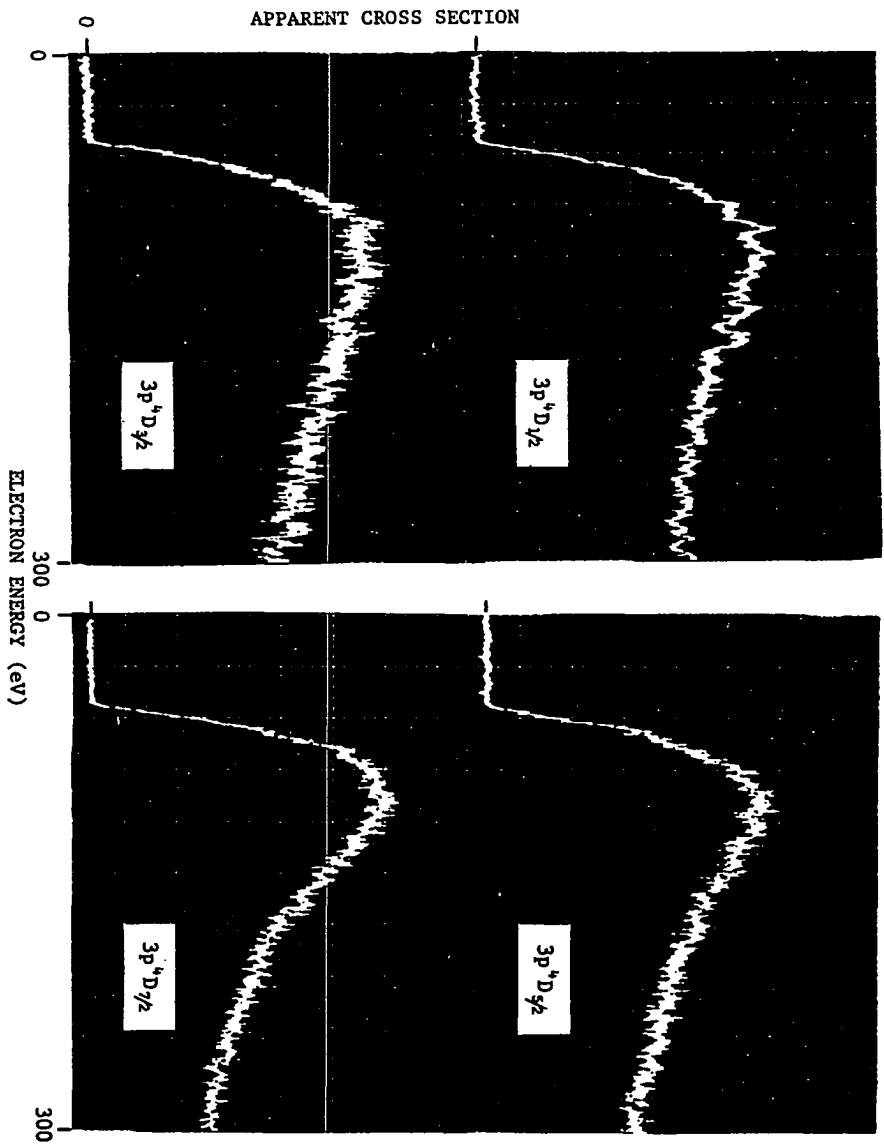


FIGURE 11. Excitation functions of the (a) $3p^4S$ and (b) $3p^4P$ levels

FIGURE 12. Excitation functions of the $3p^4 D$ levels

If one of the 2p electrons is excited without changing its spin orientation, a doublet state results. If the spin of the excited electron is flipped during the impact then a quartet configuration results. This flipping of the spin is a resonant type phenomenon and hence will give a sharper excitation function. This has been observed in numerous investigations of helium, where the situation involves singlets and triplets. The triplet levels are much sharper. This sharpness expresses itself in helium with a fast rise in the excitation function at threshold followed by a rapid decline at higher electron collision energies. This general type of behavior is seen in Figs. 10-12.

Sharpton, *et al.* ⁽²⁵⁾ have examined the singlet and triplet excitation functions of atomic neon, both experimentally and theoretically. They expressed the wave function of a state as a linear combination of the LS-basis functions of those states with the same J value as that state. Their reasoning was that since the total angular momentum is a constant of motion, then J is the only good quantum number for any type of coupling scheme which might be used. Hence, the wave function of the state under examination can be written as an expansion of a complete set of eigenfunctions corresponding to the same J value. The LS-basis functions meet this requirement. Using this method the quantum nature of a state would be a mixture of singlet (or doublet) and triplet (or quartet) components. If then this mixing was strong for a given triplet (or quartet) state, the excitation function of that triplet (or quartet) state would be broader than for a triplet (or quartet) state with little mixing since the triplet (or quartet) in the former case takes on a significant portion of the singlet (or doublet) characteristics.

If one applies this approach to the NeII levels one would expect the form of the wave function to be, e.g., for the $3p^4P_{\frac{1}{2}}$ as

$$\psi(3p^4P_{\frac{1}{2}}) = \alpha\psi^{LS}(3p^2S_{\frac{1}{2}}) + \beta\psi^{LS}(3p^2P_{\frac{1}{2}}) + \gamma\psi^{LS}(3p^4P_{\frac{1}{2}}) + \xi\psi^{LS}(3p^4D_{\frac{1}{2}}), \quad (26)$$

where ψ^{LS} represents the LS-basis wave functions and α , β , γ and ξ are the mixing coefficients. Large values of α and β contribute to large mixing and a broadening of the $3p^4P_{\frac{1}{2}}$ level. For a high J value like 5/2, one would expect less broadening since there is only one doublet level with a value J of 5/2, i.e., $3p^2D_{5/2}$. This agrees with the excitation function of $3p^4P_{5/2}$. A similar argument could be stated for the $3p^4D_{7/2}$ level. In this case, there are no other levels in the 3p family with J = 7/2. Again, it is observed that $3p^4D_{7/2}$ has a more pronounced peaked than the others. Figure 23 displays the excitation function for the $3d^4F_{9/2}$ level. Very little mixing should exist since there are no other 9/2 levels. Accordingly, this level has the most narrow excitation function found in this work.

However, the above three examples are not narrow compared to the excitation functions of other atoms. Consider Latimer and St. John's work on ArII.⁽¹⁶⁾ Figure 13 is a comparison of comparable levels in ArII and NeII.

As mentioned in Chapter II, most investigators believe the 3p levels to follow very closely LS coupling. According to the above discussion and data, it would appear that this is not the case in that an appreciable amount of mixing exists. However, if LS coupling is very poor, we would expect possible strong transitions between the quartet

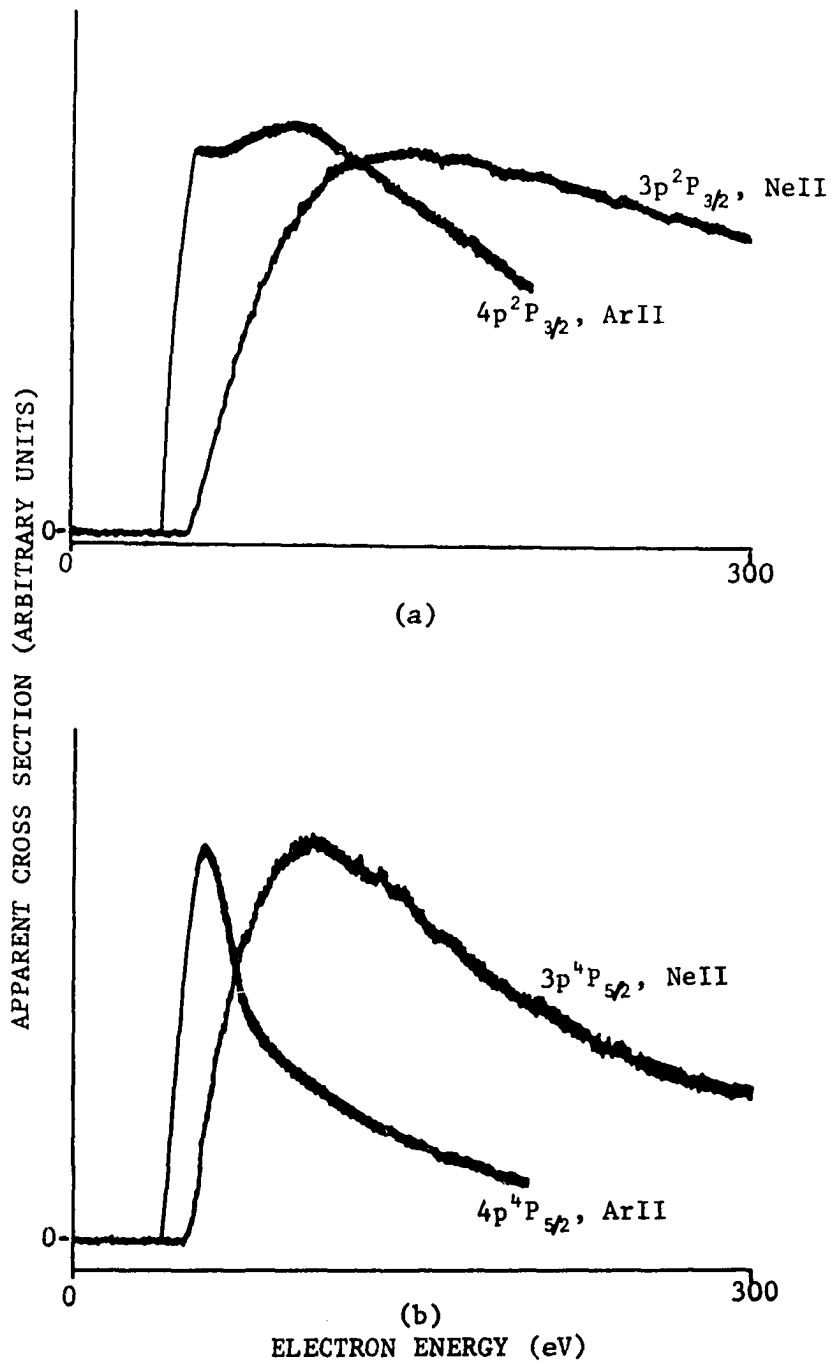


FIGURE 13. Comparison of the excitation functions between NeII and ArII for (a) doublet levels and (b) quartet levels.

and doublet states. Such is not the case. In fact only one transition of this nature was observed in this work, $3p^2D_{5/2} \rightarrow 3s^4P_{3/2}$, and it was very weak ($0.02 \times 10^{-20} \text{cm}^2$).

On the other hand, the article of Hodges *et al.*⁽²⁾ did indicate that some of their results implied that Garstang's⁽¹³⁾ intermediate coupling calculations for the 3p states are not as poor as previously thought and that LS coupling of these states are not as strong as Koopman's⁽¹⁾ experimental results indicated.

In any case, the 3p levels are thought in general to have good LS coupling. In essence then a predicament exists of having broad excitation functions which, according to Sharpton, *et al.*⁽²⁵⁾, should imply heavy mixing and the results of spectra identification and line strength experiments suggesting light mixing.

In an attempt to resolve these contradictory results, the shape of the single-ionization excitation function was examined. The low cross section values for neon and the high cross section values of argon in simultaneous ionization and excitation are in part attributed to their low and high single-ionization cross sections respectively. Perhaps the shapes of the resulting excitation functions may be attributed in part to the shape of the ionization functions. The ionization excitation function for neon as reported by Kieffer and Dunn⁽²⁶⁾ peaks at 160 eV and has the same shape as many of the functions given in this work, especially the $3p^2P_J$ levels. This is the same region of energy in which the doublets peak. In Fig. 13(a) the ArII line of Latimer and St. John's possesses two peaks, one around 54 eV and the other at 90 eV.

This type of structure was observed on several ArII levels. The ionization cross section of ArII (see Kieffer and Dunn⁽²⁶⁾) has been found to possess two peaks - one at 50 eV and the other around 100 eV. Since the shape of the neon ionization excitation function is quite broad (Kieffer and Dunn) it might be expected that if there is a relationship then the excitation functions of the 3p levels could be broadened by this relationship and not be dependent upon a heavy mixing between doublet and quartet states. It is also interesting to note that the thresholds of the ArII excitation functions rise much more rapidly after onset than those for NeII. Von Engel⁽²⁷⁾ reports the slope of the ionization cross section curve for ArI at threshold to have a slope of 71 while that for NeI was only 5.6. Bleakney⁽²⁸⁾ also reports ArI ionization cross section to rise much quicker at onset than NeI.

The sudden perturbation approximation of calculating the cross section for simultaneous ionization and excitation of the state j obtains results of the form

$$Q(j) = K(j)Q_{\text{ionization}}^+ \quad (27)$$

where $K(j)$ is a constant dependent on the state in question^(7,8). The basis for Eq. (27) is the assumption that the impacting electrons are "fast". The high energy tails of these 3p excitation functions have been investigated and presented in Chapter VIII. Also, the level cross sections have been compared to those theoretically calculated by this method⁽⁸⁾ in Chapter VII.

An area needing investigation is the excitation functions of the 3p levels of NeII. This would require a crossed-beam technique

involving an ion beam crossed with an electron beam. The comparison of such data with the present results would be of interest.

¹D Core

Figure 14 is the oscillogram of the excitation functions for the six 3p' levels of this core. The 3p'²P_J levels are particularly broad and appear to be almost flat. The rise from threshold is very slow with energy. Chapter VIII examines the high energy portion of these excitation functions. The ²D_J and ²F_J levels resemble the doublets in the ³P core. The 3p'²P_J levels gave interesting results at high energies in that they fell off as lnE/E. Bethe's⁽²⁹⁾ theoretical calculations of the ionization cross section showed an energy dependence of lnE/E.

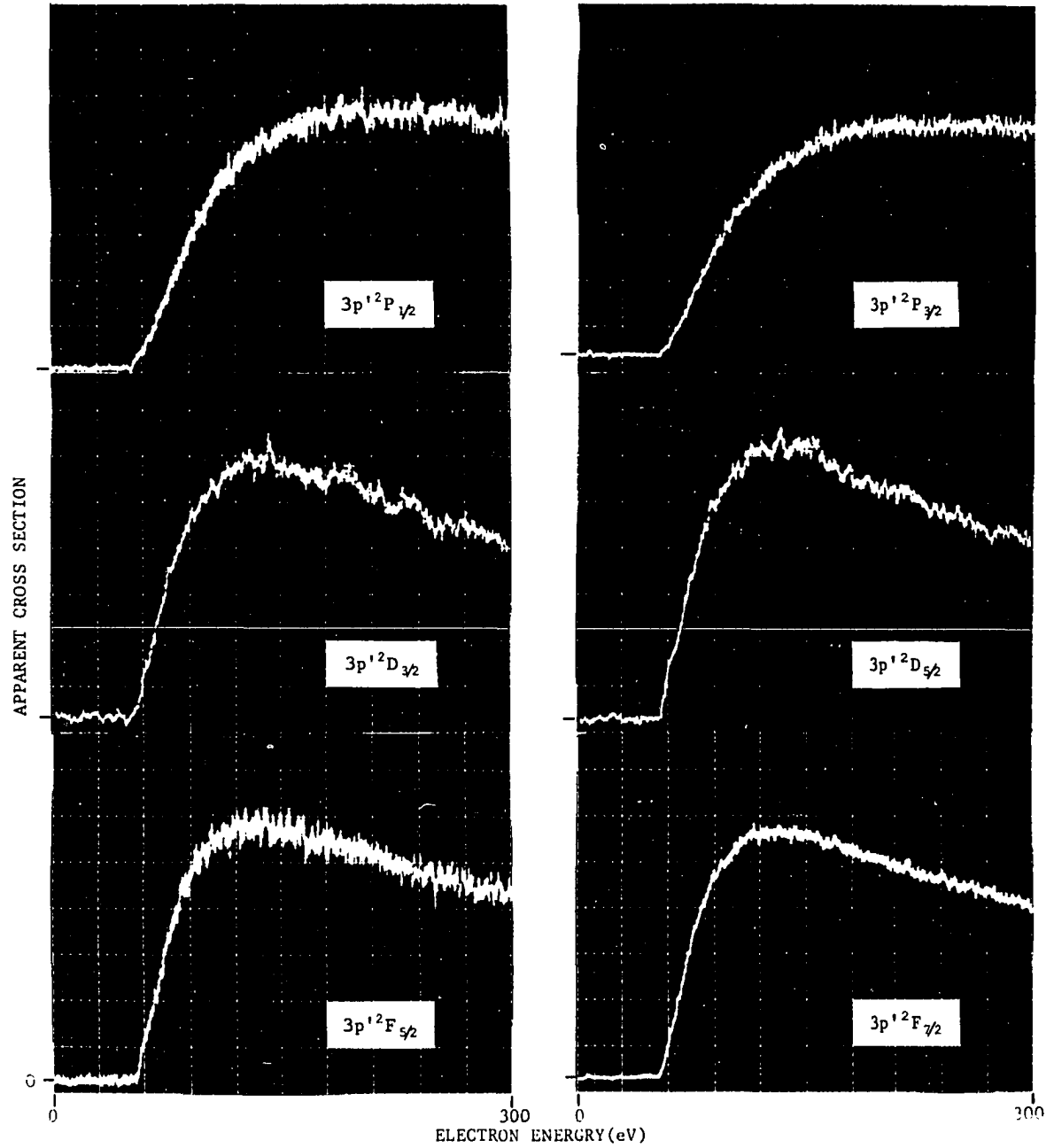
¹S Core

There are only two 3p'' levels in this core. Their excitation functions are presented in Fig. 15. These levels, 3p''²P_½ and 3p''²P_{3/2}, are very similar to the 3p'²P_½ and 3p'²P_{3/2} levels. The 3p'' levels fall off as lnE/E at high energies as well.

Apparent Cross Sections

³P Core

Table I displays the optical cross sections for the various 3s-3p transitions. The sum of those optical transitions from a certain 3p level will be the apparent cross section, Q'. These cross sections are estimated to be accurate to 10-15 per cent. The precision of the measurement depends on the strength of the line and the corresponding signal-to-noise ratio. The values stated in Table I are the averages of six measurements of each optical cross section.

FIGURE 14. Excitation functions of the (1D) $3p'$ levels

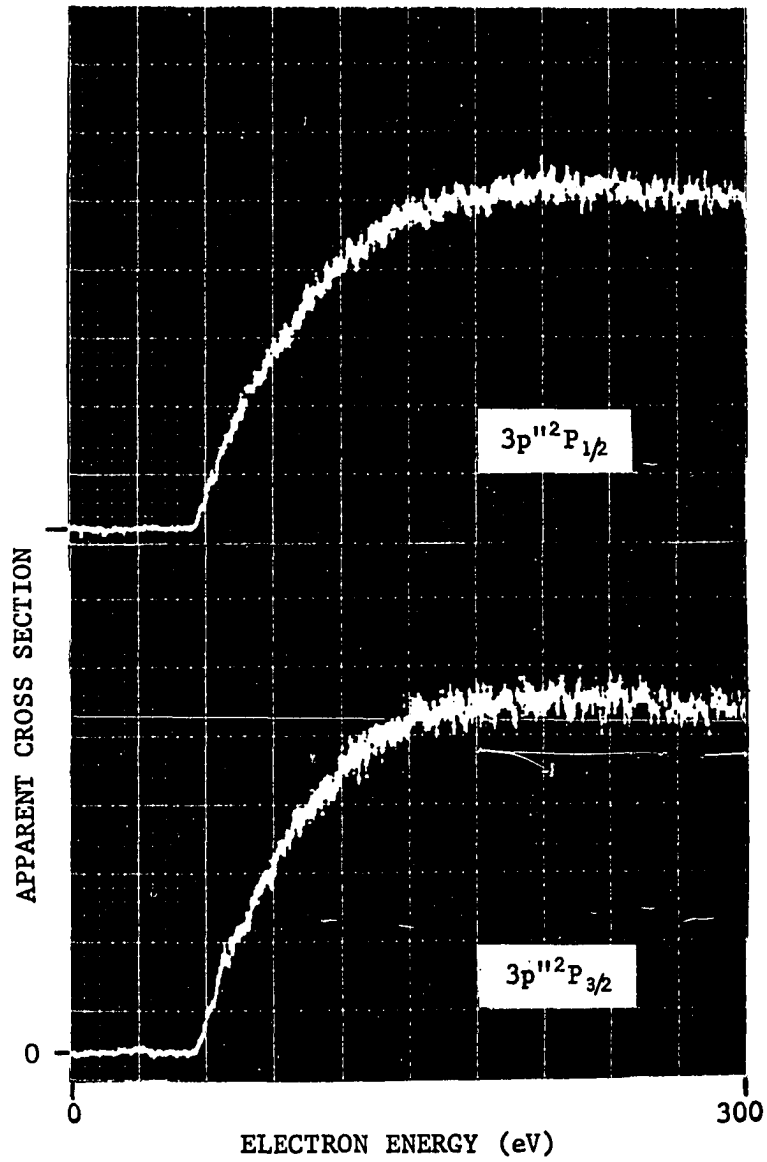


FIGURE 15. Excitation functions of the $(^1S)3p''$ levels.

Table I. Experimental Cross Sections for the (³P)3p Configurations of NeII at 150 eV
(Units of 10⁻²¹cm²).

Upper Level	3p ² S _{1/2}	3p ² P _{1/2}	3p ² P _{3/2}	3p ² D _{3/2}	3p ² D _{5/2}	3p ⁴ S _{3/2}	3p ⁴ P _{1/2}	3p ⁴ P _{3/2}	3p ⁴ P _{5/2}	3p ⁴ D _{1/2}	3p ⁴ D _{3/2}	3p ⁴ D _{5/2}	3p ⁴ D _{7/2}
Lower Level													
3s ² P _{1/2}	1.6	71.1 ^a	39.7 ^a	18.4									
3s ² P _{3/2}	8.3	11.0	130.0 ^a	5.5	27.0								
3s ⁴ P _{1/2}						1.3 ^b	1.3	5.7		6.1	5.2		
3s ⁴ P _{3/2}					0.2	2.2	7.0	2.4	4.9	1.0	6.6 ^a	12.9	
3s ⁴ P _{5/2}						2.8		8.2	15.4		0.4	3.5	15.7
Q'	9.9	82.1	169.7	23.9	27.2	6.3	8.3	16.3	20.3	7.1	12.2	16.4	15.7

^aLaser transitions in NeII laser⁽⁹⁾.

^bThis line could not be resolved and experimental branching ratio were used⁽²⁾.

The transition $3s^4p_{\frac{1}{2}}-3p^4S_{3/2}$ could not be resolved. A branching ratio must be used in such cases. Since

$$Q'(i) = \sum_{i>j} Q(ij) \quad (28)$$

then from Eq. (4)

$$Q'(i) = \sum_{\ell} \frac{A(i\ell)}{A(ik)} Q(ik) \quad (29)$$

where $\frac{A(ik)}{\sum_{\ell} A(i\ell)}$ was defined as the branching factor. Also,

$$Q'(i) = \sum_{\ell} \frac{A(i\ell)}{A(ij)} Q(ij) . \quad (30)$$

Equations (29) and (30) yield

$$\frac{Q(ik)}{Q(ij)} = \frac{A(ik)}{A(ij)} \quad (31)$$

where $\frac{A(ik)}{A(ij)}$ is defined as the branching ratio. From Eq. (31), if the branching ratio between the two lines is known as well as one of the cross sections, the optical cross section of the unknown line can be calculated. In calculating $Q(3p^4S_{3/2}, 3s^4P_{\frac{1}{2}})$, there are several branching ratios to choose from. Garstang⁽¹³⁾ has calculated the line strengths of numerous NeII levels, obtaining values for LS and intermediate coupling. The transition probabilities can then be calculated from these line strengths by the standard formulas.⁽³⁰⁾ Koozekanani and Trusty⁽⁵⁾ have calculated the transition probabilities using an intermediate coupling (IC) scheme as well. Koopman⁽¹⁾ and Hodges⁽²⁾ have measured the line strengths experimentally. Using those results which compare most favorably with this work for the desired branching ratios

will give more consistency with the rest of the data. Also, since no previous experimental work has been done in the area of which this paper is concerned, the branching ratios are the only means of comparison. Table II lists these comparisons. In this table, the notation such as $(^2S_{\frac{1}{2}}, ^2P_{\frac{1}{2}})$ has been used to represent the optical cross section of the $3p^2S_{\frac{1}{2}} \rightarrow 3s^2P_{\frac{1}{2}}$ transition or the transition probability for that transition.

From Table II, the branching ratio most favorable to my results for transitions from the $3p^4S_{3/2}$ level could be either Hodges' or Koopman's since they both agree well with mine. However, if the line strengths for the $3p^4S_{3/2} \rightarrow 3s^4P_{\frac{1}{2}}$ is examined, a considerable difference exists between Hodges and Koopman. Koopman's line strength is almost twice as large giving a cross section much greater than Hodges. The various branching ratios are given in Table III.

It would appear from Tables II and III that Koopman's line strength for the $3p^4S_{3/2} \rightarrow 3s^4P_{\frac{1}{2}}$ transition is too strong since the ratio of the $3p^4S_{3/2} \rightarrow 3s^4P_{3/2}$ line to the $3p^4S_{3/2} \rightarrow 3s^4P_{5/2}$ transition agrees quite well with the other results. Therefore, the cross section for the 3029 Å line is obtained using Hodges' data. The value of $1.3 \times 10^{-21} \text{cm}^2$ obtained compares well with the experimental value obtained (including a weak adjacent line) of $1.4 \times 10^{-21} \text{cm}^2$.

It would be hoped that a comparison of the values in Table II might help decide if LS coupling is good or poor in describing the states. In general, it is seen that one cannot really make a definite statement since the various results are not in great disagreement when one considers the nature of the calculations and experiments. This fact expresses

Table II. Comparison of Branching Ratios for $3p \rightarrow 3s$ Arrays.

	This Work	Other Experiments		Theoretical		
		Hodges ²	Koopman ¹	Garstang LS	IC	Koozekanani IC
$\frac{({}^2S_{\frac{1}{2}}, {}^2P_{\frac{1}{2}})}{({}^2S_{\frac{1}{2}}, {}^2P_{\frac{3}{2}})}$	0.19	0.18	0.19	0.5	1.03	0.06
$\frac{({}^2P_{\frac{1}{2}}, {}^2P_{\frac{1}{2}})}{({}^2P_{\frac{1}{2}}, {}^2P_{\frac{3}{2}})}$	6.46	4.41	5.38	2.0	0.96	-
$\frac{({}^2P_{\frac{3}{2}}, {}^2P_{\frac{1}{2}})}{({}^2P_{\frac{3}{2}}, {}^2P_{\frac{3}{2}})}$	0.31	0.21	0.20	0.22	0.31	0.53
$\frac{({}^2D_{\frac{3}{2}}, {}^2P_{\frac{1}{2}})}{({}^2D_{\frac{3}{2}}, {}^2P_{\frac{3}{2}})}$	3.35	3.29	4.54	5.0	3.17	1.74
$\frac{({}^4S_{\frac{3}{2}}, {}^4P_{\frac{3}{2}})}{({}^4S_{\frac{3}{2}}, {}^4P_{\frac{5}{2}})}$	0.79	0.86	0.76	0.67	0.56	0.75
$\frac{({}^4P_{\frac{1}{2}}, {}^4P_{\frac{1}{2}})}{({}^4P_{\frac{1}{2}}, {}^4P_{\frac{3}{2}})}$	0.19	0.15	0.15	0.20	0.17	0.14
$\frac{({}^4P_{\frac{3}{2}}, {}^4P_{\frac{1}{2}})}{({}^4P_{\frac{3}{2}}, {}^4P_{\frac{3}{2}})}$	2.38	2.07	1.61	3.14	2.42	1.94
$\frac{({}^4P_{\frac{3}{2}}, {}^4P_{\frac{1}{2}})}{({}^4P_{\frac{3}{2}}, {}^4P_{\frac{5}{2}})}$	0.70	0.92	0.52	0.92	1.14	0.53
$\frac{({}^4P_{\frac{3}{2}}, {}^4P_{\frac{3}{2}})}{({}^4P_{\frac{3}{2}}, {}^4P_{\frac{5}{2}})}$	0.29	0.44	0.32	0.29	0.47	0.27

Table II (Cont'd.)

	<u>This Work</u>	Other Experiments		Theoretical		
		<u>Hodges²</u>	<u>Koopman¹</u>	<u>Garstang</u> LS	IC	<u>Koozekanani</u> IC
$\frac{({}^4P_{5/2}, {}^4P_{3/2})}{({}^4P_{5/2}, {}^4P_{5/2})}$	0.32	0.47	0.27	0.43	0.30	0.25
$\frac{({}^4D_{\frac{1}{2}}, {}^4P_{\frac{1}{2}})}{({}^4D_{3/2}, {}^4P_{3/2})}$	6.10	5.15	6.02	5.05	6.09	6.60
$\frac{({}^4D_{3/2}, {}^4P_{\frac{1}{2}})}{({}^4D_{3/2}, {}^4P_{5/2})}$	13.0	17.6	6.64	6.39	15.1	19.4
$\frac{({}^4D_{3/2}, {}^4P_{3/2})}{({}^4D_{3/2}, {}^4P_{5/2})}$	16.5	24.5	8.42	8.14	15.6	20.2
$\frac{({}^4D_{5/2}, {}^4P_{3/2})}{({}^4D_{5/2}, {}^4P_{5/2})}$	3.70	3.33	2.95	2.33	3.4	3.5

Table III. Branching Ratio Involving the $3p^4S_{3/2}$ State.

	<u>Hodges</u>	<u>Koopman</u>	<u>Garstang</u>		<u>Koozekanani</u>
			<u>LS</u>	<u>IC</u>	<u>IC</u>
$\frac{({}^4S_{3/2}, {}^4P_{1/2})}{({}^4S_{3/2}, {}^4P_{3/2})}$	0.57	1.01	0.5	0.43	0.56
$\frac{({}^4S_{3/2}, {}^4P_{1/2})}{({}^4S_{3/2}, {}^4P_{5/2})}$	0.49	0.77	0.34	0.25	0.42

itself in that in some cases better agreement is obtained with LS coupling while in other instances, IC is better. One can look for large discrepancies in such data. These would be much more significant. Only four ratios show major discrepancies between experiment and theory. They are:

$$\frac{({}^2S_{\frac{1}{2}}, {}^2P_{\frac{1}{2}})}{({}^2S_{\frac{1}{2}}, {}^2P_{\frac{3}{2}})},$$

$$\frac{({}^2P_{\frac{1}{2}}, {}^2P_{\frac{1}{2}})}{({}^2P_{\frac{1}{2}}, {}^2P_{\frac{3}{2}})},$$

$$\frac{({}^4D_{\frac{3}{2}}, {}^4P_{\frac{1}{2}})}{({}^4D_{\frac{3}{2}}, {}^4P_{\frac{5}{2}})},$$

$$\frac{({}^4D_{\frac{3}{2}}, {}^4P_{\frac{3}{2}})}{({}^4D_{\frac{3}{2}}, {}^4P_{\frac{5}{2}})}.$$

The first two definitely disagree with the IC calculations but the agreement with LS values is not much better. The last two ratios are somewhat more interesting in that there is even a large discrepancy between experimental values. Obviously the line strength which is causing the trouble in the LS calculation is $({}^4D_{\frac{3}{2}}, {}^4P_{\frac{5}{2}})$. Here the IC is much better and agrees quite well with my results. Hodges' results are a little higher. It is curious that Koopman's value agrees very well with the LS value but differs by more than a factor of two from Hodges and mine. This results from a too high of a line strength for the $({}^4D_{\frac{3}{2}}, {}^4P_{\frac{5}{2}})$ transition. Perhaps from these several line

Table IV. Experimental Cross Sections for the (¹D)3p' Levels at 150 eV (Units of 10⁻²¹cm²).

Upper Level	3p' ² P _{1/2}	3p' ² P _{3/2}	3p' ² D _{3/2}	3p' ² D _{5/2}	3p' ² F _{5/2}	3p' ² F _{7/2}
Lower Level						
3s' ² D _{3/2}	47.6 ^b	16.8	14.9	17.0	26.0	
3s' ² D _{5/2}		76.4 ^b	1.7 ^a	1.6	1.9 ^a	35.7
Q'	47.6	93.2	16.6	18.6	27.9	35.7

^aLine was too weak to detect under necessary experimental conditions and experimental branching ratios were used⁽¹⁾.

^bObserved laser transition⁽⁹⁾.

Table V. Comparison of Branching Ratios for $3p' \rightarrow 3s'$ Transitions.

	This Work	Hodges	Koopman	Garstang	
				LS	IC
$\frac{(^2P_{3/2}, ^2D_{3/2})}{(^2P_{3/2}, ^2D_{5/2})}$	0.22	0.17	0.11	0.11	0.11
$\frac{(^2D_{5/2}, ^2D_{3/2})}{(^2D_{5/2}, ^2D_{5/2})}$	0.094	-	0.071	0.071	0.078
$\frac{(^2D_{3/2}, ^2D_{3/2})}{(^2D_{3/2}, ^2D_{5/2})}$	-	-	8.96	8.96	7.4
$\frac{(^2F_{5/2}, ^2D_{3/2})}{(^2F_{5/2}, ^2D_{5/2})}$	-	10.0	14.0	14.0	13.0

strengths Koopman felt that the $3p$ levels were better described in the LS coupling scheme rather than the IC.

1D Core

The optical and apparent cross sections for lines originating from the $3p'$ levels are presented in Table IV. The levels of a given doublet are quite close and barely resolvable. However, since the slits are nearly closed, the weaker lines of the doublets are not detectable and only the stronger lines present themselves for measurement. Branching ratios are used in an analogous manner as for the 3P core. Table V gives the various branching ratios.

Hodges did not give a complete listing of these line strengths and upon examination of those which he did give it is found there is not much difference in the line strengths of the experimental and theoretical origin. Koopman's values are used in determining those cross sections in Table IV which were unmeasurable. Garstang's LS and IC line strengths are almost identical and they seem to be quite insensitive to which method is used to generate them.

1S Core

Table VI contains the apparent cross sections of the $3p''$ levels of the 1S core. Since only a single $3s''$ level exists, the apparent and optical cross sections are identical.

Table VI. Experimental Cross Sections for the $(^1S)3p''$ Levels at 150 eV (units of 10^{-21}cm^2)

	$3p''^2P_{\frac{1}{2}}$	$3p''^2P_{\frac{3}{2}}$
Q'	7.4	13.7

Polarization

In the derivation of Eq. (22) it was assumed that the flux from the collision chamber was isotropic. This allows one to write

$$F(ij) = \frac{4\pi}{\Omega} F(ij, \Omega) . \quad (9)$$

However, the dipole radiation emitted by an atom after an electron impact is polarized. Figure 16(a) is a rectangular reference frame in which the Oz axis is parallel to the incident electron beam and θ is the angle the detector makes with the electron beam in the $y-z$ plane. Then the emitted dipole radiation can be thought as being due to an electric dipole in the Oz direction and two identical dipoles in the Ox and Oy directions as illustrated in Fig. 16(b).

Then

	x-dipole	y-dipole	z-dipole
Amplitude of E-vector of dipole	E_x	E_y	E_z
Intensity at Maximum	$I_x \propto E_x^2$	$I_y \propto E_y^2$	$I_z \propto E_z^2$
Classification of E-vector	\perp to Oz	\perp to Oz	\parallel to Oz
Polarization of Light relative to O_z (electron beam)	\perp	\perp	\parallel
Component of Amplitude \perp to direction of observation	E_x	$E_y \cos \theta$	$E_z \sin \theta$
Intensity of Radiation in direction of observer	$\propto E_x^2$ $= I_x$	$\propto E_y^2 \cos^2 \theta$ $= I_y \cos^2 \theta$	$\propto E_z^2 \sin^2 \theta$ $= I_z \sin^2 \theta$

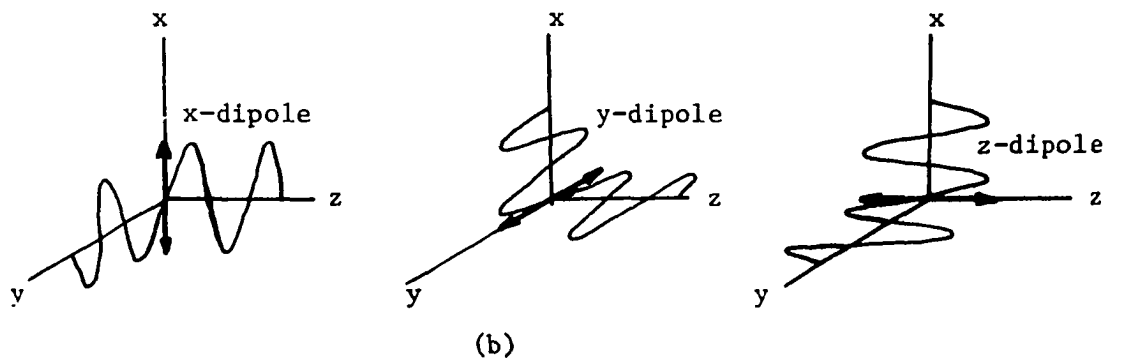
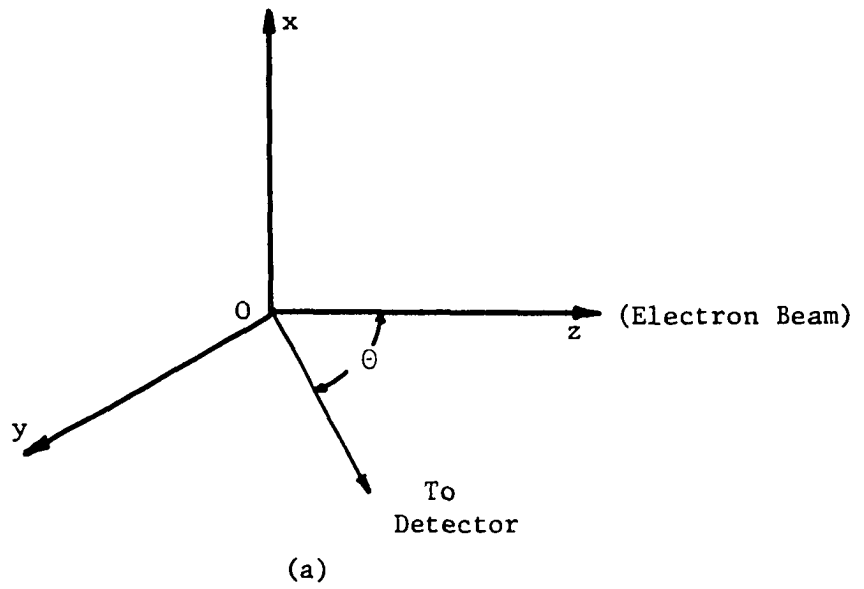


FIGURE 16: (a) Rectangular reference frame for orientation of detector relative to electron beam.
 (b) Dipole radiation for x, y and z-dipoles.

Therefore,

$$I(\theta) = I_x + I_y \cos^2\theta + I_z \sin^2\theta . \quad (32)$$

If I_x and I_y are labeled I_{\perp} and I_z as $I_{||}$, then Eq. (32) can be written

$$I(\theta) = I_{\perp}(1+\cos^2\theta) + I_{||}\sin^2\theta. \quad (33)$$

$I_{||}$ and I_{\perp} can be related to each other through the percentage polarization, P , where

$$P = 100 \left(\frac{I_{||} - I_{\perp}}{I_{||} + I_{\perp}} \right) . \quad (34)$$

The average intensity over a sphere surrounding the source of radiation is

$$\bar{I} = \frac{\int I(\theta) d\Omega}{\int d\Omega} \quad (35)$$

where

$$d\Omega = 2\pi \sin\theta d\theta . \quad (36)$$

Using Eqs. (36) and (35),

$$\bar{I} = \frac{1}{4\pi} \left[\int_0^{\pi} I_{\perp}(1+\cos^2\theta) 2\pi \sin\theta d\theta + \int_0^{\pi} 2\pi I_{||} \sin^3\theta d\theta \right] . \quad (37)$$

Integration yields

$$\bar{I} = 2/3(2I_{\perp} + I_{||}) . \quad (38)$$

$I(\theta)$ can now be written in terms of \bar{I} and P . Equations (38) and (34) give

$$I_{\perp} = \bar{I} \left[\frac{3}{2} \left(\frac{100-P}{300-P} \right) \right] , \quad (39)$$

and

$$I_{||} = \bar{I} \left[\frac{3}{2} \left(\frac{100+P}{300-P} \right) \right] . \quad (40)$$

These last two equations along with Eq. (33) yields

$$I(\theta) = \frac{3\bar{I}(100-P\cos^2\theta)}{300-P} \quad (41)$$

If the radiation is monitored at right angles to the beam, as in this experiment, then

$$I(90^\circ) = \frac{\bar{I}}{(1-P/300)} \quad (42)$$

Therefore,

$$Q = Q_{\perp}(1-P/300) \quad (43)$$

where Q is the total photon - excitation cross section and bears the same relationship to \bar{I} as Q_{\perp} , the excitation cross section obtained at right angles to the beam, does to $I(90^\circ)$. P in Eq. (43) is expressed in percentage and produces significant correction factors only if P is over 15 or 20 per cent.

Something which must be considered in the measurement of P is the degree of polarization due to the dispersing portion of the detecting system. Usually the dispersing element is a grating and the electric vectors which are parallel to the rulings have a different effective reflectance than those which are perpendicular. The instrumental polarization can be quite large and if the atomic transition is polarized, a distortion of the excitation cross section will occur. The affect of instrumental polarization on P can be shown in the following manner.

$$I_{\perp}(\text{observed}) = \alpha_{\perp} I_{\perp}(\text{true}) \quad (44)$$

$$I_{\parallel}(\text{observed}) = \alpha_{\parallel} I_{\parallel}(\text{true}) \quad (45)$$

where the α 's are the reflection coefficients of the monochromator for the respective electric vectors. Equation (34) can now be written as

$$P = 100 \left| \frac{\frac{I_{||}(\text{obs.})}{\alpha_{||}} - \frac{I_{\perp}(\text{obs.})}{\alpha_{\perp}}}{\frac{I_{||}(\text{obs.})}{\alpha_{||}} + \frac{I_{\perp}(\text{obs.})}{\alpha_{\perp}}} \right| \quad (46)$$

or as

$$P = 100 \left| \frac{\frac{\alpha_{\perp}}{\alpha_{||}} - \frac{I_{\perp}(\text{obs.})}{I_{||}(\text{obs.})}}{\frac{\alpha_{\perp}}{\alpha_{||}} + \frac{I_{\perp}(\text{obs.})}{I_{||}(\text{obs.})}} \right| \quad (47)$$

Defining

$$k = \frac{\alpha_{\perp}}{\alpha_{||}} \quad , \quad (48)$$

Eq. (47) becomes

$$P = 100 \left| \frac{k - \frac{I_{\perp}(\text{obs.})}{I_{||}(\text{obs.})}}{k + \frac{I_{\perp}(\text{obs.})}{I_{||}(\text{obs.})}} \right| \quad (49)$$

where k is a function of wavelength setting for the grating. It was determined by utilizing the standard lamp as a source of unpolarized light. The light is polarized parallel, then perpendicular, by rotating a polaroid film through 90° . Since the light is unpolarized initially, I_{\perp} and $I_{||}$ are identical upon entering the monochromator. Hence, dividing Eq. (44) by Eq. (45) gives k . Figure 17 is a plot of the instrumental polarization in terms of k as a function of wavelength.

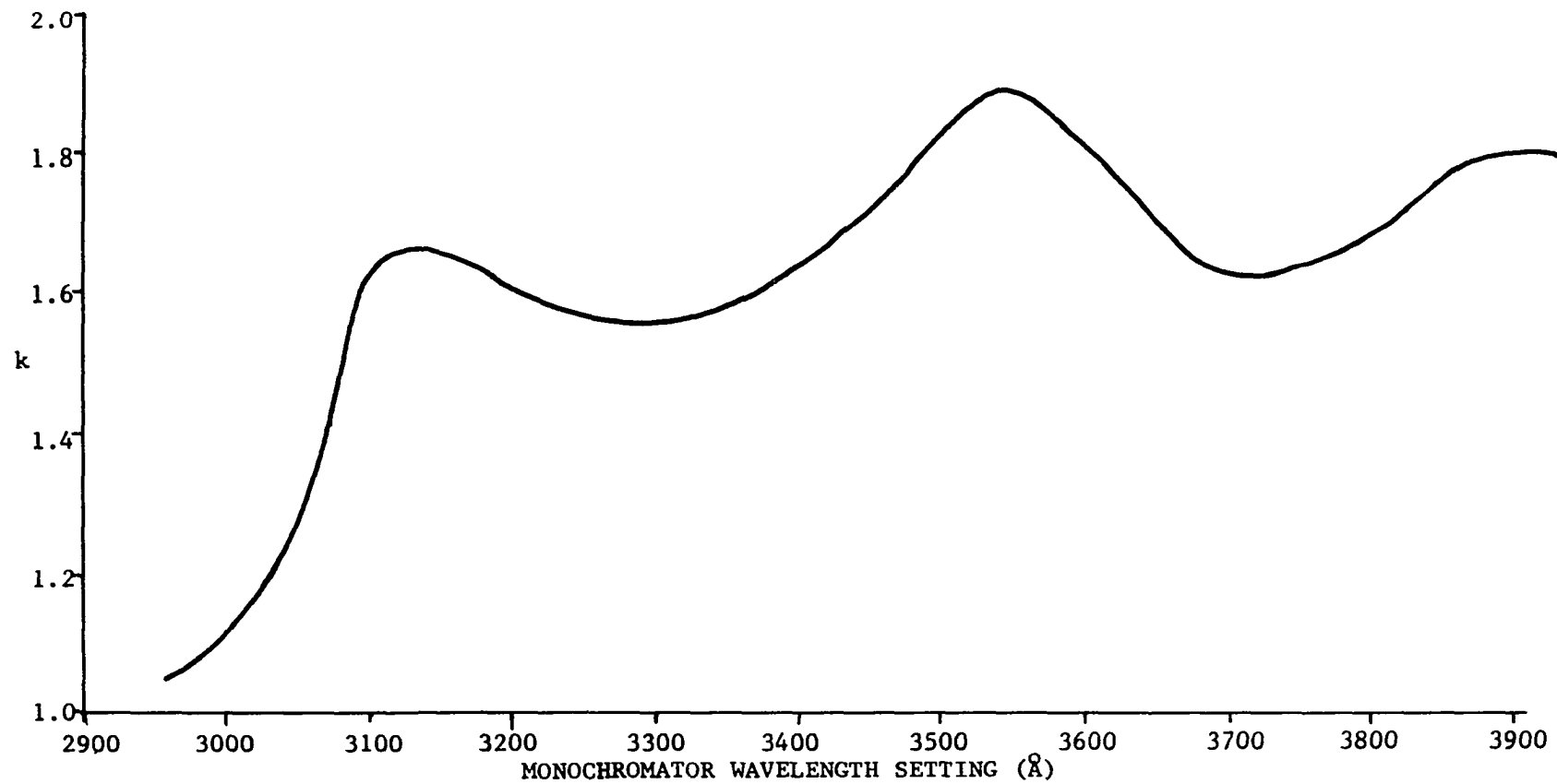


FIGURE 17. Instrumental polarization for Jarrell-Ash $\frac{1}{2}$ -meter monochromator with 1180 groves/mm grating.

There are several theoretical treatments of the polarization of radiation by electron impact. It was first treated by Oppenheimer⁽³¹⁻²⁾ and a few years later it was further developed and applied by Penney⁽³³⁾. The most recent and advanced presentation is by Percival and Seaton⁽³⁴⁾. It is predicted that the $4^1D \rightarrow 2^1P$ line in helium will have a polarization of 60 per cent at threshold. To check our procedure and methods we have examined this transition. Figure 18 compares our results with those of other experimentors. Our results compare exactly with Clout and Heddle⁽³⁵⁾ out to 100 eV. From 100 eV, our results tend to hold up and give a smaller slope. This is satisfactory since the NeII levels should have little polarization and what little they might have is near the threshold region. At higher energies, the cascade becomes more significant with a resulting depolarization of the radiation.

In taking polarization data, one must be sure that the gas pressure is not too large as a depolarization of the level occurs because of atom-atom collision. With the exception of three transitions, the polarization was zero for the 3p levels. Figure 19 is a plot of the polarization as a function of the incident electron energy for these three levels. The error bars are a rough estimate of the precision of this experiment. Since so little polarization is present and the intensity of the line is dropped significantly when only I_{\perp} or I_{\parallel} is monitored, the precision of the experiment suffers. The levels given in Fig. 19 have 5-10 per cent polarization and will not affect to any great extent the excitation functions or the cross section values listed in Tables I, IV and VI.

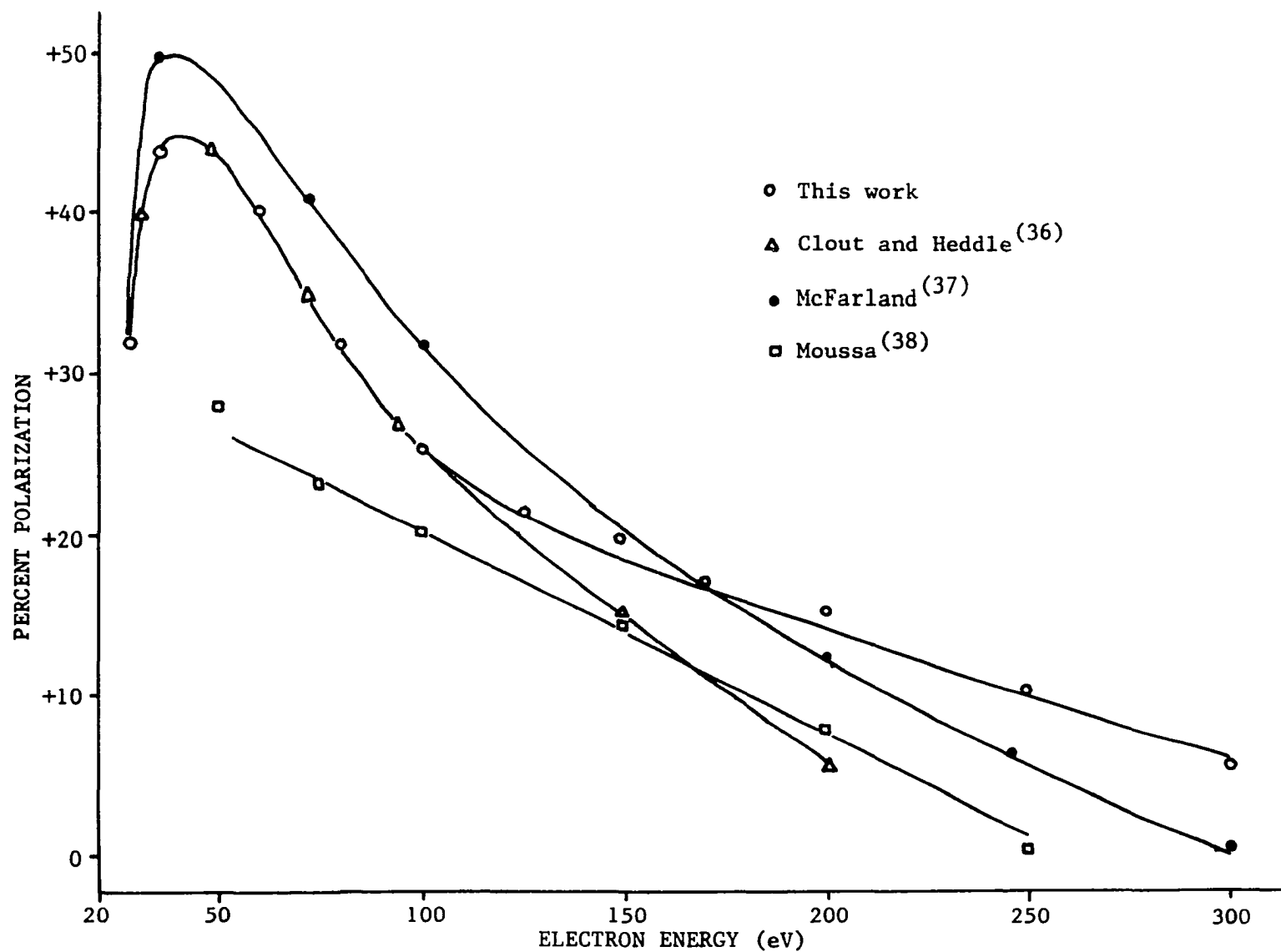


FIGURE 18. Polarization of the helium 4^1D level.

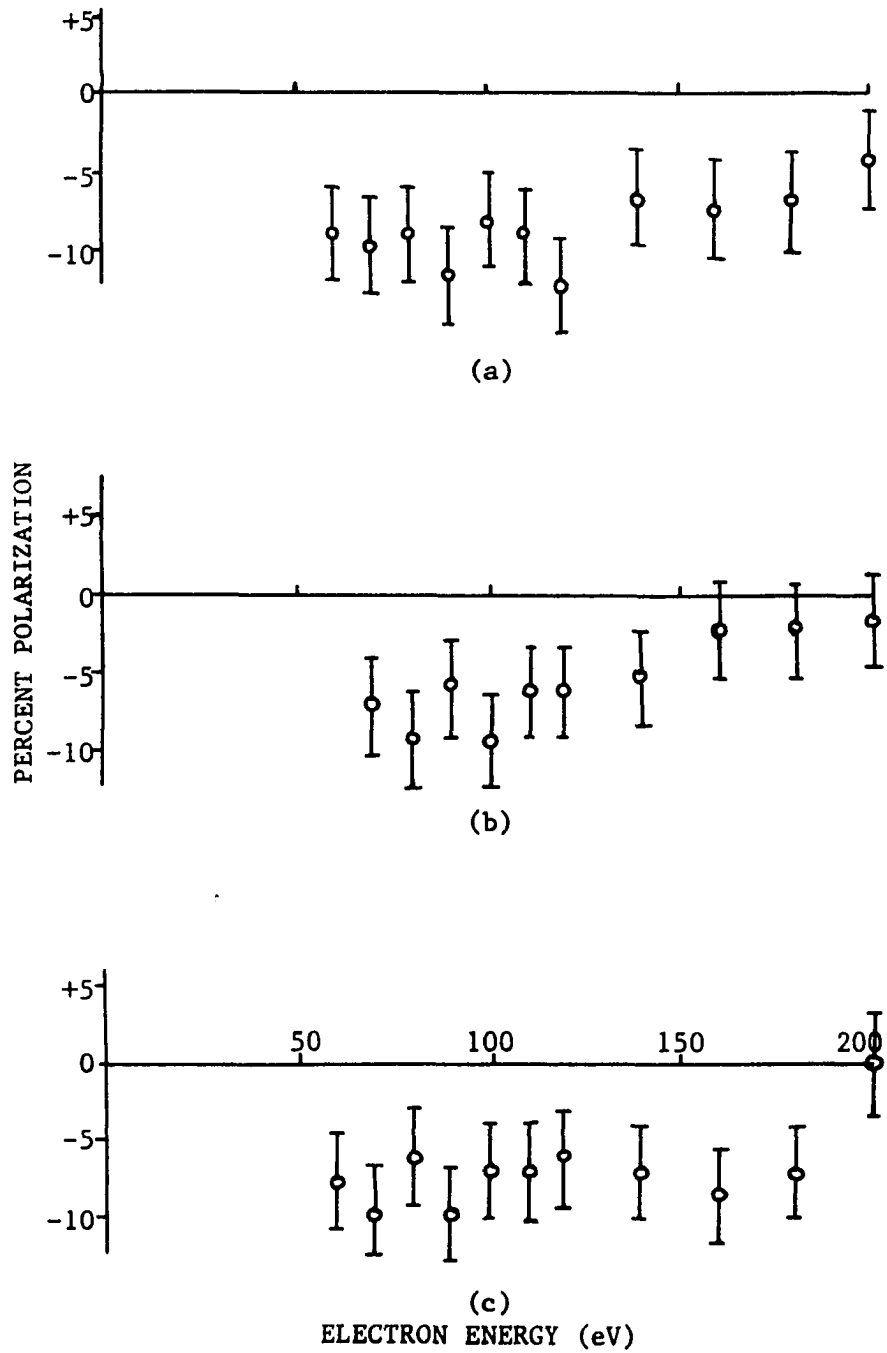


FIGURE 19. Polarization of the NeII transitions
 (a) $3p^2D_{3/2} \rightarrow 3s^2P_{1/2}$, (b) $3p^2D_{5/2} \rightarrow 3s^2P_{3/2}$
 and (c) $3p^4D_{7/2} \rightarrow 3s^4P_{5/2}$.

CHAPTER VII

CASCADE ANALYSIS

Until recently, the only transitions which were found that terminated on the 3p levels were those from the 3d and 4s levels. In a paper published in 1969, Persson⁽¹¹⁾ has identified some 4d and 5s levels which cascade into the 3p levels. These lines are very weak, however, and could not be detected by the present detection system. Hence, little error is introduced by considering only those cascade lines from the 3d and 4s levels. The cascade optical cross sections were in general, one to two orders of magnitude smaller than the 3p levels. The total cascade contribution to a given 3p level amounted to as much as 75 per cent for one extreme and as little as 3 per cent at the other extreme. The degree of confidence in the published spectral classifications diminishes for the 3d and 4s levels. This research raises some questions on several of the classifications. This will be taken up in Chapter IX.

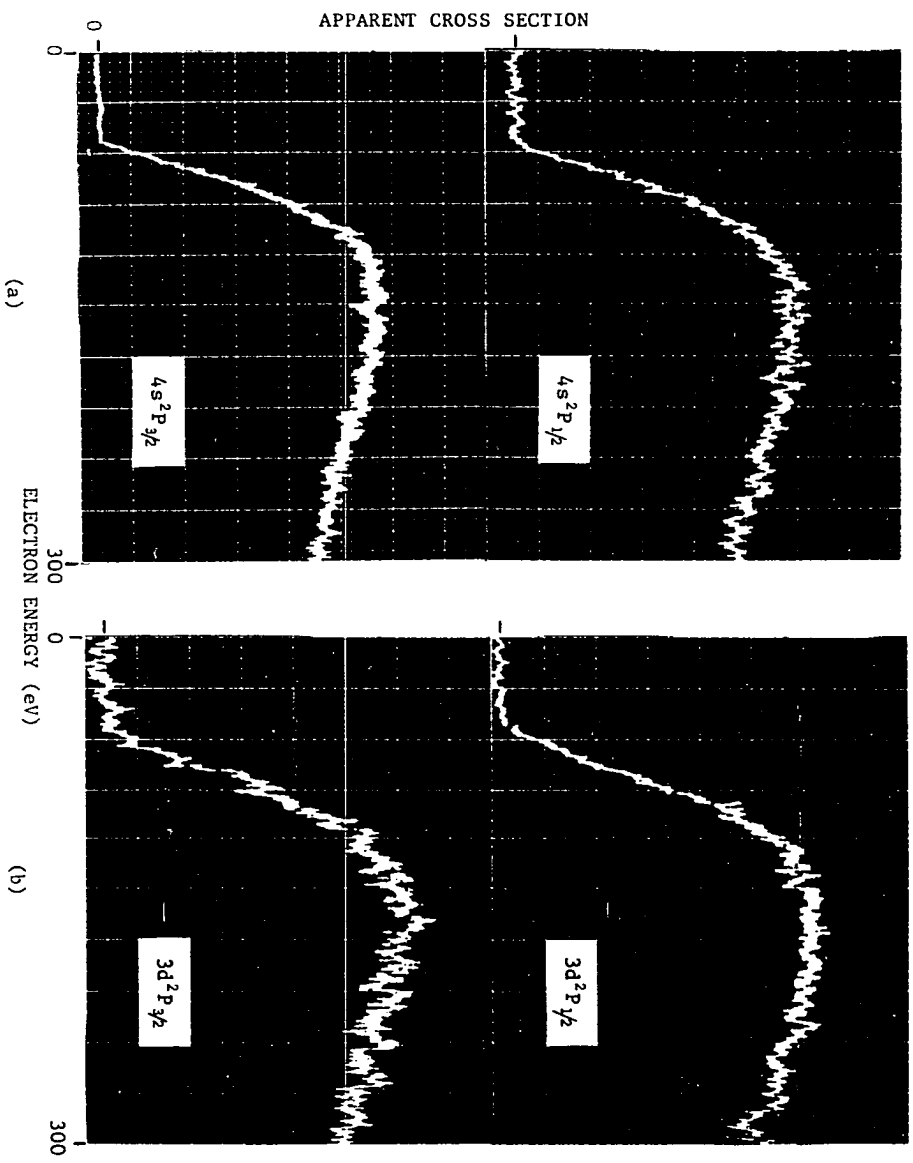
3p Core

The cascade lines from a given doublet or quartet were in general very weak and close together. These conditions made it a prerequisite that great care be taken in their measurement. Many of the cascade cross sections were at the limit of detectability of the present system

(10^{-22}cm^2) and the per cent deviation for these extremely weak lines can be as high as 50 per cent from the average. Electron beam currents were still kept at 500 μA and pressures ranged between 15 and 19 mTorr. Figures 20 and 21 are the excitation functions of the doublet 3d and 4s cascade states. As was the case for the doublet 3p levels, the excitation functions are very broad. It is still evident that as J increases, the peak of the function narrows. This is especially evident for the $3d^2F_{7/2}$ level.

Figures 22 and 23 are the excitation functions for the quartet 3d and 4s levels. There are four levels which are not presented: $3d^4P_{\frac{1}{2}}$, $3d^4D_{\frac{1}{2}}$, $3d^4F_{5/2}$ and $4s^4P_{\frac{1}{2}}$. The lines from these states were exceptionally weak and excitation functions were not obtainable. Those levels marked with an asterisk (*) are levels where some questions are present as to their classification and will be discussed in Chapter IX.⁴ As in all previous excitation function presentations, the larger J values have a more sharply peaked excitation function. This is especially pronounced in the $4s^4P$, $3d^4D$ and $3d^4F$ families.

The excitation functions of the cascade levels, therefore, seem to suggest mixing of the states is occurring in accordance with the scheme put forth by Sharpton *et al.*⁽²⁵⁾ Also, a little more evidence supports mixing in the cascade levels than existed for the 3p levels. We find relatively strong transitions between the quartet and doublet levels. The experiments of Koopman⁽¹⁾ and Hodges⁽²⁾ agree well with Garstang's⁽¹³⁾ IC calculations. Persson^(10,14), as was mentioned previously, labeled the 3d states as following an intermediate coupling between LS and $J_c l$.

FIGURE 20. Excitation functions of the (a) $4s^2P$ and (b) $3d^2P$ levels

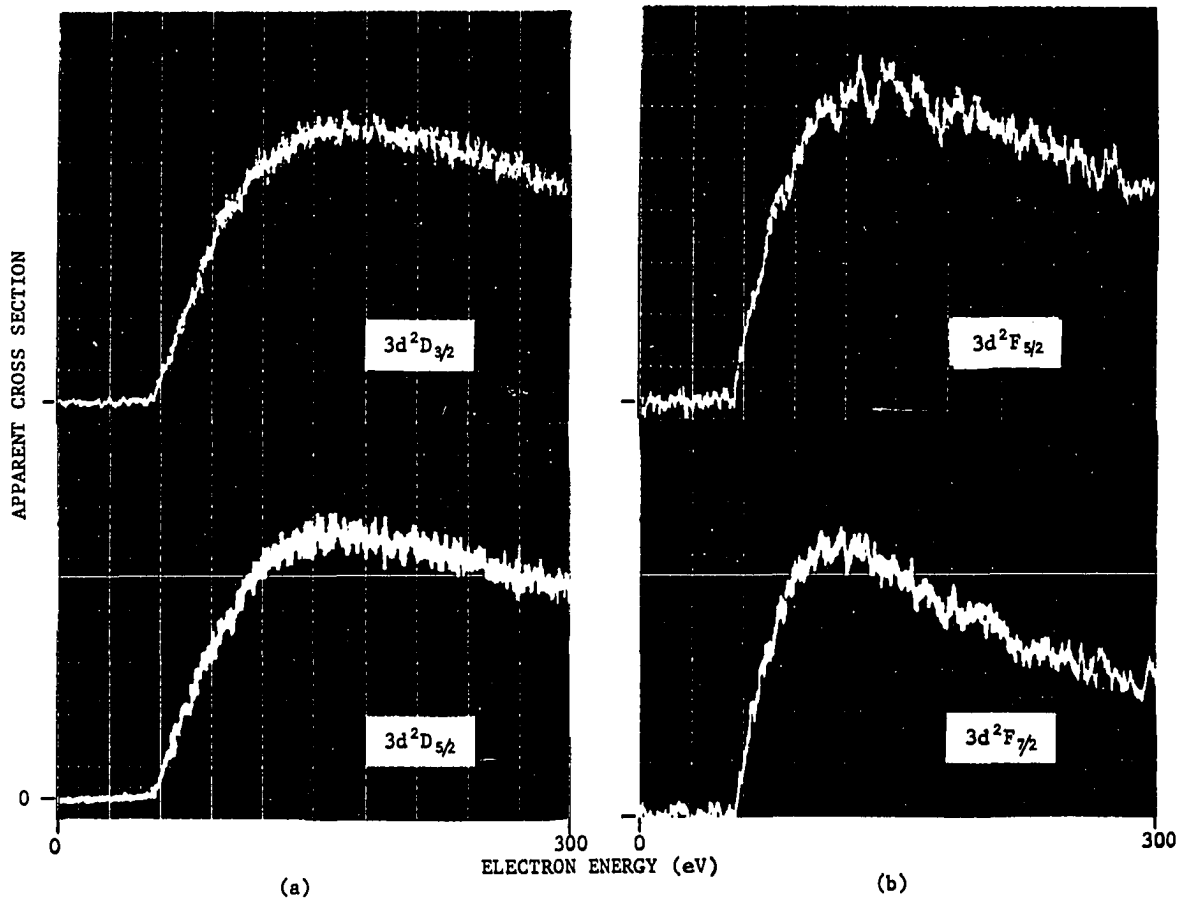


FIGURE 21. Excitation functions of the (a) $3d^2D$ and (b) $3d^2F$ levels.

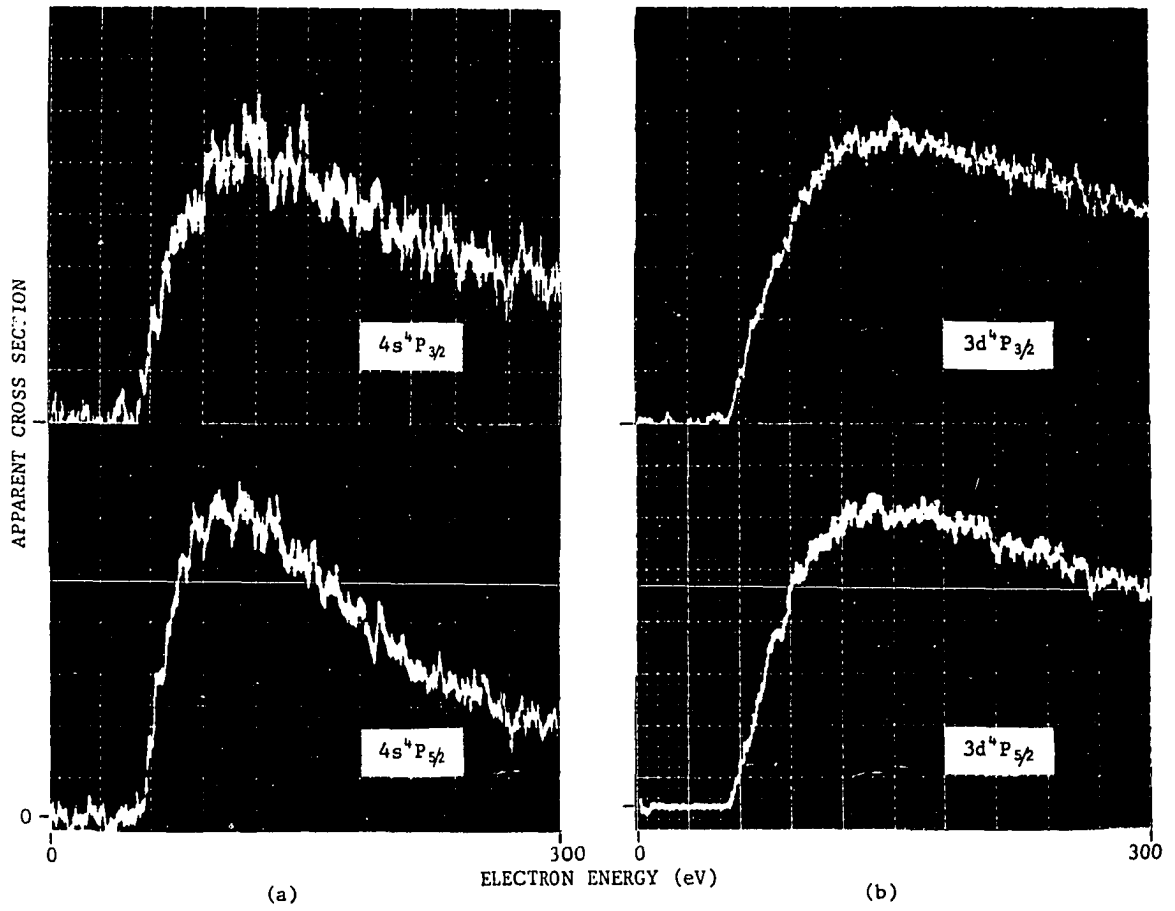


FIGURE 22. Excitation functions of the (a) $4s^4P$ and (b) $3d^4P$ levels.

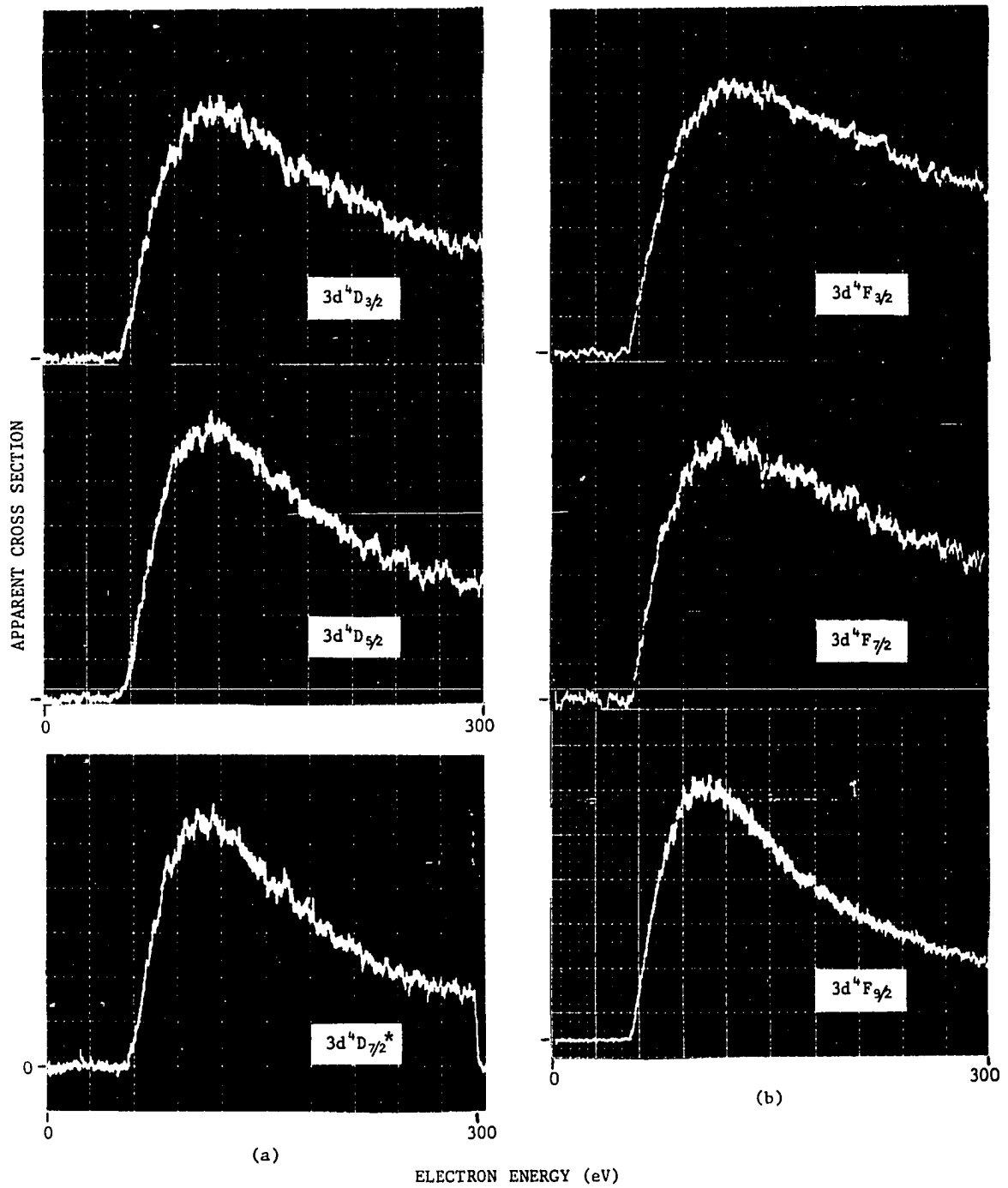


FIGURE 23. Excitation functions of the (a) $3d^4D$ and (b) $3d^4F$ levels.

Tables VII and VIII present the optical cross sections at 150 eV for the 3d and 4s states. The doublet cascade is not as infiltrated with branching ratios as the quartet system. This is because the quartet levels were in general a little weaker than the doublets as well as more difficult to resolve since the levels of a given quartet are quite close to each other. Wherever possible, Hodges⁽²⁾ experimental values were used. Otherwise, Garstang's IC calculations performed the task. Table IX contains the branching ratios of the cascade levels that were obtainable in this work compared with those which were calculated using line strengths. From Table IX one can consider the consistency of the cross sections in Table VII and VIII which were calculated using branching ratios. Also, Table IX might suggest the degree in which the 3d and 4s levels depart from LS coupling. Concerning this latter point it is seen that agreement between experimenters is not nearly as good as for the 3p levels. This is because of the lesser strength of the lines and a smaller degree of accuracy is present. One thing which is very evident is that many lines forbidden by LS coupling are present and in several cases, quite strong. Those ratios designated with an asterisk (*) denote a situation where the LS coupling calculations are totally inconsistent with experiment. The results of this work agree surprisingly well with Garstang's IC values and the calculated cross sections using these values should not be greatly in error. Also, the lack of experimental line strengths betrays the weakness of these cascade lines.

¹D Core

The number of cascade levels in this core configuration is much

Table VII. Cross Sections for the Doublet 3d and 4s Levels at 150 eV (Units of 10^{-21}cm^2).

Upper Level	$3d^2P_{\frac{1}{2}}$	$3d^2P_{\frac{3}{2}}$	$3d^2D_{\frac{3}{2}}$	$3d^2D_{\frac{5}{2}}$	$3d^2F_{\frac{5}{2}}$	$3d^2F_{\frac{7}{2}}$	$4s^2P_{\frac{1}{2}}$	$4s^2P_{\frac{3}{2}}$
Lower Level								
$3p^2S_{\frac{1}{2}}$	0.9	(1.5) ^a	0.4					0.7
$3p^2P_{\frac{1}{2}}$	0.2	1.3	0.9	-	-	-	0.3	1.9
$3p^2P_{\frac{3}{2}}$	0.3	0.6	0.6	1.8	0.3	-	-	2.2
$3p^2D_{\frac{3}{2}}$	(0.03) ^a	(0.01) ^a	0.4	0.7	2.3	-	-	0.5
$3p^2D_{\frac{5}{2}}$	-	(0.2) ^a	(0.01) ^a	0.8	(0.6) ^a	2.5	-	3.9
$3p^4S_{\frac{3}{2}}$				0.2	1.0			
$3p^4D_{\frac{1}{2}}$			0.4					
$3p^4D_{\frac{3}{2}}$				0.7	0.4			
Q'	1.4	3.6	2.7	4.2	4.6	2.5	0.3	9.2

^aBranching ratios from Garstang IC calculations⁽¹³⁾ were used to obtain these cross sections.

Table VIII. Cross Sections for the Quartet 3d and 4s Levels at 150 eV (units of 10^{-21}cm^2)

Upper Level	$3d^4P_{\frac{1}{2}}$	$3d^4P_{3/2}$	$3d^4P_{5/2}$	$3d^4D_{3/2}$	$3d^4D_{5/2}$	$3d^4D_{7/2}$	$3d^4F_{3/2}$	$3d^4F_{5/2}$	$3d^4F_{7/2}$	$3d^4F_{9/2}$	$4s^4P_{\frac{1}{2}}$	$4s^4P_{3/2}$	$4s^4P_{5/2}$
Lower Level													
$3p^4S_{3/2}$	0.6	0.9	2.7				1.3						
$3p^4P_{\frac{1}{2}}$	(0.2) ^a	(0.8) ^a		(0.8) ^b							(0.2) ^b	(0.6) ^b	
$3p^4P_{3/2}$	(0.7) ^a	(0.1) ^a	(1.0) ^b	1.5	1.9						(0.7) ^b	(0.3) ^b	0.5
$3p^4P_{5/2}$		(0.5) ^a	(1.0) ^b	(0.6) ^b	1.4	(4.5) ^b						0.4	(1.3) ^b
$3p^4D_{\frac{1}{2}}$	(0.01) ^a	(0.6) ^a		(0.06) ^a			2.0				0.8		
$3p^4D_{3/2}$	(0.06) ^a	1.0	(0.2) ^b	0.3	(0.06) ^a		(0.7) ^b	3.5			(1.1) ^b	(0.5) ^b	(0.4) ^b
$3p^4D_{5/2}$		(0.2) ^a	(0.5) ^a	(0.2) ^a	0.7	(0.07) ^a	(0.01) ^a	0.6	2.7			1.2	(0.3) ^b
$3p^4D_{7/2}$			(0.9) ^a		(0.1) ^a	1.7		(0.07) ^a	(0.3) ^a	4.4			1.2
$3p^2P_{\frac{1}{2}}$		0.3											
$3p^2D_{3/2}$			1.0					0.4					
Q'	1.6	4.4	7.3	3.5	4.2	6.3	4.0	4.6	3.0	4.4	2.8	3.0	3.7

^aBranching ratio from Garstang's IC calculations⁽¹³⁾ used.

^bBranching ratio from Hodges *et al.*⁽²⁾ experiment used.

Table IX. Branching Ratios for the Cascade Levels.

	<u>3d → 3p Arrays</u>			
	<u>This Work</u>	<u>Koopman</u>	<u>Hodges</u>	<u>Garstang</u> LS IC
$\frac{(2P_{\frac{1}{2}}, 2S_{\frac{1}{2}})}{(2P_{\frac{1}{2}}, 2P_{\frac{1}{2}})}$	4.5			2.4 5.5
$\frac{(2P_{\frac{1}{2}}, 2S_{\frac{1}{2}})}{(2P_{\frac{1}{2}}, 2P_{3/2})}$	3.0			4.6 5.1
$\frac{(2P_{\frac{1}{2}}, 2P_{\frac{1}{2}})}{(2P_{\frac{1}{2}}, 2P_{3/2})}$	0.67			2.0 0.93
$\frac{(2P_{3/2}, 2P_{\frac{1}{2}})}{(2P_{3/2}, 2P_{3/2})}$	2.2			0.20 1.5
$\frac{(2D_{3/2}, 2S_{\frac{1}{2}})}{(2D_{3/2}, 2P_{\frac{1}{2}})}$	0.44			0 0.32
$\frac{(2D_{3/2}, 2S_{\frac{1}{2}})}{(2D_{3/2}, 2P_{3/2})}$	0.67			0 0.63
$\frac{(2D_{3/2}, 2S_{\frac{1}{2}})}{(2D_{3/2}, 2D_{3/2})}$	1.0			0 0.37
$\frac{(2D_{3/2}, 4D_{\frac{1}{2}})}{(2D_{3/2}, 2S_{\frac{1}{2}})}$	1.0			0 1.6
$\frac{(2D_{3/2}, 2P_{\frac{1}{2}})}{(2D_{3/2}, 2P_{3/2})}$	1.5		2.0	5.0 2.0

Table IX (Cont'd.)

	<u>This Work</u>	<u>3d + 3p Arrays</u>		<u>Garstang</u>	
		<u>Koopman</u>	<u>Hodges</u>	LS	IC
$\frac{({}^2D_{3/2}, {}^2P_{1/2})}{({}^2D_{3/2}, {}^2D_{3/2})}$	2.2	1.0		2.1	1.2
$\frac{({}^2D_{3/2}, {}^4D_{1/2})}{({}^2D_{3/2}, {}^2P_{1/2})}$.044			0	0.52
$\frac{({}^2D_{3/2}, {}^2P_{3/2})}{({}^2D_{3/2}, {}^2D_{3/2})}$	1.5			0.41	0.59
$\frac{({}^2D_{3/2}, {}^4D_{1/2})}{({}^2D_{3/2}, {}^2P_{3/2})}$	0.67			0	1.0
$\frac{({}^2D_{3/2}, {}^4D_{1/2})}{({}^2D_{3/2}, {}^2D_{3/2})}$	1.0			0	0.61
* $\frac{({}^2D_{5/2}, {}^2P_{3/2})}{({}^2D_{5/2}, {}^2D_{3/2})}$	2.6	2.5	3.1	337.0	2.6
$\frac{({}^2D_{5/2}, {}^2P_{3/2})}{({}^2D_{5/2}, {}^2D_{5/2})}$	2.2			4.8	1.3
$\frac{({}^2D_{5/2}, {}^4S_{3/2})}{({}^2D_{5/2}, {}^2P_{3/2})}$	0.11			0	1.2
$\frac{({}^2D_{5/2}, {}^4D_{3/2})}{({}^2D_{5/2}, {}^2P_{3/2})}$	0.39		0.27	0	0.20
$\frac{({}^2D_{5/2}, {}^2D_{3/2})}{({}^2D_{5/2}, {}^2D_{5/2})}$	0.88			0	0.72

Table IX (Cont'd.)

	This Work	3d → 3p Arrays		Garstang	
		Koopman	Hodges	LS	IC
$\frac{({}^2D_{5/2}, {}^4S_{3/2})}{({}^2D_{5/2}, {}^2D_{3/2})}$	0.29			0	0.32
$\frac{({}^2D_{5/2}, {}^4D_{3/2})}{({}^2D_{5/2}, {}^2D_{3/2})}$	1.0		0.84		1.4
$\frac{({}^2D_{5/2}, {}^4S_{3/2})}{({}^2D_{5/2}, {}^2D_{5/2})}$	0.25			0	0.16
$\frac{({}^2D_{5/2}, {}^4D_{3/2})}{({}^2D_{5/2}, {}^2D_{5/2})}$	0.88			0	0.72
$\frac{({}^2F_{5/2}, {}^2P_{3/2})}{({}^2F_{5/2}, {}^2D_{3/2})}$	0.12		0.44		
$\frac{({}^2F_{5/2}, {}^4S_{3/2})}{({}^2F_{5/2}, {}^2P_{3/2})}$	3.3			0	0.16
$\frac{({}^2F_{5/2}, {}^4D_{3/2})}{({}^2F_{5/2}, {}^2P_{3/2})}$	1.3			0	
$\frac{({}^2F_{5/2}, {}^4S_{3/2})}{({}^2F_{5/2}, {}^2D_{3/2})}$	0.43			0	0.21
$\frac{({}^2F_{5/2}, {}^4D_{3/2})}{({}^2F_{5/2}, {}^2D_{3/2})}$	0.17			0	0.62
* $\frac{({}^4P_{3/2}, {}^4S_{3/2})}{({}^4P_{3/2}, {}^4D_{3/2})}$	0.90		1.1	4.6	6.0

Table IX. (Cont'd.)

	<u>This Work</u>	<u>3d → 3p Arrays</u>		<u>Garstang</u>	
		<u>Koopman</u>	<u>Hodges</u>	LS	IC
$\frac{({}^4P_{3/2}, {}^2P_{1/2})}{({}^4P_{3/2}, {}^4S_{3/2})}$	0.33			0	0.27
$\frac{({}^4P_{3/2}, {}^2P_{1/2})}{({}^4P_{3/2}, {}^4D_{3/2})}$	0.3			0	1.6
$\frac{({}^4P_{5/2}, {}^2D_{3/2})}{({}^4P_{5/2}, {}^4S_{3/2})}$	0.37		0.28	0	19
$\frac{({}^4D_{3/2}, {}^4P_{3/2})}{({}^4D_{3/2}, {}^4D_{3/2})}$	5.0		9.0	5.5	5.3
$\frac{({}^4D_{5/2}, {}^4P_{3/2})}{({}^4D_{5/2}, {}^4P_{5/2})}$	1.4		1.2	2.3	1.2
$\frac{({}^4D_{5/2}, {}^4P_{3/2})}{({}^4D_{5/2}, {}^4D_{5/2})}$	2.7		4.3	4.9	3.2
$\frac{({}^4D_{5/2}, {}^4P_{5/2})}{({}^4D_{5/2}, {}^4D_{5/2})}$	2.0		3.6	2.1	2.7
$\frac{({}^4F_{3/2}, {}^4S_{3/2})}{({}^4F_{3/2}, {}^4D_{1/2})}$	0.65			0	0.24
$\frac{({}^4F_{5/2}, {}^4D_{3/2})}{({}^4F_{5/2}, {}^4D_{5/2})}$	5.8		3.0		3.9
$\frac{({}^4F_{5/2}, {}^2D_{3/2})}{({}^4F_{5/2}, {}^4D_{3/2})}$	0.11			0	2.7

Table IX (Cont'd.)

	<u>This Work</u>	<u>3d → 3p Arrays</u>		<u>Garstang</u>	
		<u>Koopman</u>	<u>Hodges</u>	LS	IC
$\frac{({}^4F_{5/2}, {}^2D_{3/2})}{({}^4F_{5/2}, {}^4D_{5/2})}$	0.67			0	10.6
<u>4s → 3p Arrays</u>					
$\frac{({}^2P_{3/2}, {}^2S_{1/2})}{({}^2P_{3/2}, {}^2P_{1/2})}$	0.37				
$\frac{({}^2P_{3/2}, {}^2S_{1/2})}{({}^2P_{3/2}, {}^2P_{3/2})}$	0.32		0.17		
$\frac{({}^2P_{3/2}, {}^2S_{1/2})}{({}^2P_{3/2}, {}^2D_{3/2})}$	1.4		1.2		
$\frac{({}^2P_{3/2}, {}^2S_{1/2})}{({}^2P_{3/2}, {}^2D_{5/2})}$	0.18		0.11		
$\frac{({}^2P_{3/2}, {}^2P_{1/2})}{({}^2P_{3/2}, {}^2P_{3/2})}$	0.86				
$\frac{({}^2P_{3/2}, {}^2P_{1/2})}{({}^2P_{3/2}, {}^2D_{3/2})}$	3.8				
$\frac{({}^2P_{3/2}, {}^2P_{1/2})}{({}^2P_{3/2}, {}^2D_{5/2})}$	0.49				
$\frac{({}^2P_{3/2}, {}^2P_{3/2})}{({}^2P_{3/2}, {}^2D_{3/2})}$	4.4		6.9		

Table IX (Cont'd).

	<u>This Work</u>	<u>4s + 3p Arrays</u>		<u>Garstang</u>	
		<u>Koopman</u>	<u>Hodges</u>	LS	IC
$\frac{({}^2P_{3/2}, {}^2P_{3/2})}{({}^2P_{3/2}, {}^2D_{5/2})}$	0.56		0.65		
$\frac{({}^2P_{3/2}, {}^2D_{3/2})}{({}^2P_{3/2}, {}^2D_{5/2})}$	0.13		0.10		
$\frac{({}^4P_{3/2}, {}^4P_{5/2})}{({}^4P_{3/2}, {}^4D_{5/2})}$	0.33		0.47		
$\frac{({}^4P_{5/2}, {}^4P_{3/2})}{({}^4P_{5/2}, {}^4D_{7/2})}$	0.42	0.65			

smaller than in the $3p$ core (see Fig. 2). The excitation functions are given in Fig. 24. They all possess the same "broadness" as the $3p'$ levels. It would be desirable to look at the ${}^2G_{9/2}$ level and see if it is narrower than the others as was the case for the ${}^4F_{9/2}$ level. However, this was not possible as no lines from that level could be detected.

The cross sections at 150 eV are given in Table X. No branching ratios are available theoretically. Hodges *et al.*⁽²⁾ have measured some line strengths from which the branching ratios can be determined. However, their line assignments are different from Persson's⁽¹⁰⁾ in seven of the fourteen lines they measured. One line is even in a different core than Persson assigned it. Therefore, some doubt exists as to the validity of any branching ratios used in conjunction with my data. With this in mind, only one branching ratio of the four available from Hodge's data was used, the one for which there was agreement on the line assignments.

$1S$ Core

No lines were observed that terminate on the two $3p''$ levels of this configuration.

Level Cross Sections of the $3p$, $3p'$ and $3p''$ Levels

The level cross section was defined by Eq. (8). By adding the values in the rows of Tables VII, VIII and X, the amount of cascade is obtained into that $3p$ level which represents that row. Subtracting this quantity from the apparent cross section of that particular $3p$ level given in Tables I, IV and VI will give the level cross section. The

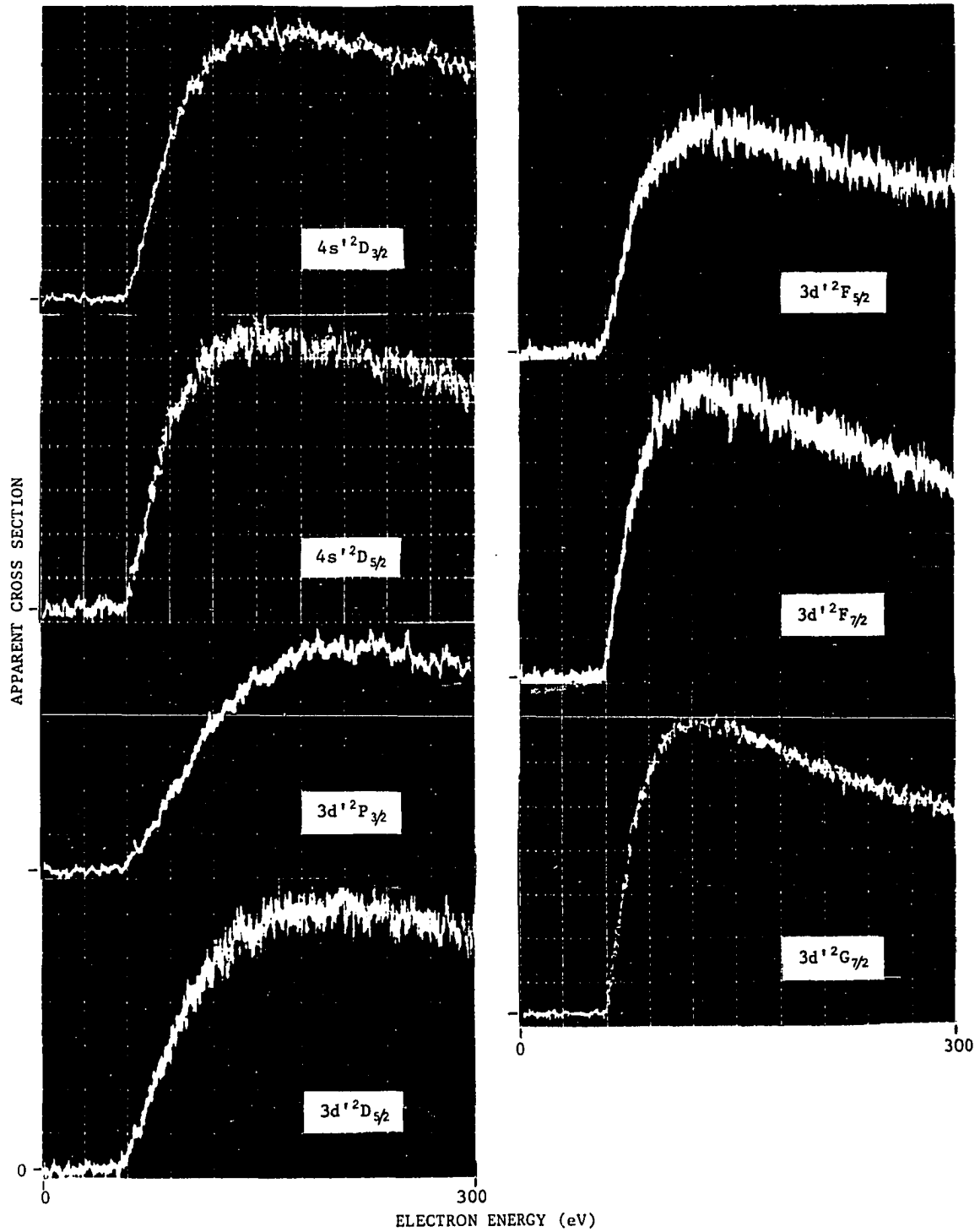


FIGURE 24. Excitation functions of the (1D) $4s'$ and (1D) $3d'$ levels.

Table X. Cross Sections of the 3d' and 4s' Levels at 150 eV (units of 10^{-21}cm^2).

Upper Level	$3d'2S_{\frac{1}{2}}$	$3d'2P_{\frac{1}{2}}$	$3d'2P_{\frac{3}{2}}$	$3d'2D_{\frac{3}{2}}$	$3d'2D_{\frac{5}{2}}$	$3d'2F_{\frac{5}{2}}$	$3d'2F_{\frac{7}{2}}$	$3d'2G_{\frac{7}{2}}$	$4s'2D_{\frac{3}{2}}$	$4s'2D_{\frac{5}{2}}$
Lower Level										
$3p'2p_{\frac{1}{2}}$	0.3	0.2	(0.2) ^a							
$3p'2p_{\frac{3}{2}}$		0.3	1.2		0.9					3.3
$3p'2D_{\frac{3}{2}}$		0.2		0.4		1.8				
$3p'2D_{\frac{5}{2}}$					1.7		2.6			3.3
$3p'2F_{\frac{5}{2}}$						0.5		4.4	3.6	
$3p'2F_{\frac{7}{2}}$							0.8			4.2
Q'	0.3	0.7	1.4	0.4	2.6	2.3	3.4	4.4	3.6	10.8

^aDetermined with branching ratios obtained by Hodges⁽²⁾.

level cross sections are given in Table XI along with the per cent cascade into that level. The 3p quartet levels are quite heavily weighted with cascade and these cascade lines are in turn dependent upon Garstang's theoretical branching ratios. Therefore, in the cascade contribution we would not expect less than 20 or 30 per cent error. The remaining lines should be much more accurate (10-15 per cent) since they are relatively strong and the cascade was less subjected to branching ratios.

As was denoted in Table XI, the $3p^4S_{3/2}$ direct cross section is not included. This is because some question exists on the cascade contribution to this level and will be discussed in Chapter IX.

Comparison with Theoretical Cross Sections

The only theoretical work which has been done on the cross sections for simultaneous ionization and excitation of neon by electron impact is by Koozekanani.⁽⁸⁾ He utilized the sudden perturbation approximation method. The basic assumption of this method is that the Hamiltonian of the atom changes in a very short time compared to the involved relaxation time. For our situation it means a fast electron strips away one of the bound valence electrons of the neutral atom in a very short time compared to the relaxation of the ion.

Koozekanani calculated only five cross sections. Comparison of results are given in Table XII.

In general, the results differ by a factor of two or three, but show surprising agreement for the $3p^2D_{3/2}$ level. Further comparison with this calculation scheme can be made at high energies since the sudden perturbation theory yields a cross section which has the same

Table XI. Level Cross Sections of the 3p Levels*
(Units of 10^{-21}cm^2) at 150 eV.

Level	Cross Section	Per cent Cascade
$3p^2S_{\frac{1}{2}}$	6.4	35
$3p^2P_{\frac{1}{2}}$	77.2	6
$3p^2P_{3/2}$	163.9	3
$3p^2D_{3/2}$	18.6	22
$3p^2D_{5/2}$	19.2	29
$3p^4P_{\frac{1}{2}}$	5.7	31
$3p^4P_{3/2}$	8.6	41
$3p^4P_{5/2}$	10.6	48
$3p^4D_{\frac{1}{2}}$	3.2	55
$3p^4D_{3/2}$	3.3	73
$3p^4D_{5/2}$	9.9	40
$3p^4D_{7/2}$	7.0	55
$3p^12P_{\frac{1}{2}}$	46.9	1
$3p^12P_{3/2}$	77.5	7
$3p^12D_{3/2}$	14.2	14
$3p^12D_{5/2}$	11.0	41
$3p^12F_{5/2}$	19.4	30
$3p^12F_{7/2}$	30.7	14
$3p^{11}2P_{\frac{1}{2}}$	7.4	0
$3p^{11}2P_{3/2}$	13.7	0

*The $3p S_{3/2}$ level is not included in this table. It will be discussed in Chapter IX.

Table XII. Comparison of Sudden Perturbation Calculated Cross Sections and Experimental Level Cross Sections at 150 eV (Units of 10^{-21}cm^2)

Level	Experimental	Sudden Perturbation
$3p^2S_{\frac{1}{2}}$	6.4	20.8
$3p^2P_{\frac{1}{2}}$	77.2	138.6
$3p^2P_{\frac{3}{2}}$	163.9	311.1
$3p^2D_{\frac{3}{2}}$	18.6	16.2
$3p^4D_{\frac{3}{2}}$	3.2	0.6

energy dependence as the single-ionization cross section. In the above calculations, $Q_{\text{ion}}(150 \text{ eV}) = 0.77 \times 10^{-16} \text{ cm}^2$ was used. (26)

CHAPTER VIII

HIGH ENERGY CONSIDERATIONS

Most calculation schemes, such as the sudden perturbation, in theoretical cross section work assume the incident electron is fast, i.e., large energy. When this is done, the calculations are most valid at high energies - say five or ten times threshold. Therefore, it is highly desirable to determine the energy dependence of the excitation functions at large energies.

This measurement has been done for the $3p$, $3p'$ and $3p''$ levels of NeII from 300 eV to 1000 eV. The output of the lock-in-amplifier was fed into a time-base chart recorder. The voltage drive was electronic and linear. Since the scan started at 300 eV and the oscillograms are from 0-300 eV, one can determine the cross section at high energies by normalizing the two at 300 eV.

$3p$ Core

Figures 25 and 26 are the optical excitation functions of the doublet and quartet $3p$ levels, respectively. The data was then analyzed by plotting $\ln Q'$ versus $\ln E$. This is done in Figs. 27 and 28. The cascade portion of the tail must then be measured to determine the level excitation function.

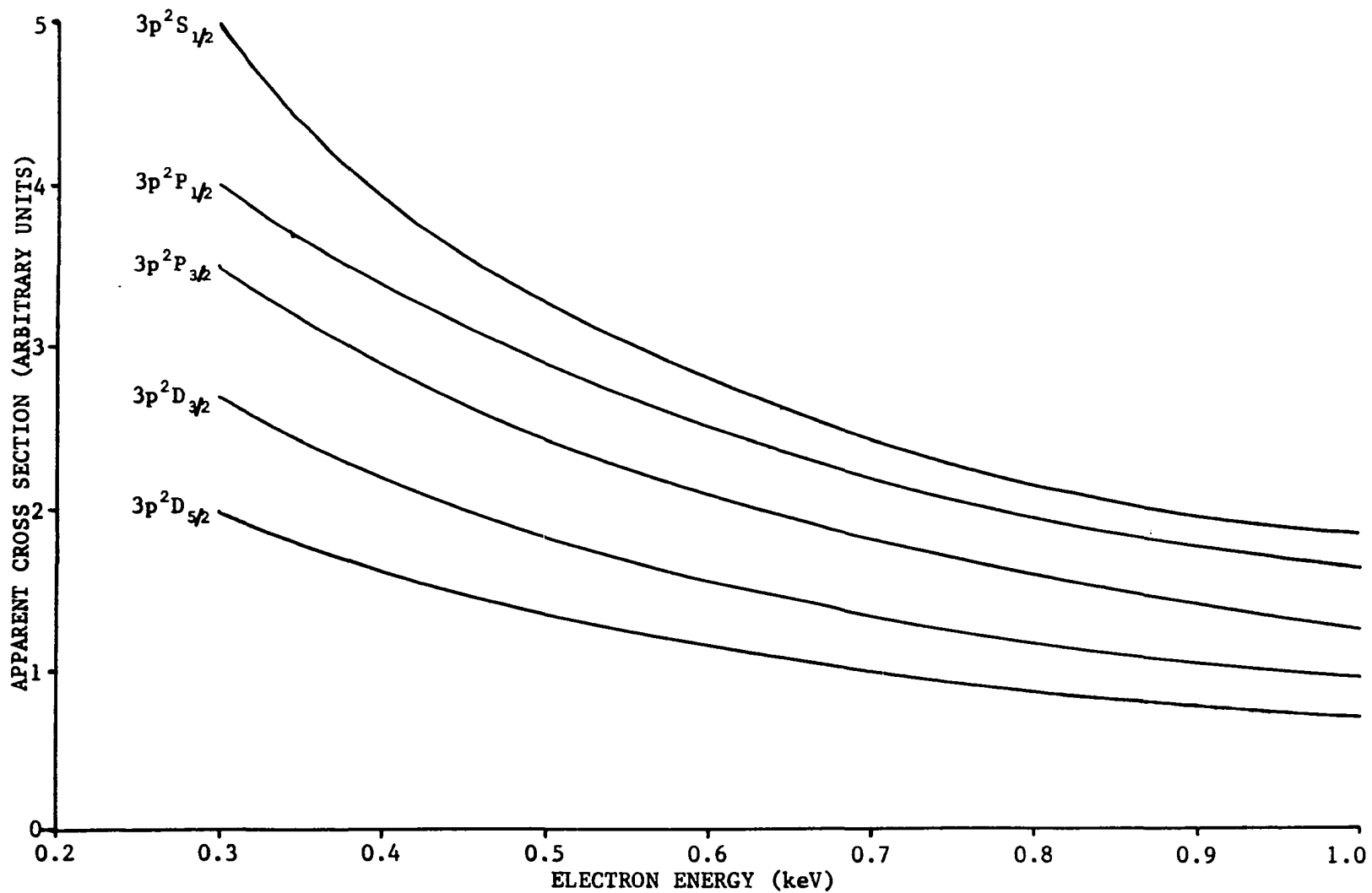


FIGURE 25. High energy portion of the 3p doublet excitation functions.

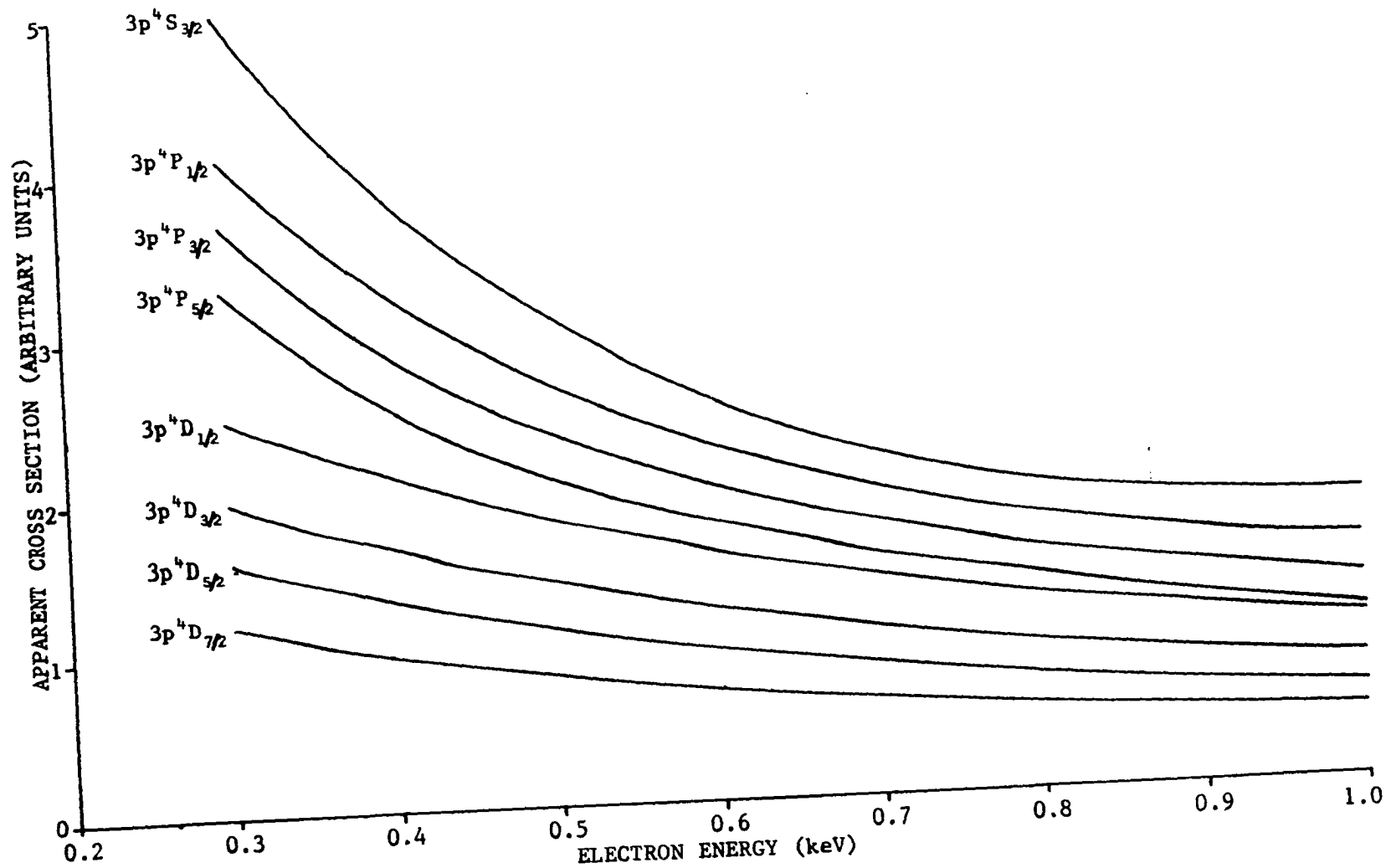


FIGURE 26. High energy portion of the 3p quartet excitation functions.

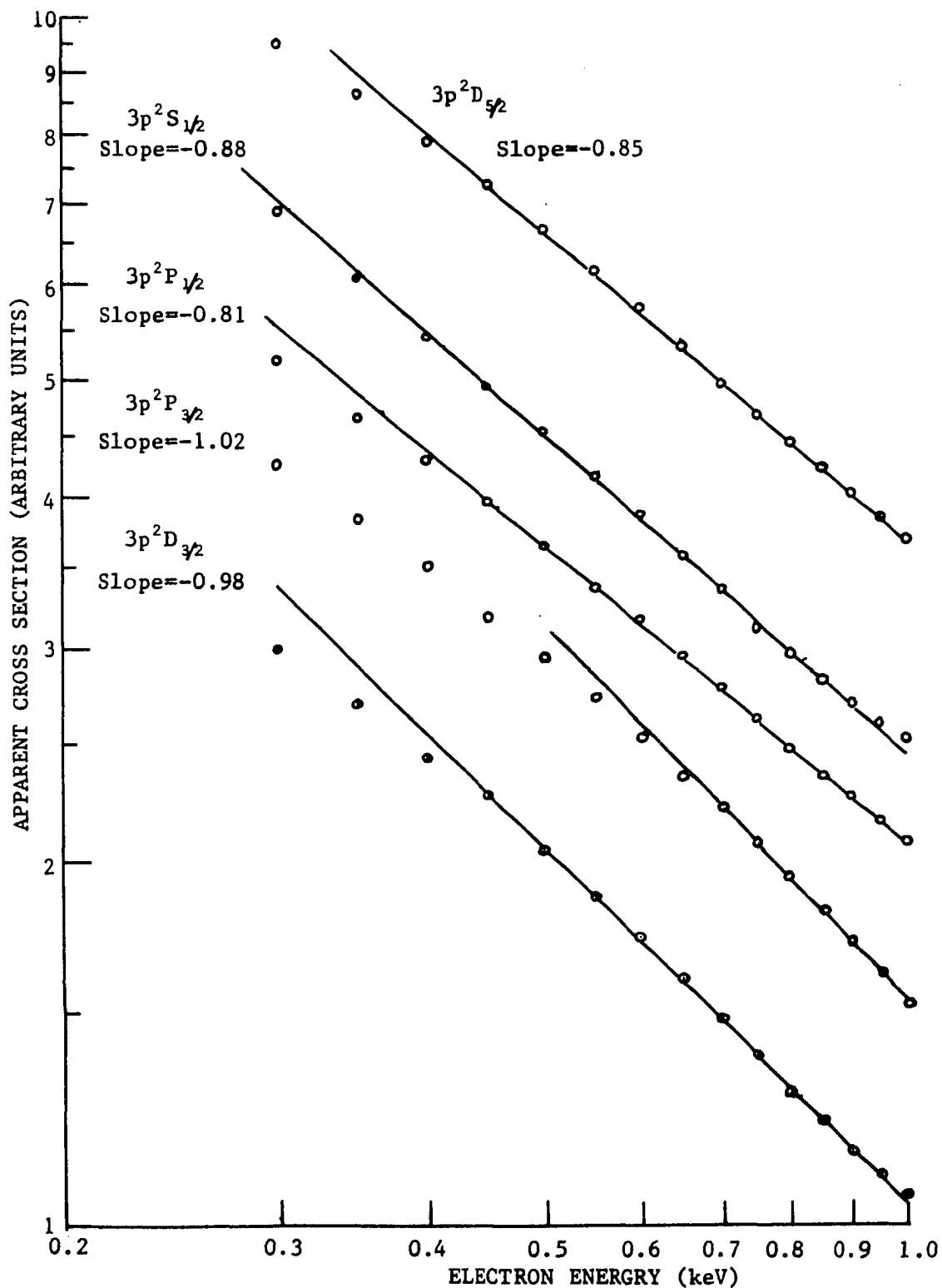


FIGURE 27. $\ln Q'$ vs. $\ln E$ for the 3p doublet levels.

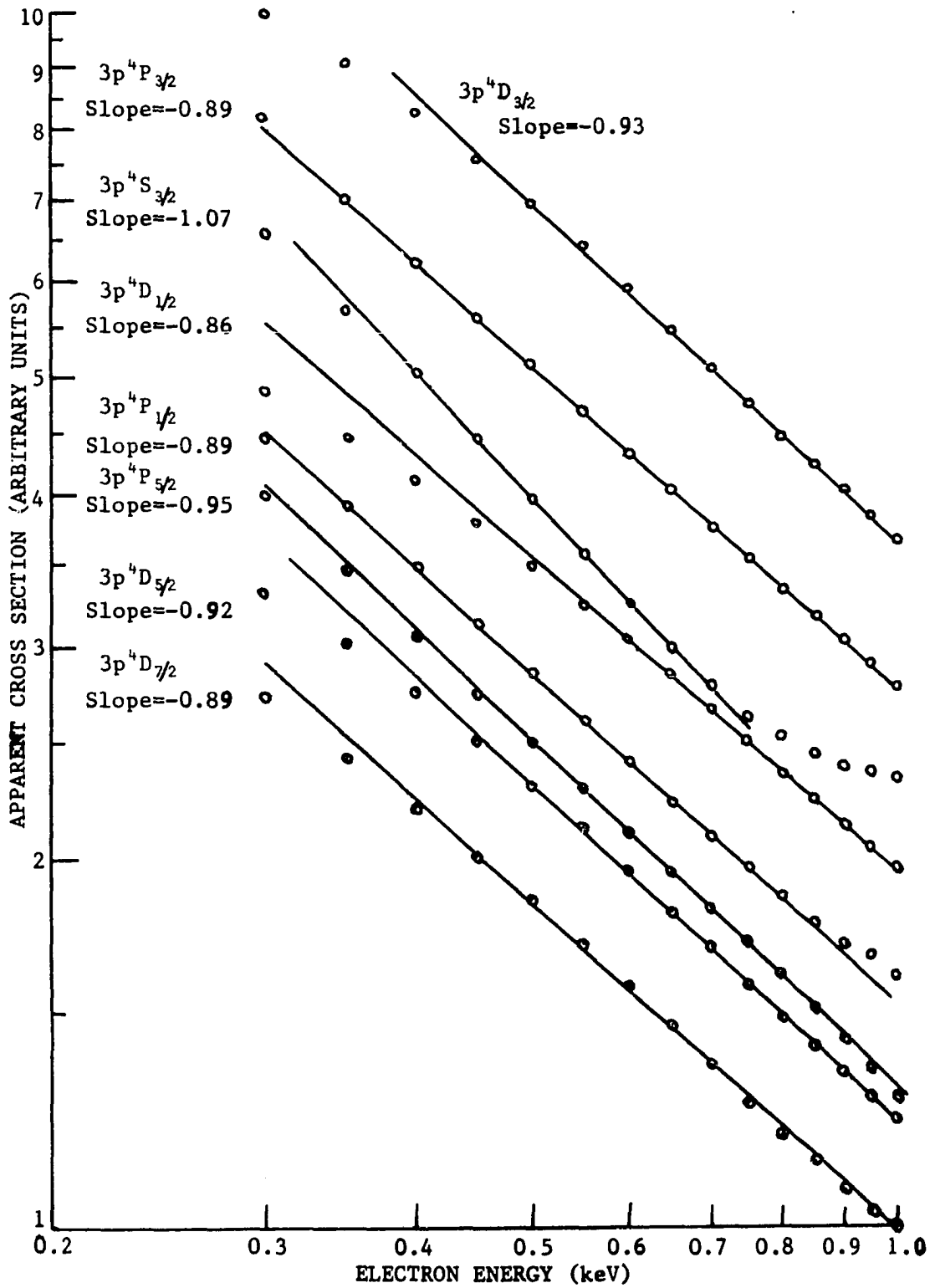


FIGURE 28. $\ln Q'$ vs. $\ln E$ for the 3p quartet levels.

Figures 29 and 30 are the cascade curves. These curves were much more difficult to monitor since Q decreases with energy and the lines were not strong even at low energies. Those levels, e.g., $3d^4F_{9/2}$ and $3d^4D_{7/2}$, which fell rapidly with energy became very difficult to measure. Figure 31 is the $\ln Q$ vs. $\ln E$ graph of those 3p levels whose slope changed when cascade was subtracted out. It is evident that the cascade lines have a shape similar to the 3p levels and thereby do not change the slope to any great degree.

Four of the optical excitation functions fall off as $E^{-1.0}$. Others have found $E^{-1.0}$ dependence for simultaneous ionization and excitation of Ar⁽¹⁶⁾ and He⁽³⁸⁾. The remaining levels vary in the range of $E^{-0.8}$ to $E^{-0.9}$. The $3p^4S_{3/2}$ graph has an unusual upturn at the tail of the plot. The $3p^4P_{\frac{1}{2}}$ has a similar but smaller effect. Since none of the other lines possess such an effect it must be a characteristic of the levels and not due to some process such as excitation by slower secondary electrons.

The sudden perturbation scheme of calculation has been discussed previously and from it

$$Q(j,E) = K(j)Q_{\text{ion}}^+(E) , \quad (27)$$

where

$Q(j,E)$ = the level cross section of state j of the ion
at energy e .

$K(j)$ = a constant dependent on the state in question.

$Q_{\text{ion}}^+(E)$ = the cross section at energy E for single-ionization without additional excitation.

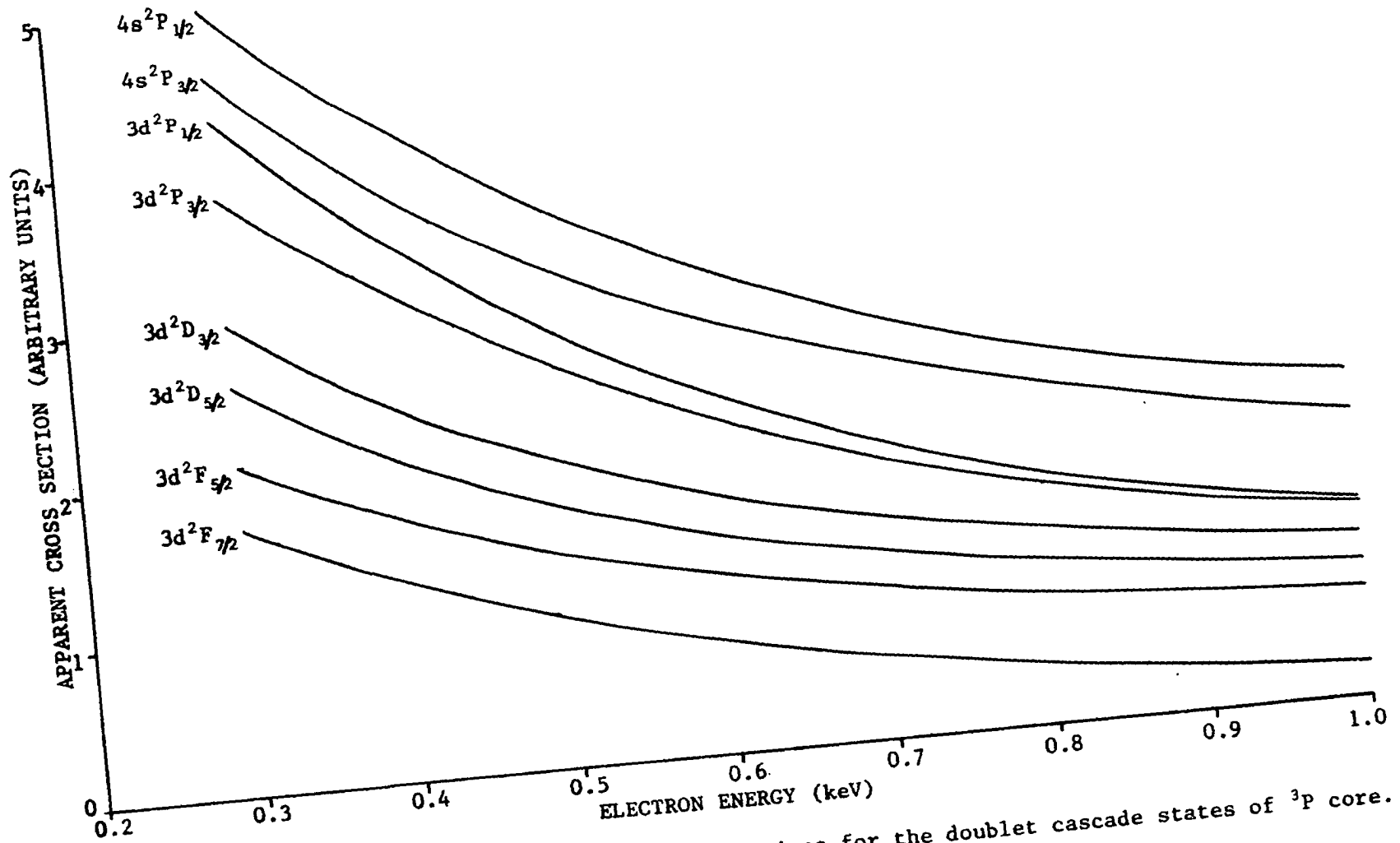


FIGURE 29. High energy portion of excitation functions for the doublet cascade states of 3P core.

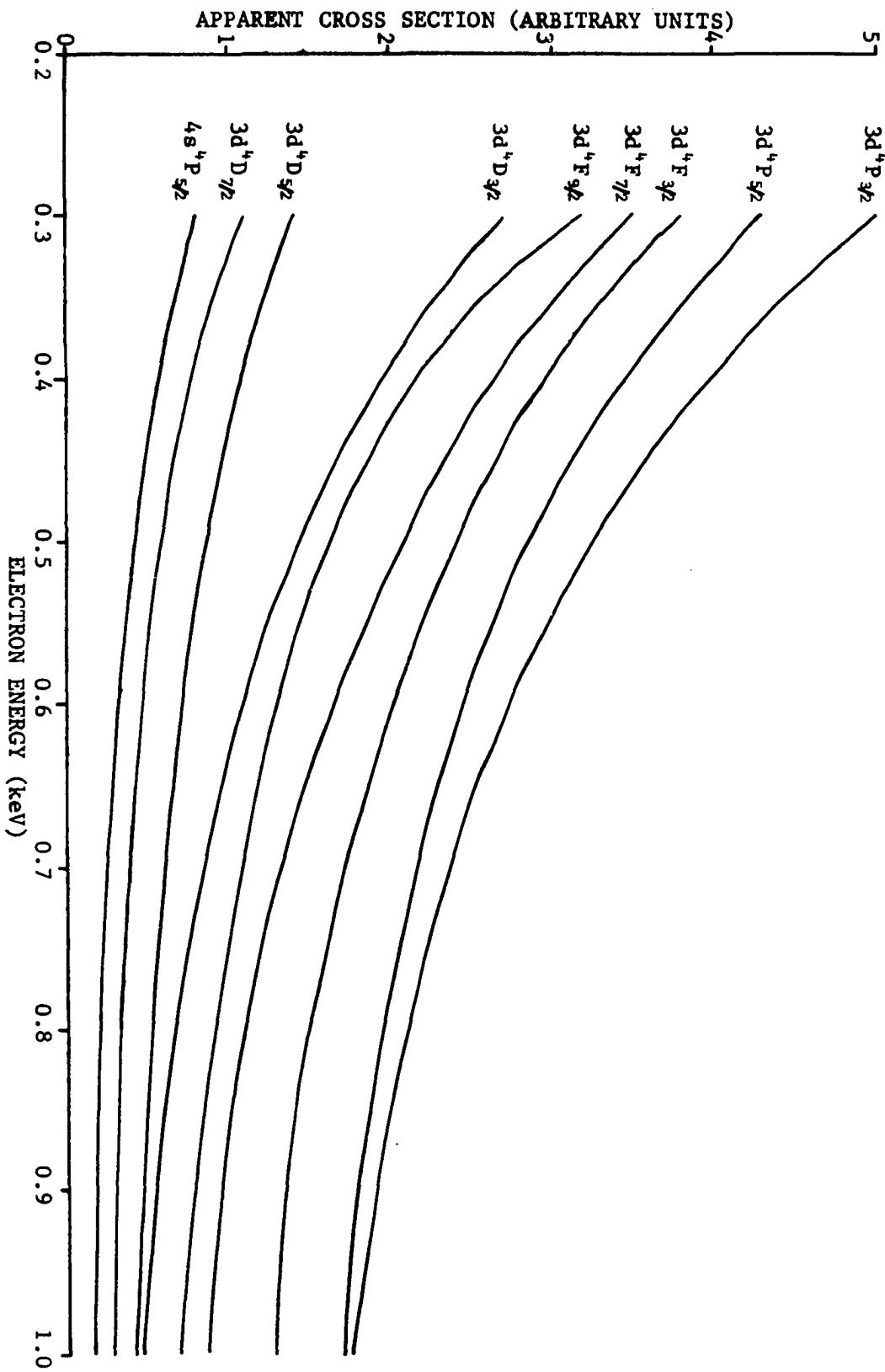


FIGURE 30. High energy portion of excitation functions for the quartet cascade states of 3P core.

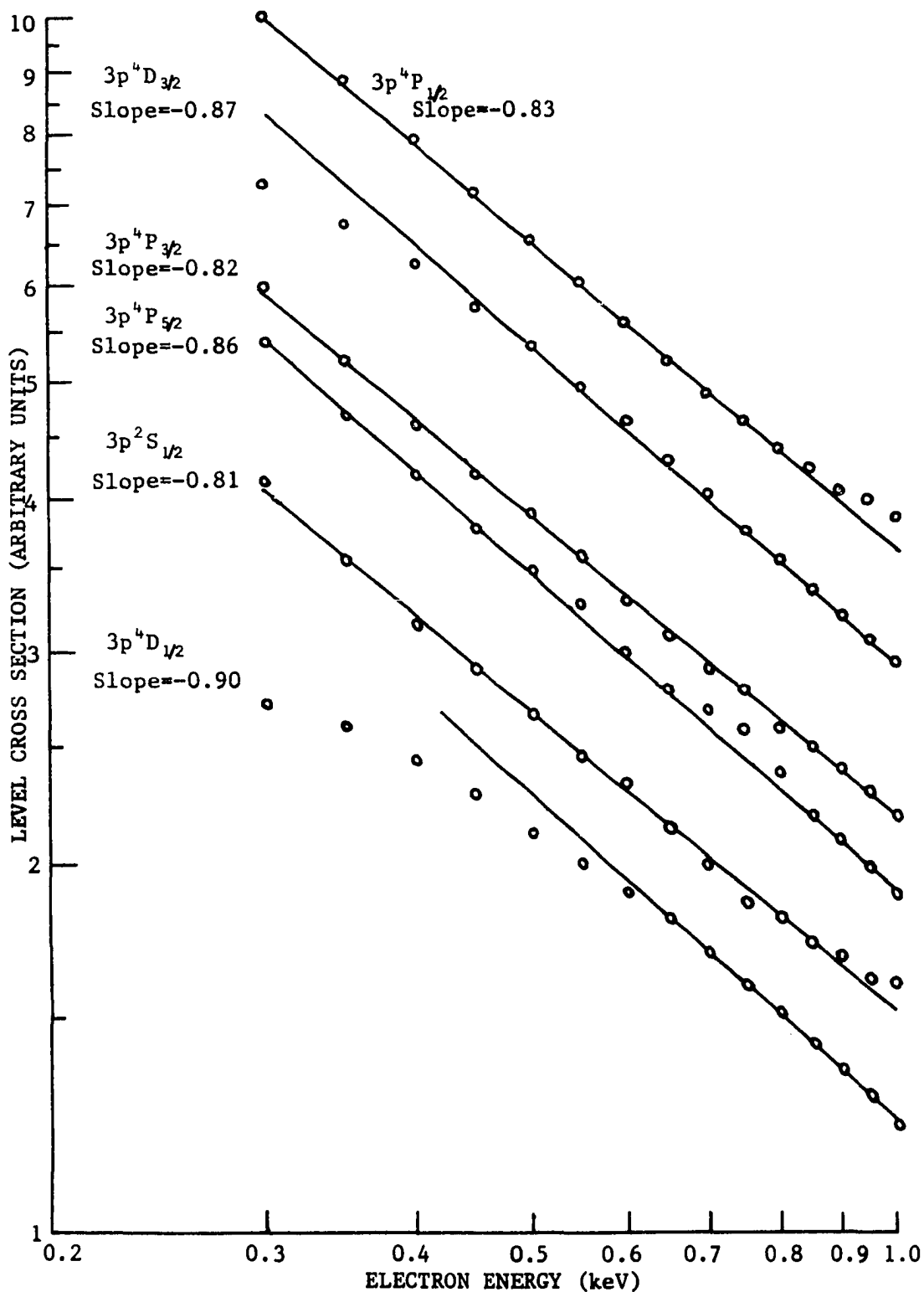


FIGURE 31. $\ln Q$ vs. $\ln E$ for those 3p levels where the subtraction of cascade has changed their slope.

Therefore, the cross section should fall with energy in the same manner as the single-ionization cross section. Figure 32 is a graph of $\ln Q$ versus $\ln E$ for the total ionization cross section.⁽³⁹⁾ Bleakney⁽²⁸⁾ has shown that $Q_{\text{ion}}^+ / Q_{\text{ion}}^{\text{TOTAL}} \approx 0.9$ after 200 eV. So for practical purposes, Fig. 32 is the plot for single-ionization. It's slope is -0.74. This plot begins to deviate from its linearity between 500-600 eV - similar to many $\ln Q$ versus $\ln E$ graphs of the 3p levels.

The similar slopes of the 3p excitation functions at high energies and the ionization cross section, as well as the broadness of the 3p optical excitation functions which are generally accepted as LS coupled, tend to persuade this author that ionization cross section affects to some extent the energy dependence of the simultaneous ionization and excitation cross section.

¹D Core

A procedure identical to that carried out for the ³P core lines was followed for the (¹D)3p' levels. The amount of cascade was much less in these cases. Figures 33 and 34 are the 3p' curves and cascade levels, respectively. It was found that the 3p'²P_{1/2} and 3p'²P_{3/2} curves had a $\ln E/E$ energy dependence. The 3p'²D_{5/2} fell off as $E^{-1.0}$ when cascade was removed. Cascade for the other states affected the slopes very little. The remaining curves had slightly smaller slopes than the 3p levels. Figure 35 is the $\ln E$ versus (Q'E) and Fig. 36 represents $\ln Q'$ versus $\ln E$. When cascade was removed, the slopes remained unchanged.

The two $(\ln E)/E$ results are very interesting. Bethe⁽²⁹⁾ found a $\ln E/E$ energy dependence for the ionization cross section from theoretical

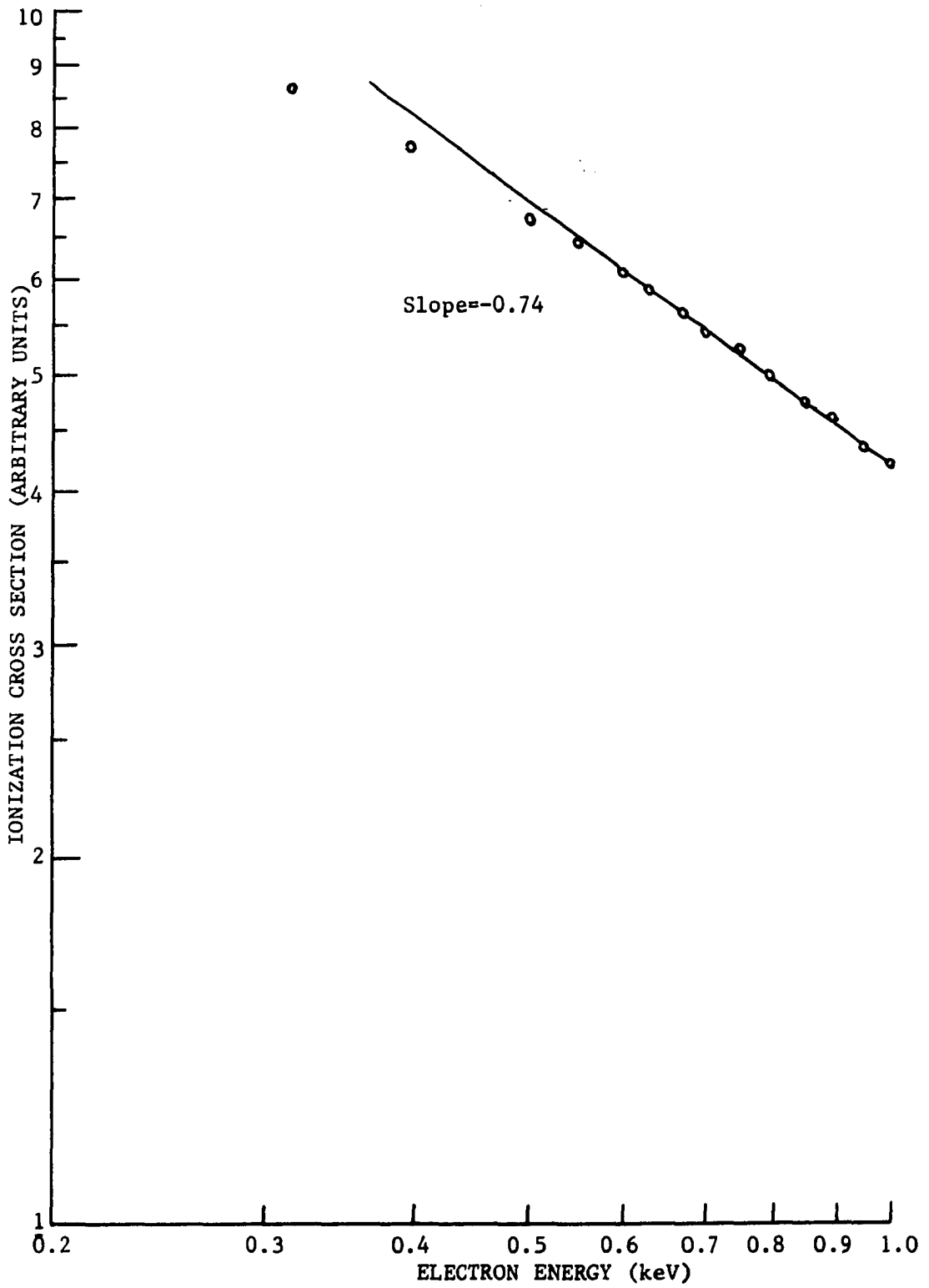


FIGURE 32. $\ln Q$ vs. $\ln E$ for the total ionization of NeI by electron impact.

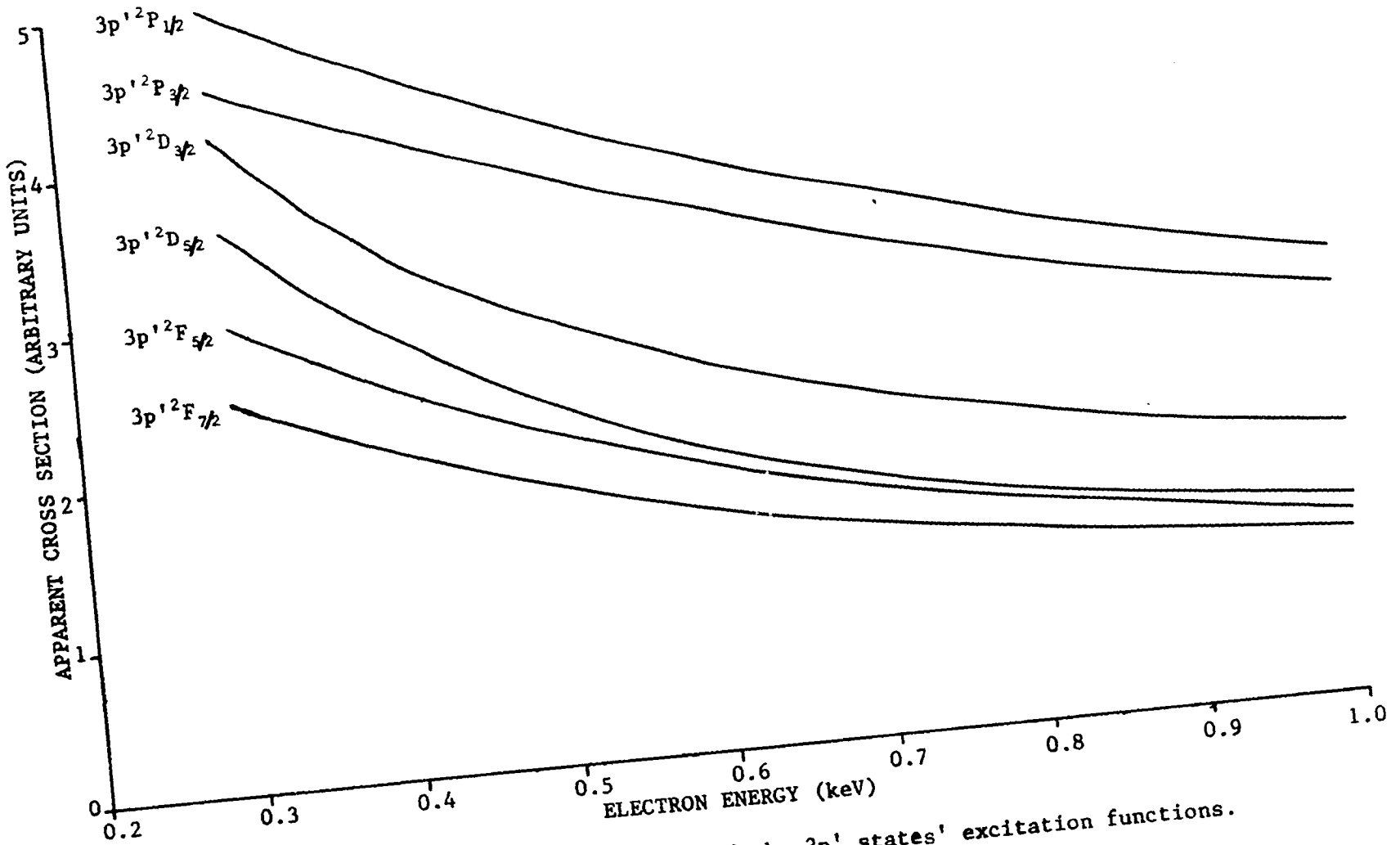


FIGURE 33. High energy portion of the 3p' states' excitation functions.

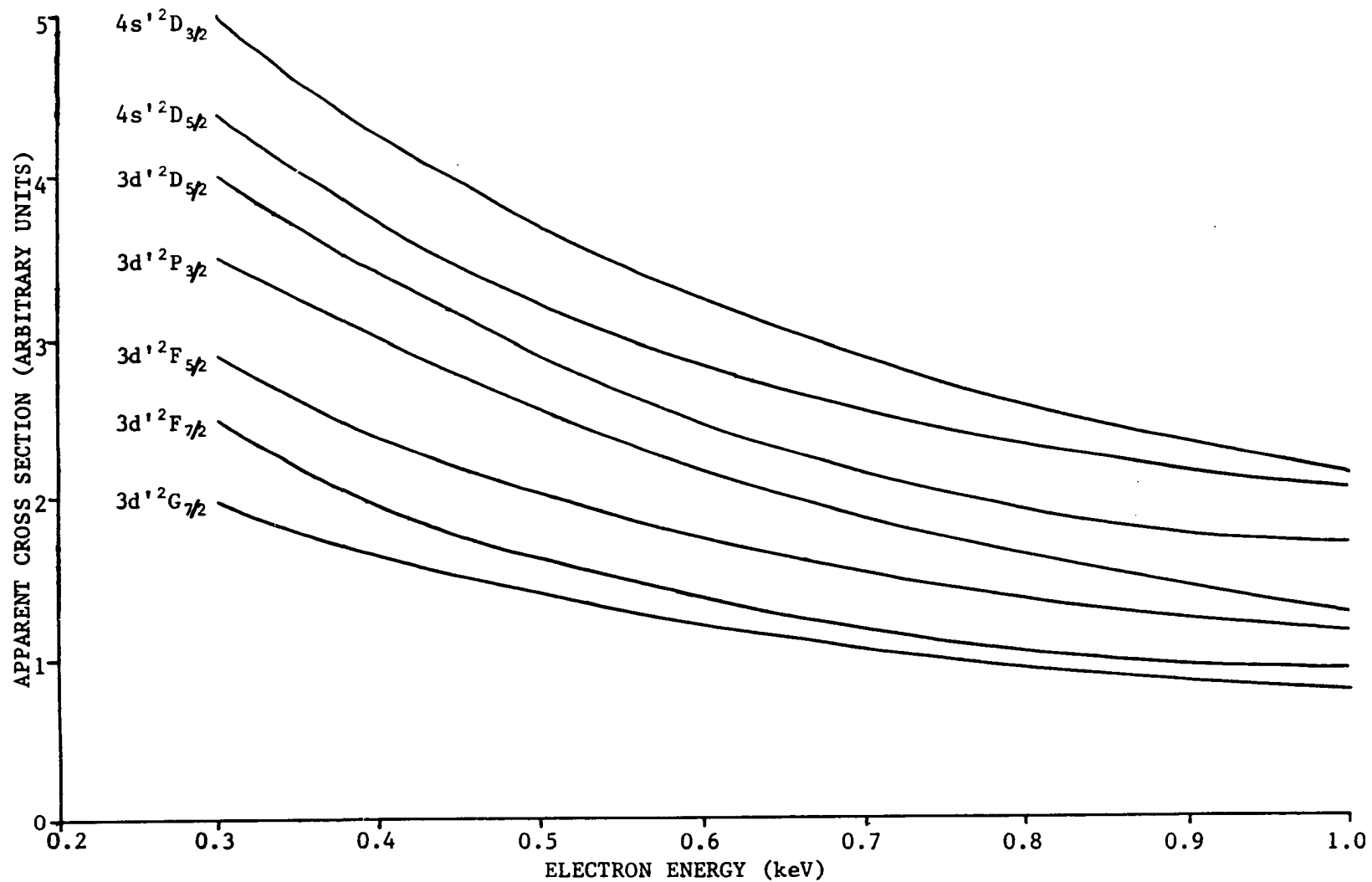
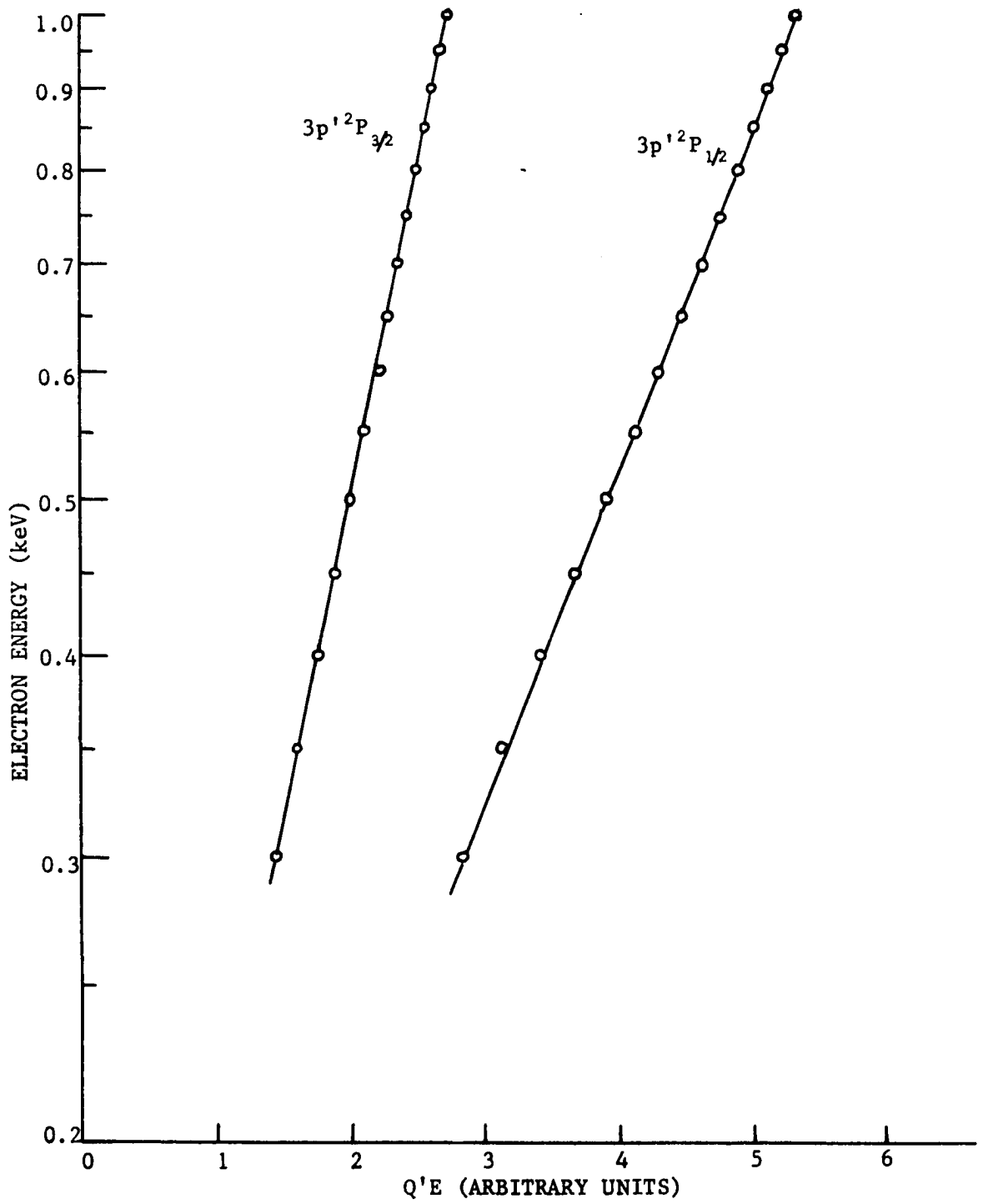


FIGURE 34. High energy portion of excitation functions for the cascade states of 1D core.

FIGURE 35. $\ln E$ vs. $Q'E$ for the $3p'^2P$ levels.

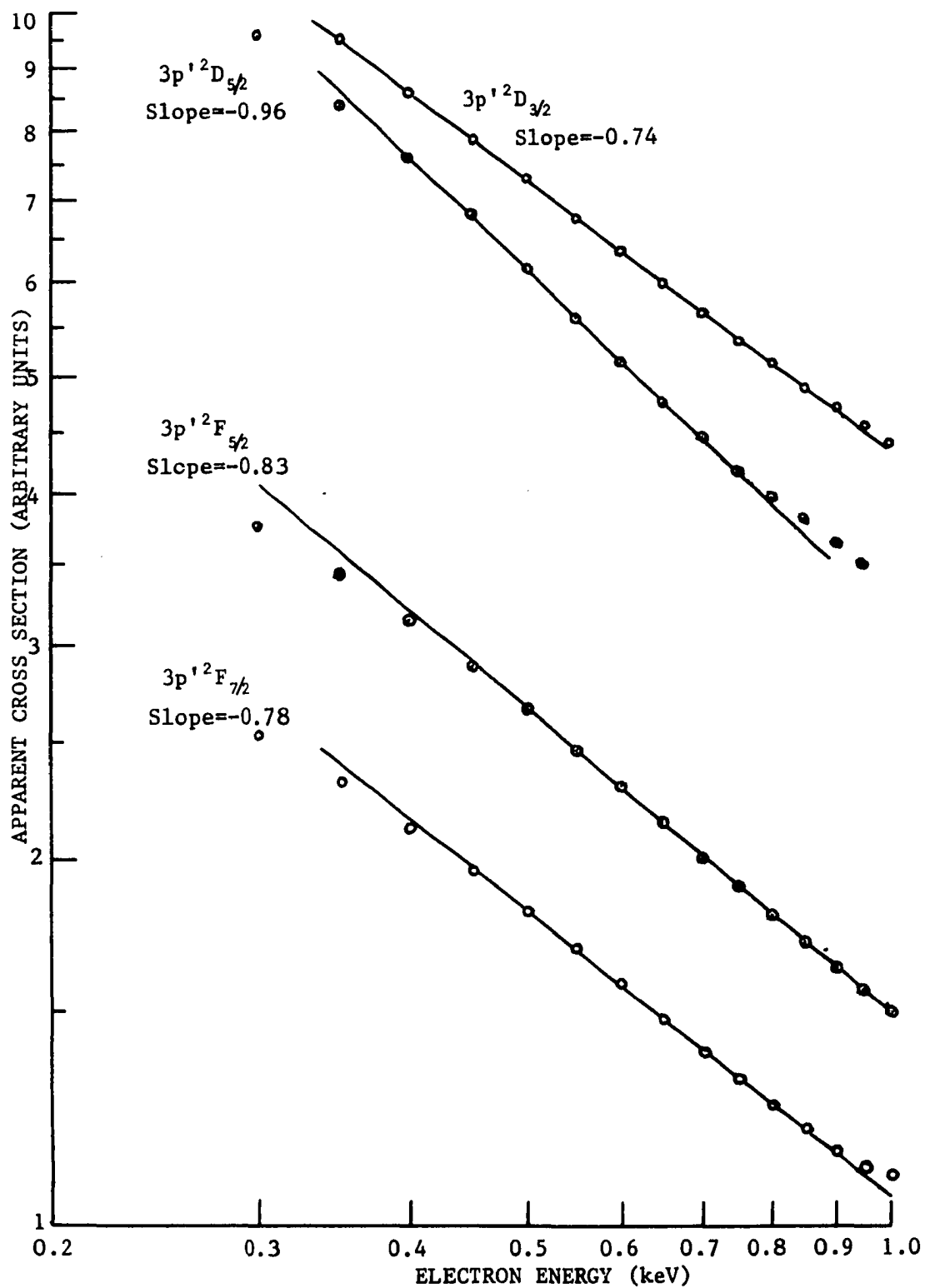


FIGURE 36. $\ln Q'$ vs. $\ln E$ for the $3p'{}^2D$ and 2F levels.

considerations. It would be interesting to compare some sudden perturbation calculations for these two levels with these measured cross sections.

¹S Core

Since no cascade appears for the 3pⁿ levels, the level and apparent cross sections are identical. Figure 37 shows the high energy tails of the two levels of this configuration. Figure 38 shows they follow a $\ln E/E$ energy dependence up to around 800-900 eV.

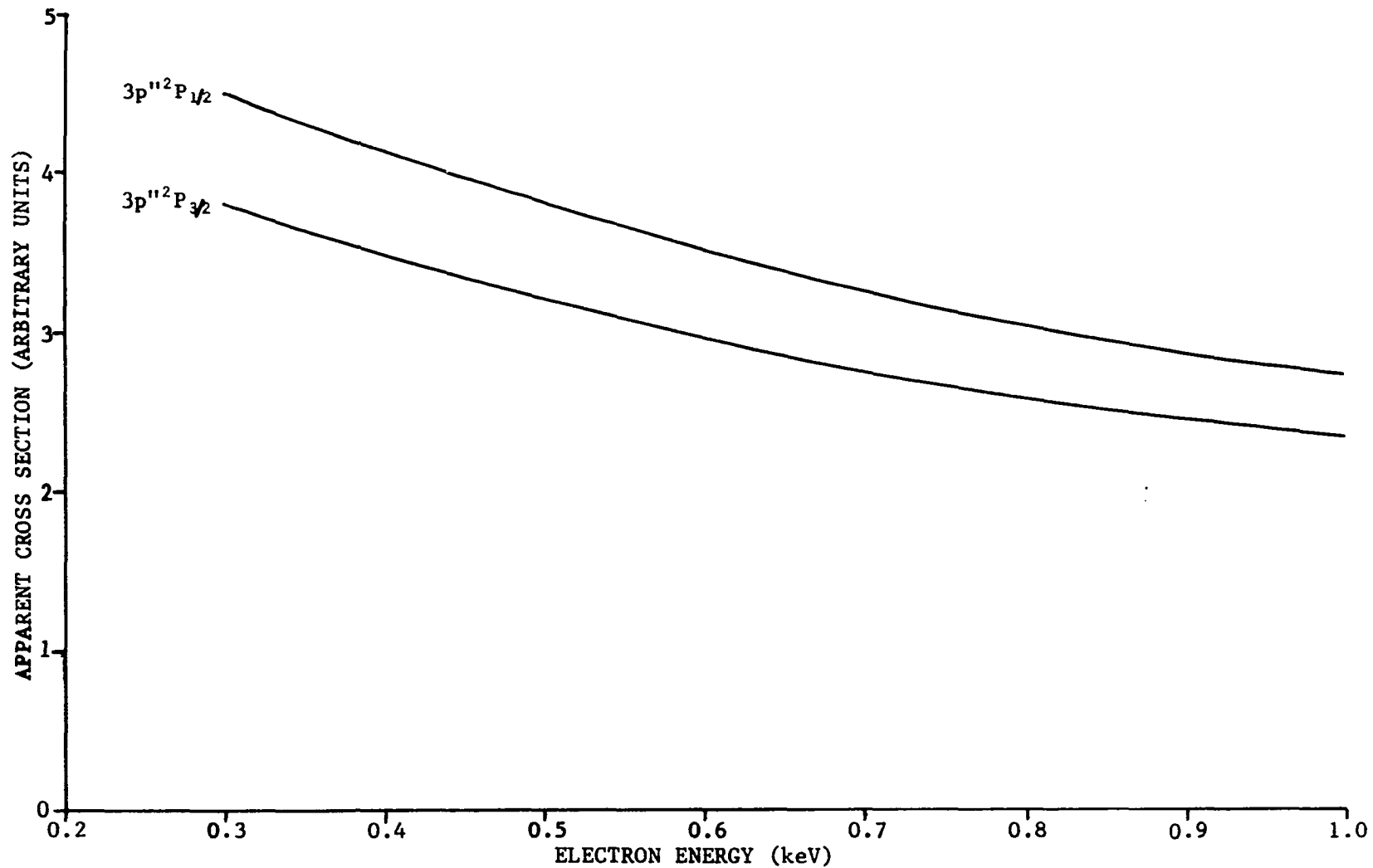
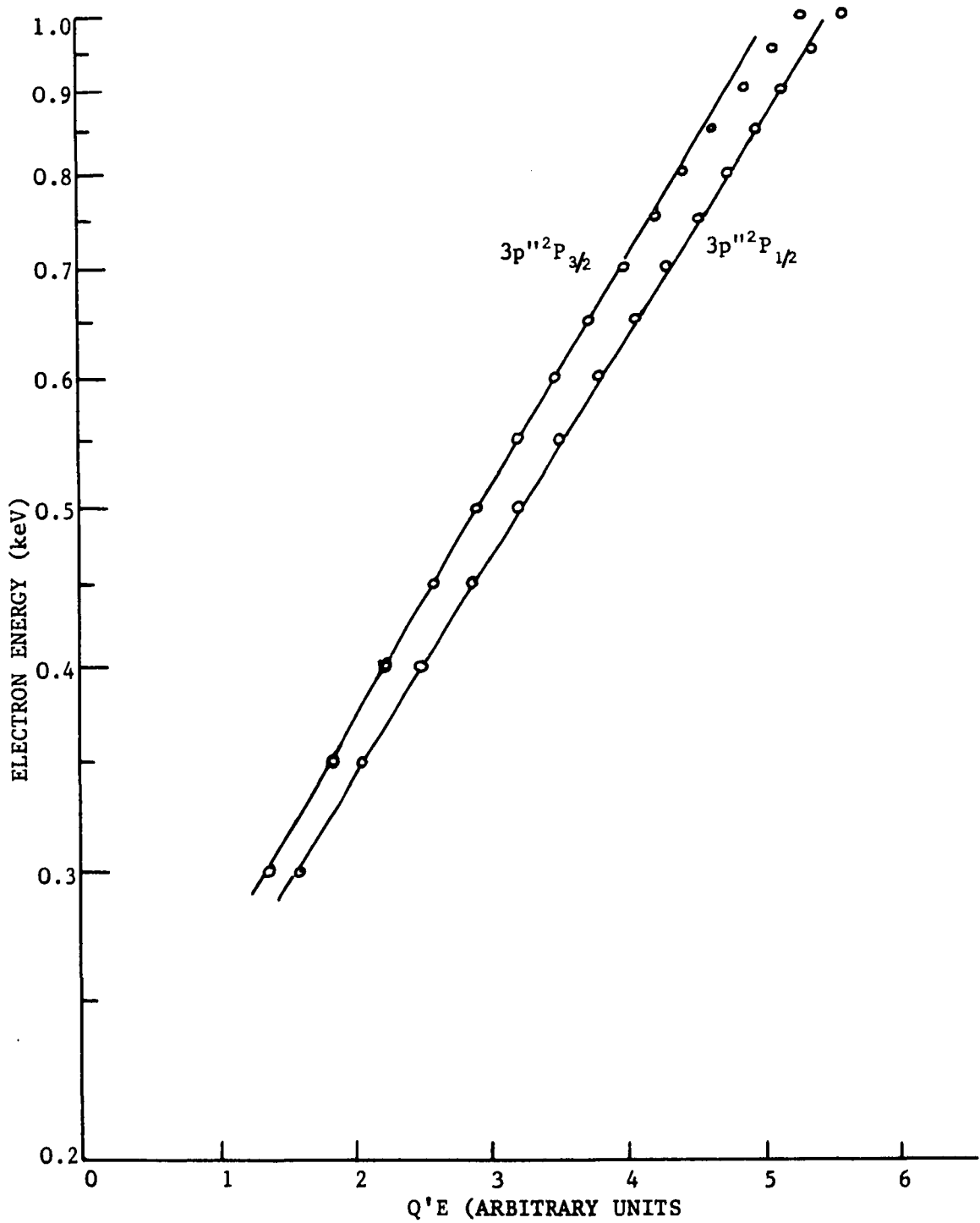


FIGURE 37. High energy portion of the $3p''$ excitation functions.

FIGURE 38. λnE vs. $Q'E$ for the $3p^{112}P$ levels.

CHAPTER IX

CASCADE INTO $3p^4S_{3/2}$ AND RELATED TOPICS

As was mentioned earlier, the cascade analysis of $3p^4S_{3/2}$ has been left until now. The reason for this delay can be readily determined from Fig. 39. Six cascade transitions have been measured and their total contribution to the cross section at 150 eV is $6.7 \times 10^{-21} \text{cm}^2$. The apparent cross section of the $3p^4S_{3/2}$ level consists of three optical transitions which total $6.3 \times 10^{-21} \text{cm}^2$. This yields a negative level cross section - a physically impossible condition. The possibilities for such a result can be listed as follows:

- (i) Error in the measurement of the optical cross sections involved; this may involve incorrect data collected from the collision chamber or from the standard lamp.
- (ii) Misclassification of transitions involved.
- (iii) Other channels of decay from the $3p^4S_{3/2}$ level which were not observed.

The first possibility can be checked by carefully repeated measurements. Also, it can be investigated by measuring cross sections in the same wavelength region for other atoms and then comparing with the original authors. This was done with helium⁽²³⁾ and neon⁽²⁵⁾. The agreement was very favorable. As another check on the standardization procedure, the intensity as a function of wavelength of the standard

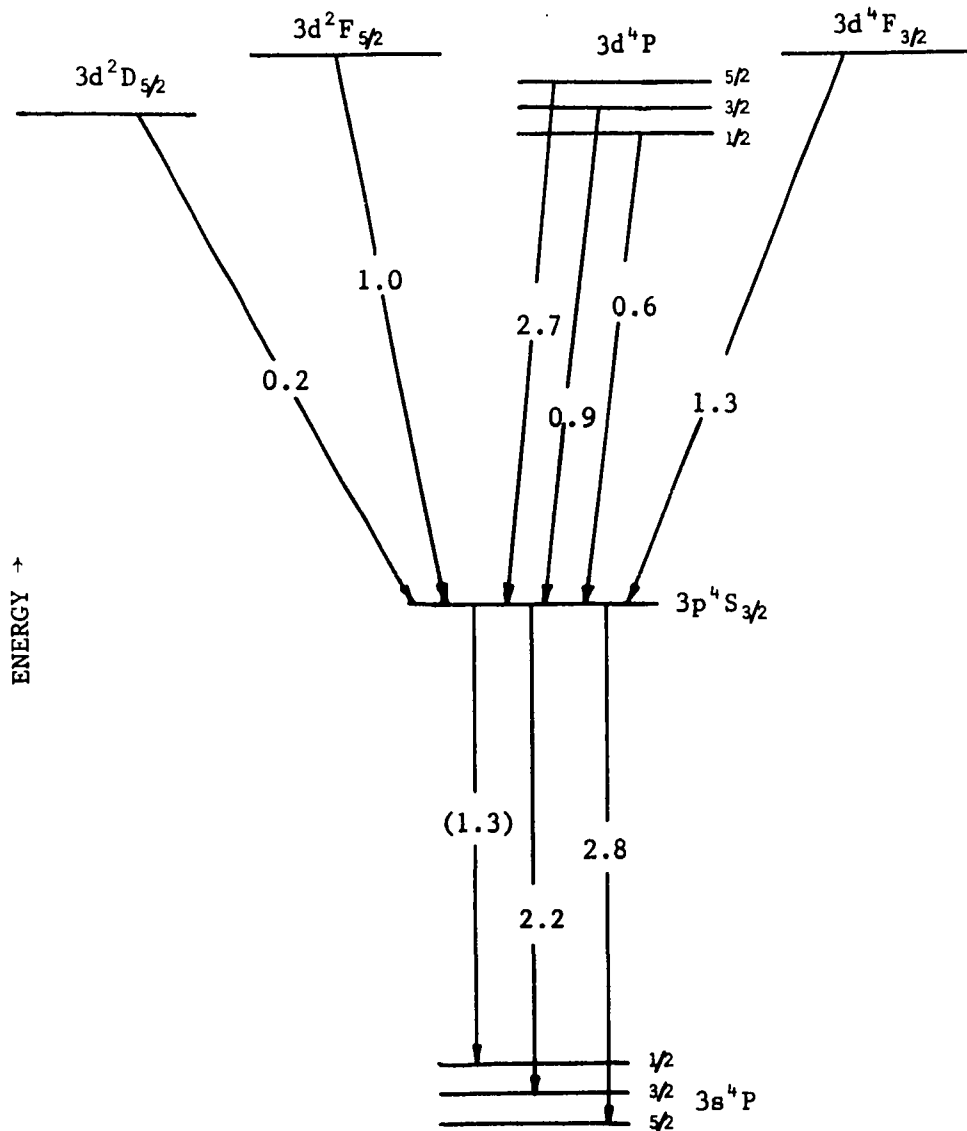


FIGURE 39. Levels involved in the calculation of the apparent and level cross section of $3p^4S_{3/2}$. The energy of the levels is not to scale. Cross sections are at 150 eV and in units of 10^{-21} cm².

lamp which was used throughout this research was compared with a newly acquired standard lamp. Identical results were obtained.

The second possibility is believed to be the strongest contender for the source of the problem. As was mentioned at the first of this paper, the analysis of the NeII spectra is very early in its development.. Persson's newly acquired results^(10,12) have shown various misclassifications in the 3d states; in particular, the previously designated $^2F_{5/2,7/2}$ and $^4F_{5/2,7/2}$ should be $^4F_{5/2,7/2}$ and $^2F_{5/2,7/2}$, respectively. Other experimenters use different newly acquired line identifications. This is very evident in Hodges *et al.*⁽²⁾ work which was just published and which we have used extensively. They used different 3d²F and 3d⁴F classifications and half of their assignments for lines originating from the 3d' levels were different than Persson's. As further evidence in the confusion in the spectral assignments let us consider the spectral line 2866 Å. Striganov and Sventitskii⁽⁴⁰⁾ have designated it as unclassified, being either of NeIII or NeIV. Denis *et al.*⁽³⁾ in their recently published paper on the mean lives of multiply ionized neon have quoted the unpublished results of S. Lindeberg for 2866 Å. He classifies it as a NeIII line coming from the transition 3p¹F→3s¹D. We have observed this line as well and Fig. 40(a) is the excitation function from 0 to 500 eV. The onset voltage of the 2866 Å line has been examined carefully by running the electron beam acceleration voltage drive very slowly and displaying the signal on a time-base chart recorder. Also, an operational amplifier-inverter was constructed in order to bias the voltage on the horizontal sweep of the oscilloscope so that the left hand side of the oscillogram can be zeroed at higher voltages. Figure

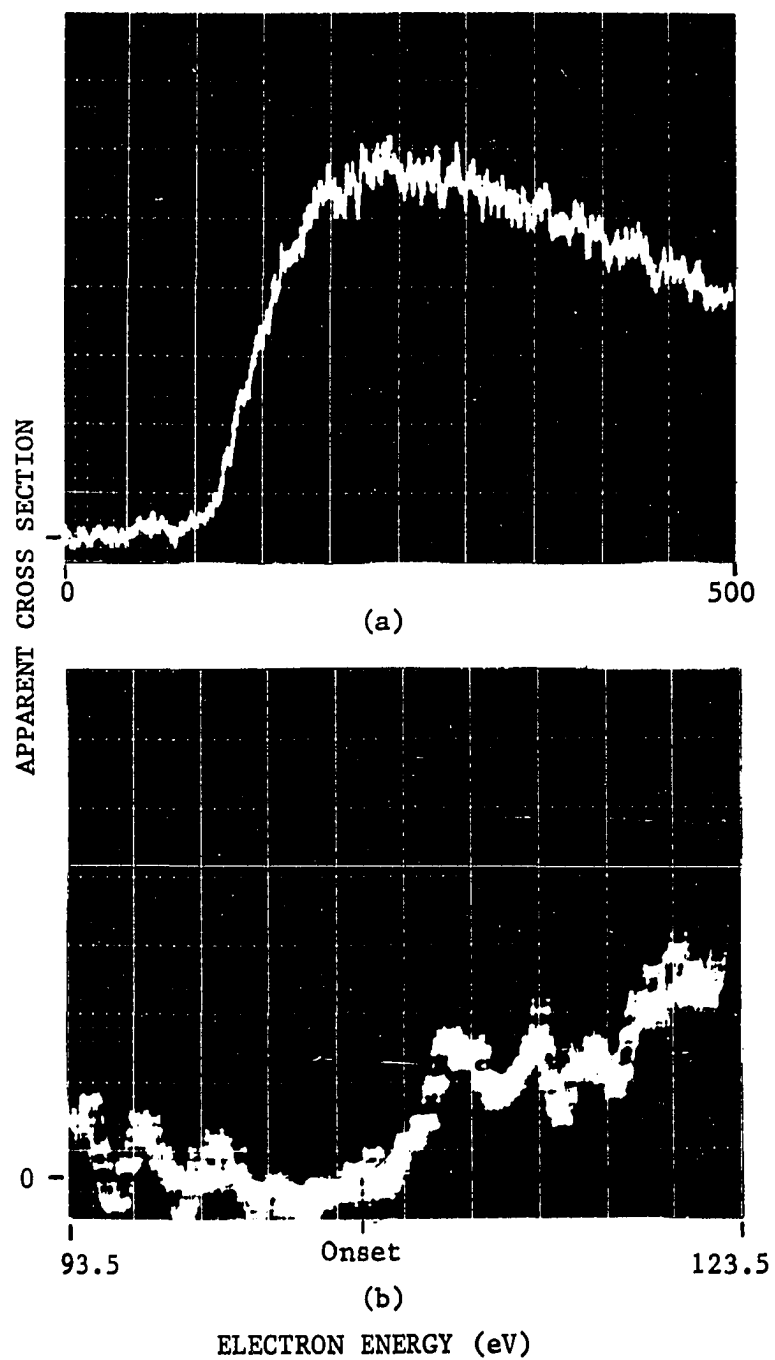


FIGURE 40. (a) Excitation function for the 2866 Å line.
(b) Onset voltage for the 2866 Å line.

40(b) is such a scan from 93.5 eV to 123.5 eV. The gain was quite high and this was coupled to the above amplifier, which had a little oscillation in it since the bias on the operational amplifier was pushed above its normal value in order to obtain the appropriate scale settings. Linearity of the amplifier operation remained, however. The resulting oscillogram reveals an onset of about 106-107 eV. The chart recordings also showed an onset at 107 eV. The energy of a photon of wavelength 2866 Å is 4.33 eV. Therefore, from Ref. 40 the line is definitely a NeIII. line whose terminal level is either $3s^5S$ or $3s^3S$.

The above discussion illustrates how the optical excitation function can be used as a tool in spectral classification. Another example of the use of optical excitation functions as aids in line identification concerns some results obtained for lines originating out of the $3d^4F$ levels. Reference 40 had the lines 3388.46 Å and 3561.23 Å originating from the $3d^4F_{5/2}$ levels. Therefore, the optical excitation functions of these two lines should be identical. Analysis of these functions revealed that they were not the same. The 3388.46 Å excitation function fell off less rapidly - a difference of 7 per cent in the ratio of the intensity at 150 eV to the intensity at 300 eV for the two lines. It was this result that caused a search for other line identifications. The article of Persson *et al.* ⁽¹⁰⁾ was obtained and it was found and they had discovered a new line at 3388.95 Å from the transition $3d^1 2S_{1/2} + 3p^1 2P_{1/2}$. Therefore, the optical excitation function of the line at 3388 Å I was observing was not fully resolved from this newly found 1D core line. We have seen that the 1D core excitation functions are very broad; the new line

was holding the composite excitation function up at higher energies. By narrowing the slits and exercising great care, I was able to resolve these two lines at 3388 Å. Taking the excitation function of the resolved $3d^4F_{5/2}$ line at 3388.42 Å gave agreement with the $3d^4F_{5/2}$ line at 3561 Å. Persson also suggested these upper states were 2F , not 4F . Even though the excitation function did not identify any lines, it certainly revealed that something was wrong in the spectra. Persson has found numerous other cases where two lines reside in a spectral region previously thought to be occupied by but one line.

A similar situation was found concerning the $3d^4D_{7/2}$ level. The line 3329 Å has been identified as belonging to the transition $3d^4D_{7/2} \rightarrow 3p^4D_{7/2}$. The transition $3d^4D_{7/2} \rightarrow 3p^4P_{5/2}$ has been assigned to 3034.46 Å. Figure 41 is the excitation function of 3329 Å. It appears quite broad and 3034.46 Å should have the same energy dependence. Unfortunately, 3034.46 Å line lies only 0.12 Å away from a weaker line (Persson⁽¹⁰⁾ indicates the weak line is half as strong). Since this is below the minimum resolution of the present monochromator, it cannot be fully resolved. However, by setting to the side of the 3034.46 Å line, we can get an intensity which is free from the adjacent line. This allows an excitation function to be determined even though its cross section can not. Figure 23(a) contains the $3d^4D_{7/2}$ level due to the 3034.46 Å transition. Clearly, it is not broad but happens to be one of the most narrow functions obtained. The two lines cannot be from the same upper state. As evidence from Fig. 23(a), the line giving the narrow excitation function was chosen as the true excitation function of $3d^4D_{7/2}$. The choice was based upon the experimental trend that as J

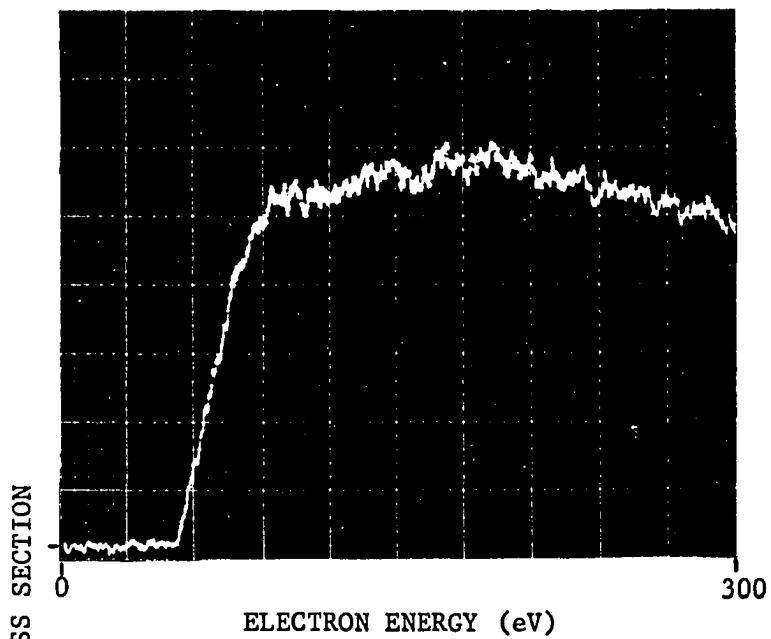


FIGURE 41. Excitation function of the 3329 Å line.

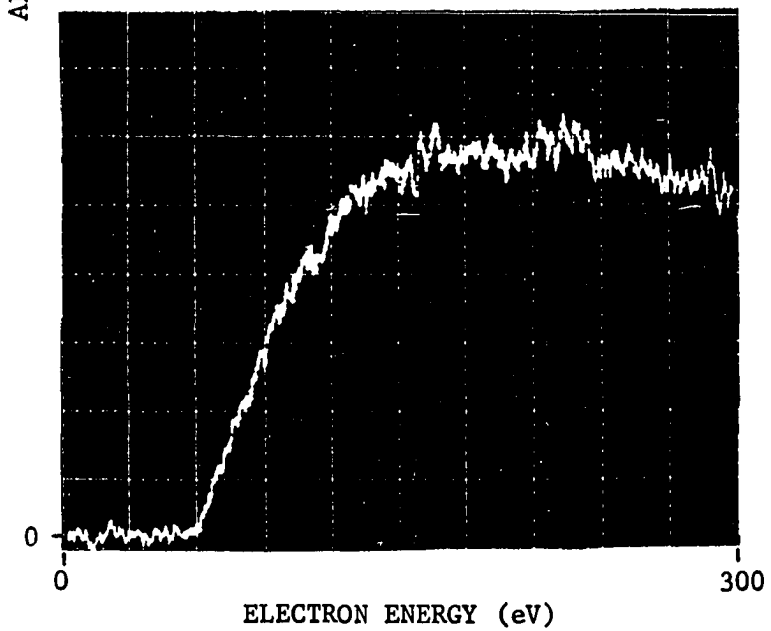


FIGURE 42. Excitation function of the 3626 Å line.

increased for a given L family, the excitation function becomes more peaked. From Fig. 23(a) it can be observed that the 3034 Å line fits this trend quite well while the 3329 Å line would be an anomalous condition to previous results. Examination of Fig. 41 reveals a peaking at about 100 eV, followed by a slight dip and then a much broader peak. It is noticed that the 3034 Å line peaks at 100 eV as well. A possible explanation for the discrepancy between $3d^4D_{7/2}$ excitation function in Fig. 41 and that contained in Fig. 23(a) is that there are two lines at 3329 Å which are as yet unresolvable, with almost identical wavelengths. Then we would see the resultant of the two lines. The $3d^4D_{7/2}$ being the sharp component, giving rise to the first peak, and the other component consisting of some line which is very broad.

A similar condition could be present in some of the cascade lines into $3p^4S_{3/2}$, thereby giving too large a cross section, particularly for those coming from the $3d^4P_{5/2}$ and $3d^4F_{3/2}$ level.

One final statement may be made concerning the uncertainty of the spectra. A line was found at 3626 Å of which no previous mention has been made in the literature. The closest line to it is a NeII line at 3628 Å, whose excitation function is given in Fig. 20(b) for the $3d^2P_{3/2}$ level. Figure 42 is the excitation function for the 3626 Å line. Its threshold is around 60 eV which would put its energy in the vicinity of the $3d'$ levels, probably a 2S or 2F configuration or some higher 3P core level, say 4p or 5p. It certainly has the broad shape of a 1D core level with the slow rise after onset.

The fourth possibility for a negative cascade is that the $3p^4S_{3/2}$ level may have other channels of depopulation - such as atom-atom

collision or multiple excitation by electron collision. These processes do not seem very likely since they would betray themselves in a non-linearity of the line intensity when the pressure or current is altered. Such was not the case.

Persson⁽¹⁴⁾ has made available a list of all his measured transitions into and out of the level $3p^4S_{3/2}$. In essence, our experimental conditions are very similar in that he used a hollow cathode to produce his excited atoms and ions. He supplied relative intensity measurements with his data. These intensities are rough estimates in that no account was made for the spectral sensitivity of the detecting-system. In any case, the combined intensity of transitions into the $3p^4S_{3/2}$ level equals 133 units. The total intensity out of the level is only 42. Even if he overestimated the intensity of each cascade line by a factor of three, it would leave no room for direct excitation of the $3p^4S_{3/2}$ level.

It is then the feeling of this author that the spectral identification of the 3d levels is not yet complete and accurate, thereby giving rise to a negative cross-section for the $3p^4S_{3/2}$ level.

CHAPTER X

RESONANT FEATURES IN ATOMIC NEON

In 1963, Schulz⁽⁴¹⁾ observed sharp anomalies at 19.3 eV in the electron total elastic-scattering cross sections in helium. The observation of similar sharp anomalies, hereafter called resonances, were found around 16 eV in neon by Schulz⁽⁴²⁾ and Simpson.^(43,44) Simpson and Fano⁽⁴³⁾ attributed these resonances in helium and neon to the formation of negative ion states. They pictured the negative ion as resulting from the insertion of the impacting electron to the lowest excited configuration of the atom with a binding energy around 10 eV. Addition of an electron to higher configurations is also possible but would be more difficult to observe.

Kuyatt *et al.*⁽⁴⁵⁾ have observed similar resonances in a number of gases (Ar, Kr, Xe, Hg, He and Ne) in elastic scattering of electrons. Several of these resonances in He, Ne and Hg are associated with higher excited configurations than the lowest excited configuration of the atom. They have also examined the inelastic components of the electron total-scattering cross section and found these resonances in He, Ne and Xe.

This chapter deals with the observation of some resonant effects in the optical excitation cross sections of atomic neon. These resonances have been interpreted as resulting from these short lived Ne^- states.

The beam current and gas pressure were kept constant at 100 μ A and 10 mTorr, respectively. The apparatus is the same as previously discussed except for the monochromator and photomultiplier tube. A $\frac{1}{4}$ -meter Jarrell-Ash monochromator was used in these experiments with a grating blazed at 6000 \AA . Since the previously used EMI 6256B photomultiplier tube's spectral limit is 6500 \AA and several of the neon lines observed were above this limit, an EMI 9558 tube was employed. This tube possesses an S-20 spectral response.

The optical excitation functions of the ten 2P levels of neon were determined from 16.62 eV to 20.62 eV. Paschen notation is used for these levels and a 2P level would correspond to a 3p electron coupled to either the $2p_{\frac{1}{2}}$ and $2p_{3/2}$ core. These optical excitation functions are presented in Fig. 43. Fine structure was observed for the $2P_3$, $2P_4$, $2P_6$, $2P_8$, $2P_9$ and $2P_{10}$ functions. The $2P_{10}$ resonance has been observed previously by Sharpton⁽¹⁸⁾ and Feltsan *et al.*⁽⁴⁶⁾

Since the $2P_{10}$ resonant feature is so strong, it was associated with the strong #6 resonance structure found by Kuyatt⁽⁴⁵⁾ at 18.56 ± 0.03 eV. Calibrating the $2P_{10}$ resonance at 18.56 eV led to consistent values for the onset energies published by the National Bureau of Standards⁽⁴⁷⁾ for the 2P excitation functions.

The resonances on the $2P_8$ and $2P_9$ excitation functions have identical energies of 18.70 eV. Likewise, the $2P_3$, $2P_4$ and $2P_6$ resonances fall at 18.82 eV. From Fig. 44, it is seen that this would put one of the resonant levels in the vicinity of the $2P_4$ level and the other between the $2P_1$ and $2P_2$ levels. The short dashed lines on the left side

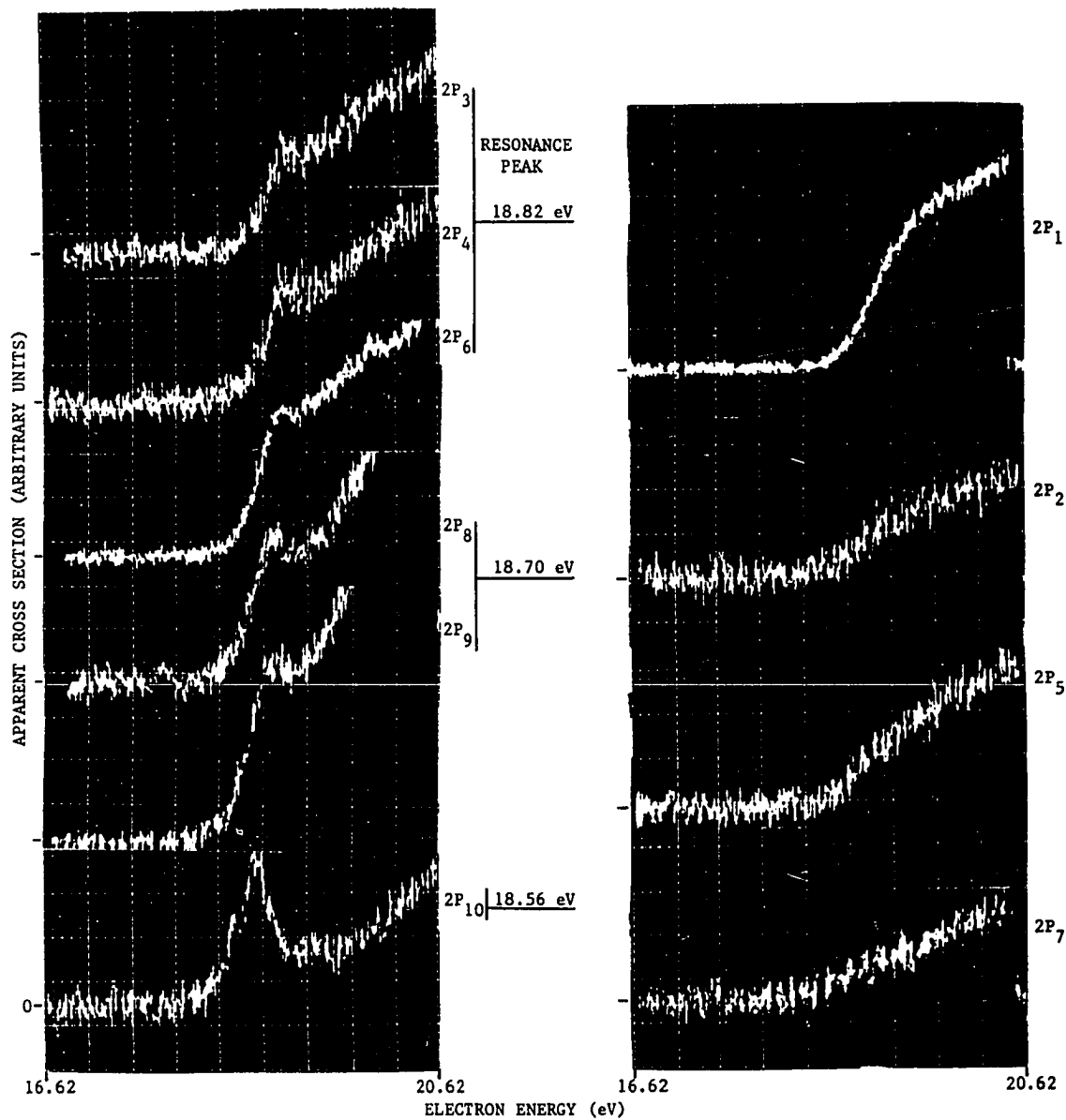


FIGURE 43. Resonant peaks observed in the excitation functions of the 2P levels of atomic neon.

ATOMIC NEON LEVELS

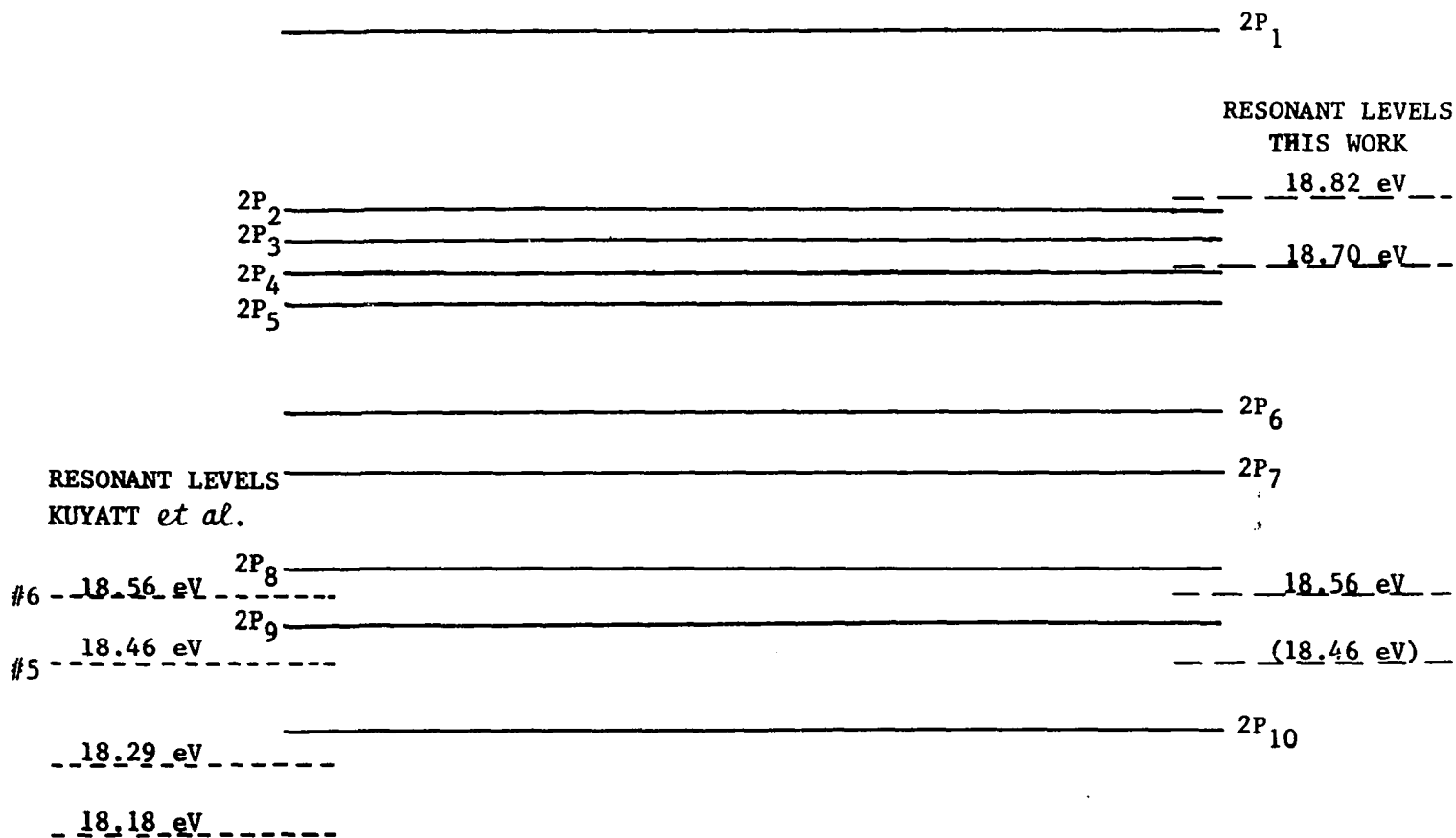


FIGURE 44. Energy level diagram (not to scale) of the 2P levels of atomic neon and the associated negative ion states.

of Fig. 44 are some of the resonant levels found by Kuyatt⁽⁴⁵⁾. The long dashed lines on the right are those resonant levels we have observed.

It is believed these resonant features on the optical excitation functions are due to cascading from the compound state of an electron and a neon atom, commonly called Ne^- . Therefore, the basic process we are considering is thus given by the equation



where in general the final atomic state is not the same as the initial state. In our situation, Ne^* would be one of the 2P levels. If the reaction in Eq. (50) was very large it would be a large source of populating these 2P levels and give rise to the anomalies in Fig. 43. The state designations for $(\text{Ne}^-)^*$ is a little more difficult. Kuyatt⁽⁴⁵⁾ believes his resonances given in Fig. 44 are formed by the addition of a 3p or 3d electron to the $2p^53p$ states of neon. The two new states are probably associated with the $2p^53p$ levels as well. In support of this is the interesting observation concerning the spacing of these upper Ne^- levels. Kuyatt⁽⁴⁵⁾ found his resonances at 16.0 and 16.1 eV, 18.2 and 18.3 eV and 18.46 and 18.56 eV. That is, the resonances occur in pairs separated by about 0.1 eV. The two new states reported here at 18.70 and 18.82 eV also occur as a pair separated by approximately 0.1 eV. It is impossible that these sharp anomalies are due to cascade from higher neutral neon levels since the resonances occur at energies lower than the thresholds of these higher atomic levels.

We expected to see similar peaks in all the excitation functions except for perhaps $2P_1$. Consider the $2P_8$ and $2P_9$ features in Fig. 43. From the figure it can be seen that each of these could easily be two peaks at 18.70 eV and 18.82 eV which are not resolved. The lack of resolution is expected since the difference between these two resonant levels is only 0.12 eV while our resolution of the electron energy is only 0.4 eV. In the $2P_{10}$ case, it was always observed that shoulders existed on both sides of the peak. The shoulder on the high energy side has about the same height as the 18.70 eV resonance and is located at that energy. The optical cross section for the $2P_{10}$ feature is much greater than the other two resonances. The low energy shoulder lies approximately 0.1 eV below the peak, and hence can be associated with the #5 structure of Kuyatt. From Fig. 43 it is evident that no fine structure was obtained in the $2P_1$, $2P_2$, $2P_5$ and $2P_7$ functions. However, by displaying the signal on a time base chart recorder where the energy scale could be expanded much more, slight "humps" were observed in the $2P_5$ and $2P_7$ excitation functions in the energy region of the 18.70 and 18.82 eV resonances. Also, if one examines Fig. 7 in Kuyatt's paper, one can perceive of slight indentions in the transmitted electron current at the same energies of the two new resonant levels reported here.

One can utilize the strong and sharp $2P_{10}$ resonance as a calibration point for the electron beam energy as well as an estimate of the energy resolution.

Finally, Pichanick and Simpson⁽⁴⁸⁾ have observed several resonant structures in the total metastable cross sections of neon in the

vicinity of 18.7-19.0 eV. It is quite possible that the Ne^- states are feeding into the metastable states of neon.

CHAPTER XI

SUMMARY

The simultaneous ionization and excitation cross section by electron impact for the 3p, 3d and 4s levels in neon of the 3P , 1D and 1S cores have been examined. Ultra-high vacuum techniques were employed and the system was extremely free of impurities. The excitation functions were quite broad; some of the 3p' and 3p'' were practically flat. In all, over 100 optical cross sections have been measured and over 50 excitation functions from threshold to 1000 eV were obtained. The optical cross section values represent an average of five or six measurements. The repeatability was better than 1 or 2 per cent for the strong 3p lines. The cascade lines from the 3d and 4s levels of the various cores are very weak - some were just at the limit of detectability. The error of these cascade cross sections will range from 10 to 50 per cent. The direct excitation cross sections were obtained for the 3p, 3p' and 3p'' levels. Polarization effects were examined and only three levels exhibited any polarization and this was less than 10 per cent.

There are no previous experimental results for direct comparison. The branching ratios can be compared, however, and our results were in general agreement with Koopman⁽¹⁾ and Hodges *et al.*⁽²⁾ From these branching ratios and their comparison with LS and intermediate coupling

calculations, the lack of strong lines between doublet and quartet levels and the general tendency of the quartet excitation functions to be more peaked than the doublets, leads one to accept the $(^3P)3p$ levels as being well designated by LS coupling. In conjunction with this and the exceptionally broad excitation functions, it appears that the ionization cross section influences the energy dependence of the simultaneous ionization and excitation cross section. The high energy portion of the excitation functions tended to bear this out as well. The sudden perturbation approximation has been applied to several of the $3p$ levels⁽⁸⁾ and even though it gives an ionization cross section energy dependence, its numerical values for the cross sections were two or three times greater than the experimental values of those levels for which it was applied. This is not unexpected considering the assumptions which were made in this approximation. It is my opinion that more theoretical work is needed in the sudden perturbation or some other theory which will yield an energy dependence similar to the ionization cross section.

Some questions were raised concerning the accuracy of line identification in the NeII spectrum since some of the excitation functions for the alleged same level were radically different. Also, a negative cross section of the $3p^4S_{3/2}$ level was obtained and the source of such a condition was attributed to improper line classification. Several new levels were examined and illustrated the use of the optical excitation function as an aid in line identification.

New resonant features were discovered in the $3p$ levels of atomic neon and were attributed to cascade from Ne^- states.

ADDENDUM

Dr. Willy Persson of the Lund Institute of Technology, Lund, Sweden, has notified me concerning more of his recent work on the line assignments for NeII.

On p.114 of this report I mentioned observing an unidentified line at 3626 Å. Its excitation function verified the origin as NeII and it has an optical cross section of $1 \times 10^{-21} \text{cm}^2$ at 150 eV. Dr. Persson has identified this line as $(^3P)3d^4P_{5/2} - (^3P)5p^2P_{3/2}$. The onset of the excitation function hinted that it should be from a high level of the 3P core.

Dr. Persson has also made available the LS purity of some of the levels. From Figs. 22 and 23 it is noted that the $3d^4P_{3/2}$ and $3d^4P_{5/2}$ levels are broader than the other quartet levels. In fact they resemble very closely the doublet levels. This would imply a large degree of mixing. Dr. Persson's work supports such a conclusion. He finds these two levels are only 50 per cent pure in LS coupling. He also mentions the $3d^4D_J$ levels are about 95 per cent pure. From Figs. 22 and 23 we see that the $3d^4D_J$ levels are relatively narrow. The $3d^4D_{7/2}$ level is 96 per cent pure and this tends to enhance the conclusion that the 3034 Å is the true $3d^4D_{7/2}$ excitation function rather than the 3329 Å line.

REFERENCES

1. D. W. Koopman, J. of the Opt. Soc. of Am. 54, 1354 (1964).
2. D. Hodges, H. Marantz and C. L. Tang, J. of the Opt. Soc. of Am. 60, 192 (1970).
3. A. Denis, P. Ceyzériat and M. Dufay, J. of the Opt. Soc. of Am. 60, 1186 (1970).
4. H. Hertz, Zeitschrift für Naturforschung 24, 1937 (1969).
5. S. H. Koozekanani and G. L. Trusty, J. of the Opt. Soc. of Am. 59, 1281 (1969).
6. Charlotte Froese, Phys. Rev. 137A, 1644 (1965).
7. S. H. Koozekanani, IEEE J. of Quant. Electronics QE-2, 770 (1966).
8. S. H. Koozekanani, IEEE J. of Quant. Electronics QE-4, 59 (1968).
9. W. P. Bridges and A. N. Chester, IEEE J. Quantum Electron QE-1, 66 (1965).
10. W. Persson and L. Minnhagen, Arkiv for Fysik 37, 273 (1967).
11. W. Persson, J. of the Opt. Soc. of Am. 59, 285 (1969).
12. To be published in Physica.
13. R. H. Garstang, Monthly Notices Roy. Astron. Soc. 114, 118 (1954).
14. Private communication.
15. L. Minnhagen, Arkiv för Fysik 18, 97 (1960).
16. L. Minnhagen, Arkiv för Fysik 25, 203 (1963).
17. I. D. Latimer and R. M. St. John, Phys. Rev. A 1, 1612 (1970).
18. F. Sharpton, Ph.D. Dissertation, Univ. of Oklahoma (1968).
19. R. W. Christy, J. of Appl. Phys. 31, 1680 (1960).

20. K. M. Poole, Proc. Phys. Soc. (London) B66, 541 (1953).
21. N. G. Utterback and T. Griffith, Jr., Rev. Sci. Instr. 37, 866 (1966).
22. R. M. St. John, "Calibration of a Spectroscopic System", Methods of Experimental Physics, Vol. 8, 27 (1969), Academic Press, Inc., N. Y.
23. J. D. Jobe, Excitation Processes in Helium (a Ph.D. dissertation), 14 (University of Oklahoma, 1968).
24. J. C. de Vos, Physica 20, 715 (1954).
25. F. A. Sharpton, R. M. St. John, C. C. Lin and F. E. Fajen, Phys. Rev. A 2, 1305 (1970).
26. L. J. Kieffer and J. H. Dunn, Rev. of Mod. Phys. 38, 1 (1966).
27. A. von Engel, Ionized Gases (Clarendon Press, Oxford, 1965), Table 3.7, pg. 63.
28. W. Bleakney, Phys. Rev. 36, 1303 (1930).
29. H. A. Bethe, Ann. Physik 5, 325 (1930).
30. See for example, E. U. Condon and G. H. Shortley, Theory of Atomic Spectra (Cambridge Univ. Press, N. Y., 1953), Eqs. (1) and (3) on pp. 97 and 98.
31. J. R. Oppenheimer, Proc. Nat'l. Acad. Sci. (U.S.) 13, 800 (1927)
32. J. R. Oppenheimer, Z. Physik 43, 27 (1927).
33. W. G. Penny, Proc. Nat'l. Acad. Sci. (U.S.) 18, 231 (1932).
34. I. C. Percival and M. J. Seaton, Phil. Trans. Roy. Soc. (London) A251, 113 (1958).
35. P. N. Clout and D.W.O. Heddle, J. Opt. Soc. Am. 59, 715 (1969).
36. R. H. McFarland, Physical Rev. 156, 55 (1967).

37. H. R. Moustafa Moussa, Thesis, Leiden (1967).
38. H. R. Moustafa Moussa and F. J. DeHeer, Physica 36, 646 (1967).
39. P. T. Smith, Physica Rev. 36, 1293 (1930).
40. A. R. Striganov and N. S. Sventitskii, Tables of Spectral Lines of Neutral and Ionized Atoms (IFI/Plenum, N.Y., 1968).
41. G. J. Schulz, Phys. Rev. Letters 10, 104 (1963).
42. G. J. Schulz, in "Proceedings of the Third International Conference on the Physics of Electronic and Atomic Collisions", edited by M.R.C. McDowell (North-Holland Publishing Co., Amsterdam, 1964), p. 124.
43. J. A. Simpson and U. Fano, Phys. Rev. Letters 11, 158 (1963).
44. J. A. Simpson, in "Proceedings of the Third --- (see 42) -----", p. 128.
45. C. E. Kuyatt, J. A. Simpson and S. R. Mielezarek, Phys. Rev. 138, A385 (1965).
46. P. V. Feltsan, I. P. Zapesochny and M. M. Povch, Ukrainium Phys. Journal 11, 1222 (1966).
47. "Atomic Transition Probabilities, H. through Nd", NSRDS-NBS4, 1, p. 128.
48. F.M.J. Pichanick and J. A. Simpson, Phys. Rev. 168, 64 (1969).